

---

# **Aircraft Automatic-Flight-Control System with Inversion of the Model in the Feed-Forward Path Using a Newton-Raphson Technique for the Inversion**

---

G. Allan Smith, George Meyer, and Maurice Nordstrom

---

(NASA-TM-88209) AIRCRAFT  
AUTOMATIC-FLIGHT-CONTROL SYSTEM WITH  
INVERSION OF THE MODEL IN THE FEED-FORWARD  
PATH USING A NEWTON-RAPHSON TECHNIQUE FOR  
THE INVERSION (NASA) 96 p

N87-11796

Unclas  
44853

CSCL 01C G3/08

July 1986



National Aeronautics and  
Space Administration

---

# **Aircraft Automatic-Flight-Control System with Inversion of the Model in the Feed-Forward Path Using a Newton-Raphson Technique for the Inversion**

---

G. Allan Smith,  
George Meyer, Ames Research Center, Moffett Field, California  
Maurice Nordstrom, Sterling Software, Palo Alto, California

July 1986

**NASA**

National Aeronautics and  
Space Administration

**Ames Research Center**  
Moffett Field, California 94035



## NOMENCLATURE

A	aircraft acceleration vector
$A_C$	smooth commanded acceleration vector
$A_i$	rough commanded acceleration vector
$A_T$	total commanded acceleration vector
B	Jacobian matrix for trim procedure
D	force controls
Dpitch	normalized pitch command, six-degree-of-freedom trim variable or four-degree-of-freedom trim variable
Droll	normalized roll command, six-degree-of-freedom trim variable or four-degree-of-freedom trim variable
Dyaw	normalized yaw command, six-degree-of-freedom trim variable or four-degree-of-freedom trim variable
E	perturbed error vector for trim procedure
$E_{REF}$	reference error vector for trim procedure
$E2(\theta)$	elementary direction cosine matrix for rotation about the second axis through an angle $\theta$ , similar notation for other angles, where
	$E2(\theta) = \begin{vmatrix} \cos \theta & 0 & -\sin \theta \\ 0 & 1 & 0 \\ \sin \theta & 0 & \cos \theta \end{vmatrix}$
EF	force equations error vector
EM	moment equations error vector
F	force vector acting on aircraft in Earth reference axes
$F_b$	force vector acting on aircraft in body axis
G	gravity vector

**PRECEDING PAGE BLANK NOT FILMED**

J aircraft moment of inertia matrix, where

$$J = \begin{vmatrix} I_{xx} & 0 & I_{xz} \\ 0 & I_{yy} & 0 \\ -I_{xz} & 0 & I_{zz} \end{vmatrix}$$

m aircraft mass

$M_b$  moment vector acting on aircraft in body axes

R aircraft position vector

$R_c$  smooth commanded position vector

$R_i$  rough commanded position vector

$S(\omega)$  skew symmetric matrix function of the angular velocity vector, where

$$S(\omega) = \begin{vmatrix} 0 & \omega(3) & -\omega(2) \\ -\omega(3) & 0 & \omega(1) \\ \omega(2) & -\omega(1) & 0 \end{vmatrix}$$

T trim perturbed variables

TBR direction cosine transformation matrix from Earth reference axes-to-body axes; symbol implies R to B

TRB inverse (transpose) of TBR; symbol implies B to R

U aircraft controls

V aircraft velocity vector

$V_c$  smooth commanded velocity vector

$V_i$  rough commanded velocity vector

$V_w$  wind velocity vector

$V_{wb}$  velocity of aircraft with respect to wind in body axes

VATOL vertical attitude takeoff and landing (acronym)

$\alpha$  aircraft angle of attack

$\alpha_c$  commanded angle of attack, six-degree-of-freedom trim variable

$\beta$  aircraft sideslip angle  
 $\beta_c$  commanded sideslip angle for six-degree-of-freedom trim  
 $\Delta A_c$  translational regulator acceleration correction vector  
 $\Delta \dot{\omega}_c$  rotational regulator angular acceleration correction vector  
 $\Delta T_c$  trim variables correction vector  
 $\Delta T$  trim variables perturbation vector  
 $\Gamma_c$  commanded flightpath angle for six-degree-of-freedom trim  
 $\Gamma_v$  flightpath angle  
 $\psi_c$  commanded heading angle for six-degree-of-freedom trim  
 $\psi_v$  heading angle  
 $\phi_E, \theta_E, \psi_E$  roll, pitch, and yaw Euler angles with respect to Earth reference axes  
 $\phi_p, \theta_p, \psi_p$  roll, pitch, and yaw Euler angles with respect to perpendicular axes  
 $\phi_c$  commanded roll angle, six-degree-of-freedom trim variable  
 $\phi_{pc}$  commanded roll angle for six-degree-of-freedom trim in perpendicular reference  
 $\theta_{pc}$  commanded pitch angle, six-degree-of-freedom trim variable in perpendicular reference  
 $\psi_{pc}$  commanded yaw angle, six-degree-of-freedom trim variable in perpendicular reference  
 $\omega$  aircraft angular velocity vector, body axes  
 $\omega_i$  rough commanded angular velocity vector  
 $\dot{\omega}$  aircraft angular acceleration vector, body axes  
 $\dot{\omega}_c$  smooth commanded angular acceleration vector  
 $\dot{\omega}_T$  total commanded angular acceleration vector

## Subscripts

b	body axes
c	commanded
E	Earth reference axes
i	rough input
p	perpendicular reference axes
REF	reference
T	total
v	derived from velocity vector
w	wind

## Superscripts

$\cdot$	time derivative
$-1$	matrix inverse

AIRCRAFT AUTOMATIC-FLIGHT-CONTROL SYSTEM WITH INVERSION OF THE  
MODEL IN THE FEED-FORWARD PATH USING A NEWTON-RAPHSON  
TECHNIQUE FOR THE INVERSION

G. Allan Smith, George Meyer, and Maurice Nordstrom\*

SUMMARY

A new automatic flight-control system concept suitable for aircraft with highly nonlinear aerodynamic and propulsion characteristics and which must operate over a wide flight envelope has been investigated at NASA Ames Research Center. This exact model follower inverts a complete nonlinear model of the aircraft as part of the feed-forward path. The inversion is accomplished by a Newton-Raphson trim of the model at each digital computer cycle time of 0.05 seconds.

The combination of the inverse model and the actual aircraft in the feed-forward path allows the translational and rotational regulators in the feedback path to be easily designed by linear methods. An explanation of the model inversion procedure is presented. An extensive set of simulation data for essentially the full-flight envelope for a vertical attitude takeoff and landing aircraft (VATOL) is presented. These data demonstrate the successful, smooth, and precise control that can be achieved with this concept. The trajectory includes conventional flight from 200 to 900 ft/sec with path accelerations and decelerations, altitude changes of over 6000 ft and 2g and 3g turns. Vertical attitude maneuvering as a tail sitter along all axes is demonstrated. A transition trajectory from 200 ft/sec in conventional flight to stationary hover in the vertical attitude includes satisfactory operation through lift-curve slope reversal as attitude goes from horizontal to vertical at constant altitude. A vertical attitude takeoff from stationary hover to conventional flight is also demonstrated.

INTRODUCTION

Some current high performance fighter aircraft and helicopters, and many of those proposed for the future, have control and stability difficulties over some portions of their flight envelopes. These difficulties arise from highly nonlinear aerodynamic and propulsion characteristics, from undesirable coupling between axes, and from the extreme range of flight conditions encountered over the flight

---

\*Work done while employed by Informatics General Corporation (now Sterling Software), Palo Alto, California.

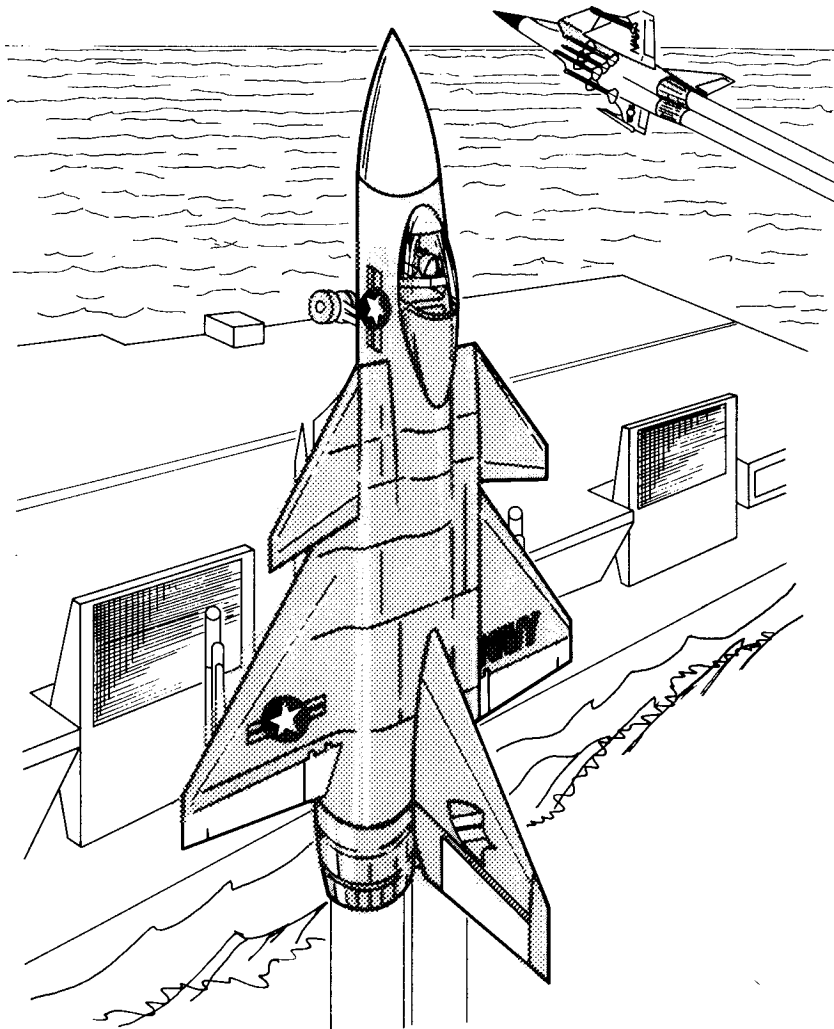
regime. There may be instances where automatic flight control will be desirable for these aircraft over at least a portion of the flight regime. Examples include precision trajectory control during night landing on a carrier at sea, terrain following with a helicopter, hover-mode control of a vertical attitude takeoff and landing aircraft (VATOL), and of course complete automatic control is required for remotely piloted vehicles and cruise missiles.

A new automatic flight control system concept that is suitable for trajectory control of aircraft with such challenging characteristics and requirements is being investigated at NASA Ames Research Center. The implementation of this concept is made possible by the airborne digital computer. This is a total aircraft flight-control system that combines attitude and thrust control in a unified system for operation over the full flight envelope.

The flight-control system is an exact model follower that uses essentially all of the aerodynamic and propulsion data that would be found in a complete model used for simulation studies. A unique feature of the control system is the continuous real-time inversion of the complete nonlinear model of the aircraft forces and moments for the purpose of defining the aerodynamic and propulsion control commands based on trajectory commands and regulator outputs.

This control-system concept has been developed in a series of theoretical studies (refs. 1,2,3). Successful flight tests of the concept have been conducted in the augmentor wing jet short takeoff and landing (STOL) research aircraft (ref. 4), in the De Havilland DHC-6 aircraft (ref. 5), and in a Bell UH1H helicopter (ref. 6). Simulator studies of a carrier landing system were reported in reference 7. Preliminary results of a simulation of hover mode control for a VATOL were given in reference 8. The overall structure of the control system has been described in the above references so only a brief explanation of the general system configuration will be given in this report. The emphasis will be on a new direct trim technique for the continuous real-time inversion of the nonlinear aircraft model as part of the control system, and a discussion of extensive simulation results of its application to control of a conceptual VATOL aircraft over the full-flight regime from vertical attitude hover through transition to normal attitude flight. Preliminary results with this new inversion technique were presented in reference 9.

Figure 1(a) is an artist's conception of a Navy VATOL (tail sitter) suitable for launch and recovery at the side of a small ship. In figure 1(b) (see ref. 10), the major dimensions and the inertia values are given and the basic delta wing and canard configuration is shown. The aerodynamic and propulsion characteristics of this proposed aircraft were developed by Vought Corporation (ref. 10), and are used in the simulation discussed in this report. This conceptual aircraft was chosen to illustrate the extensive flight regime and range of nonlinear characteristics that can be accommodated by the Ames control system.

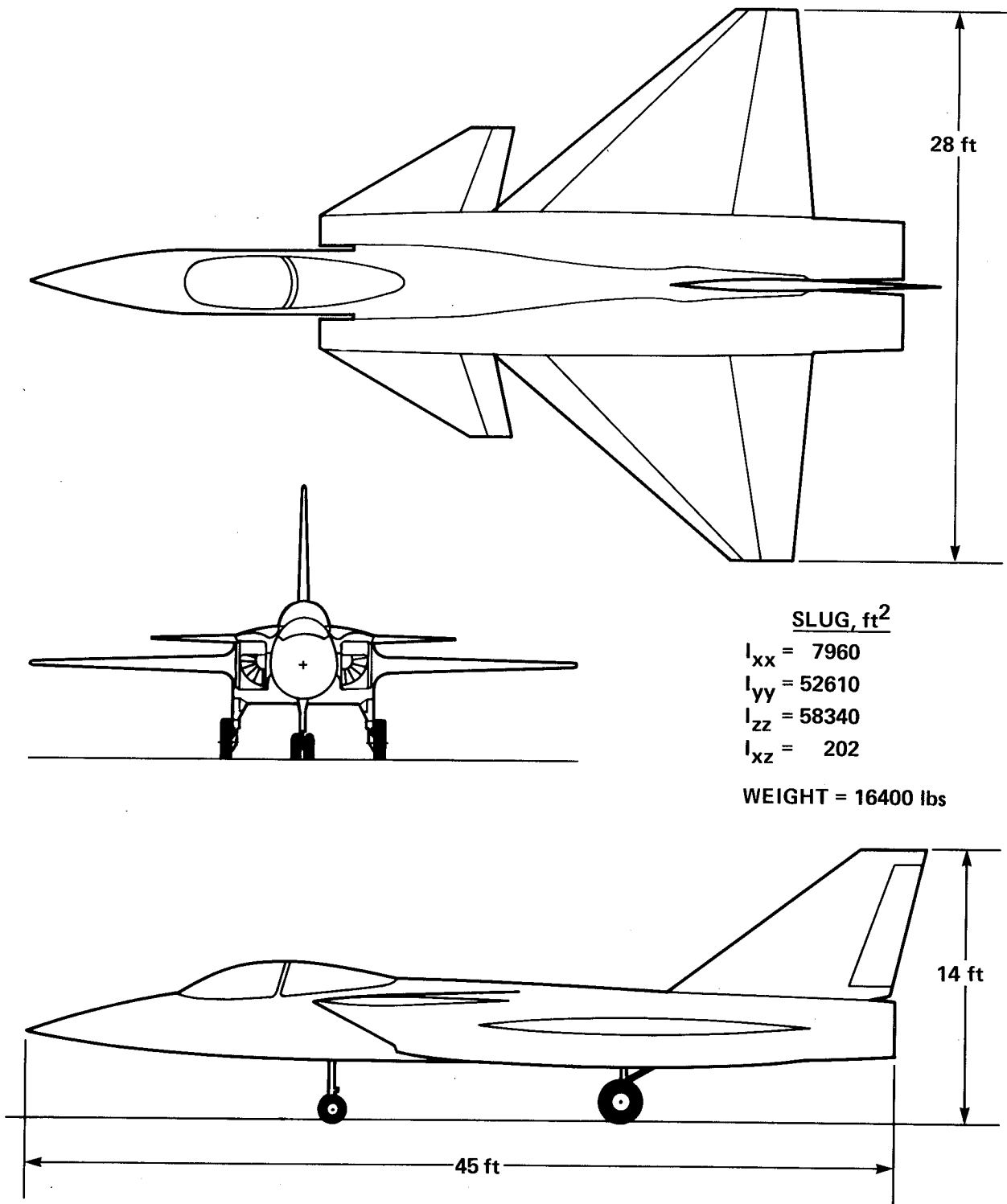


(a) Artist's conception.

Figure 1.- VATOL aircraft used in simulation study.

### THE CONTROL SYSTEM CONCEPT

The Ames control system concept has several key features. Fundamentally, it employs a feed-forward controller with a command section and a control section as shown in figure 2, in addition to a conventional feedback loop. To simplify the description of the concept, the attitude dynamics will be neglected in this introductory section of the report so that the four control variables  $D$  in figure 2 may be taken as thrust and attitude (given by the three Euler angles of roll, pitch, and yaw). The feed-forward controller is shown in solid lines and the feedback control is shown with dotted lines. The signals in this diagram are three-dimensional vectors with appropriate subscripts, except for the four controls,  $D$ .



(b) Preliminary design.

Figure 1.- Concluded.

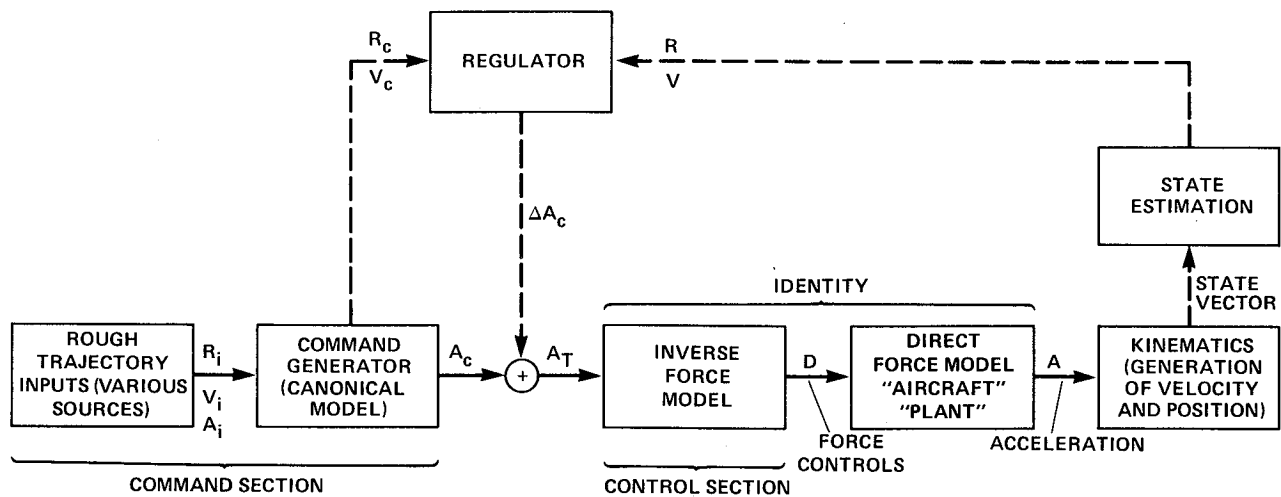


Figure 2.- Essential aspects of the Ames control concept.

The command generator in the command section generates smooth position  $R_c$ , velocity  $V_c$ , and acceleration  $A_c$  command vectors in Earth-reference inertial axes (north, east, and down) in response to rough trajectory command inputs  $R_i$ ,  $V_i$ , and  $A_i$ . These rough inputs may be supplied from an air traffic control system, from ground vectoring or from a trajectory time history either stored in the computer or generated on line by a pilot using the conventional controls or a sidestick controller to command selected components of acceleration in body axes.

The control section of the feed-forward controller is an inverse of the aircraft force model and computes the aircraft thrust and attitude needed to produce the total commanded acceleration vector  $A_T$ . If the inverse model was perfect and there were no disturbances acting on the aircraft, it would follow the commanded acceleration exactly so there would be no need for feedback. Because these conditions are not met in practice, feedback is used as indicated by the dotted loop. The loop is conceptually closed around the series combination of the aircraft force model and its inverse force model, which for this simplified preliminary discussion, constitute an identity. The regulator can thus be easily designed by linear methods.

The command generator in figure 2 accepts the rough input trajectory commands that may not be executable because of discontinuities or because of the absence of some components of the vectors, and it produces a complete and consistent set of smooth executable position, velocity, and acceleration command vectors. This is accomplished by using a simple canonical model of the desired aircraft response, which for this introductory description, would consist of three strings of two integrators each, one string for each of the three channels which correspond to the inertial components of the input command vectors (north, east, down). Sideslip angle,  $\beta$ , is directly controllable as a commanded input (usually commanded to be zero). Adjustment of gains and limits provides smooth output vector commands as discussed in reference 1. The aircraft position and velocity  $R$  and  $V$  are compared with the smooth commands in the regulator and produce an acceleration correction

vector,  $\Delta A_c$ , which is added to the feed-forward command  $A_c$  to give the total commanded acceleration vector,  $A_T$ . The feedback signal,  $\Delta A_c$ , is usually small when compared to the feed-forward command,  $A_c$ . A brief description of the command generator and the regulator is given in appendix A.

### THE AIRCRAFT MODEL

As in any simulation study, the aircraft is represented by a mathematical model, usually called the plant in control theory terminology. For this study, the control system itself also contains a model which is inverted, and hence, is referred to as the inverse model after it is inverted, or as the aircraft model while it is being inverted. In fact, two inverse models exist in the control system as will be discussed later. These inverse models are essentially the same as the plant model, but they have slight differences for this study. If desired, the differences can be exaggerated for purposes of studying mismatch effects, and in an actual physical installation in an aircraft, they might differ substantially from the real aircraft characteristics in some portions of the flight envelope. Also, there is a simple canonical model of the desired aircraft dynamics which is used in the command generator section of the control system.

A complete description of the aircraft aerodynamic and propulsion characteristics is given in reference 11, which includes the equations used in the simulation to calculate all forces and moments acting on the aircraft. These calculations use the DATCOM procedure, a complete aerodynamic force computation routine developed by the Douglas Aircraft Company under Air Force sponsorship (ref. 12). A detailed engine model with afterburner is used to calculate thrust and ram drag.

A flow diagram of the aircraft model calculations is shown in figure 3. This generally conventional model has been specialized to represent the VATOL aircraft used in this simulation. The four input commands,  $U$ , are normalized thrust,

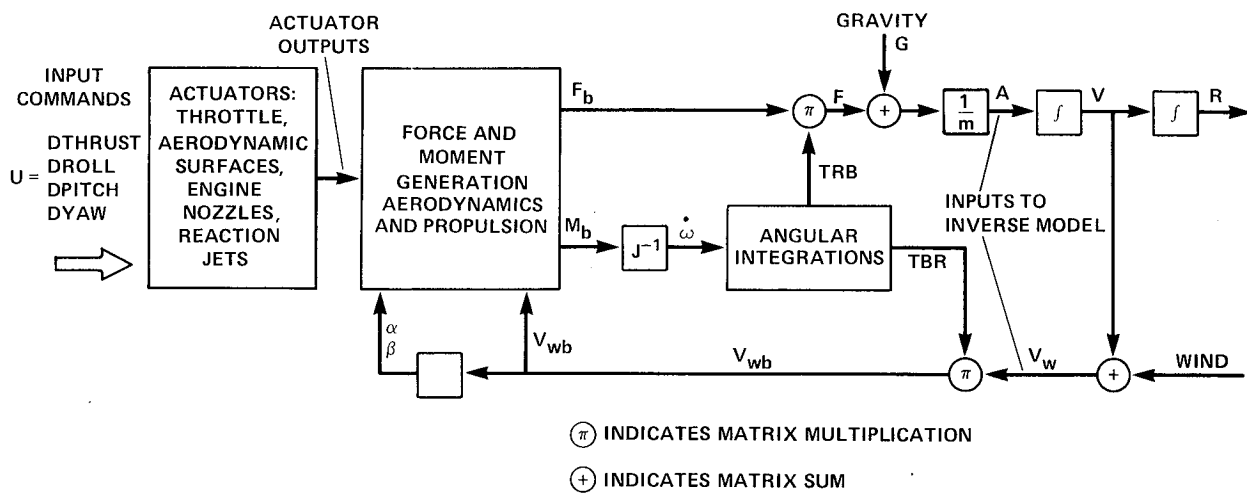


Figure 3.- Aircraft model.

Dthrust, which is converted to a throttle displacement, and three normalized angular acceleration commands, Droll, Dpitch, Dyaw, which are converted to aircraft control surface and engine nozzle deflections. For example, a value of 0.6 for Dpitch would call for approximately 60% of the maximum available pitch angular acceleration. This is scaled and sent to the elevon and engine nozzle actuators to cause about a 60% deflection of each. The VATOL jet engine has an output nozzle capable of swivelling through plus or minus 15° in both pitch and yaw. The four input commands are divided appropriately between the various controls which include throttle, elevons, rudder, leading-edge wing flaps, trailing-edge canard flaps, nozzle angle, and engine bleed air jets at the wing tips for roll control in the hover mode.

The outputs of the control actuators are sent to the force- and moment-generating section where aerodynamic forces for each surface are computed as a function of angle of attack,  $\alpha$ , angle of sideslip,  $\beta$ , and velocity,  $V_{wb}$ . The symbol  $V_{wb}$  represents the velocity with respect to the air in body axes which are taken as positive along the aircraft longitudinal axis, out the right wing, and in the direction of the landing gear. Fuselage drag is also computed and thrust calculations include such refinements as engine gyroscopic moments and thrust losses caused by nozzle turning angle and bleed air used for roll control. The body axis torque moments,  $M_b$ , in figure 3 are used with the aircraft inertia matrix,  $J$ , and the Euler angle-rate equations to calculate angular acceleration,  $\dot{\omega}$ . Integrations then provide angular velocity,  $\omega$ , and aircraft attitude which is expressed as TRB, which is the direction cosine matrix of rotation from reference axes to body axes. For display purposes, this matrix is usually expressed in terms of the three conventional Euler angles,  $\psi_E$ ,  $\theta_E$ ,  $\phi_E$ ; alternatively, five angles including angle of attack,  $\alpha$ , and sideslip angle,  $\beta$ , can be used as will be discussed presently. The inverse (transpose) TRB is used to transform  $F_b$ , the force in body axes, from body axes to reference axes. The addition of the gravity vector,  $G$ , and division by the aircraft mass,  $m$ , yields the acceleration vector,  $A$ . This acceleration vector is the essential output of interest for the direct model. Integrations to give velocity,  $V$ , and position,  $R$ , are included in the figure.

The control section of the feed-forward controller is functionally the inverse of the complete aircraft model just described. The input to the inverse model is the total acceleration command vector,  $A_T$ , and conceptually it is applied at the point A in figure 3. Note that the vector velocity of the aircraft with respect to wind in Earth reference axes,  $V_{wb}$ , is also needed as an input to the inverse model in order to calculate the velocity dependence of aerodynamic forces and moments. This velocity information will require instrumentation and estimation capability on board an actual aircraft. Errors in modeling the velocity will be largely compensated by the feed-back loop and regulator. The operation of the trajectory control system should now be clear and attention will be directed to the details of the model inversion process which differs substantially from the scheme used for previous applications of this concept.

## THE MODEL INVERSION PROCESS

In the early implementations of this control system concept (refs. 4 and 5) the model inversion was performed with the aid of extensive two- and three-dimensional tables of nonlinear aerodynamic data relating lift and drag coefficients to angle of attack and thrust. Real-time interpolation of the data was done by the airborne digital computer. Although simplifications of the aircraft model and approximations in the nonlinear aerodynamic and propulsion data were necessary to permit the inversion, simulation and flight-test results were generally satisfactory. However, a substantial amount of analysis was required to construct the inverse tables and to determine what level of detail was necessary.

The new model inversion technique avoids the actual computation of inverse nonlinear data and does not require simplifications or approximations. Instead, it relies entirely on the complete nonlinear equations of the aircraft model and data which would be used for the normal simulation studies made during the design and development of the aircraft. The data can be modified by flight-test results.

The inversion of the model is done by carrying out a trim of the aircraft model at each computer-loop-cycle time; i.e., twenty times per second. This is a Newton-Raphson trim of the aircraft model similar to that which is usually done at the start of a simulation run to determine initial control settings. However, these trims are done for specified commanded accelerations rather than for the usual case of zero acceleration, and they are done at each computer-loop-cycle time and not just at the start of a run. The Newton-Raphson procedure is a multivariable adaptation of Newton's method for finding the root of an equation by calculating a local derivative and using a linear extrapolation to find an approximation to the root in an iterative fashion. The term "trim" is used in the aerodynamic sense to mean a balance between desired accelerations and the actual forces and moments acting on the aircraft. All quantities in the trim equations are the actual full values and are not deviations from a reference as is sometimes indicated by the term "trim" in control system analysis.

Figure 4 is a simplified conceptual diagram of the model trim procedure and will be recognized by those engaged in aircraft simulation studies as being similar to the procedure used for initial trim at the start of a simulation run. The trim procedure balances the force and moment trim-vector error equations which are:

$$EF = F_b + TBR_c(G - mA_T)$$

$$EM = M_b + S(\omega_c)J\omega_c - J\dot{\omega}_c$$

They represent three scalar force equations and three scalar moment equations, respectively. The gravity vector is  $G$ , the aircraft mass is  $m$ , the moment of inertia matrix is  $J$ , and  $S(\omega_c)$  is the skew symmetric matrix function of the angular velocity. These equations are written in aircraft body axes so the gravity and

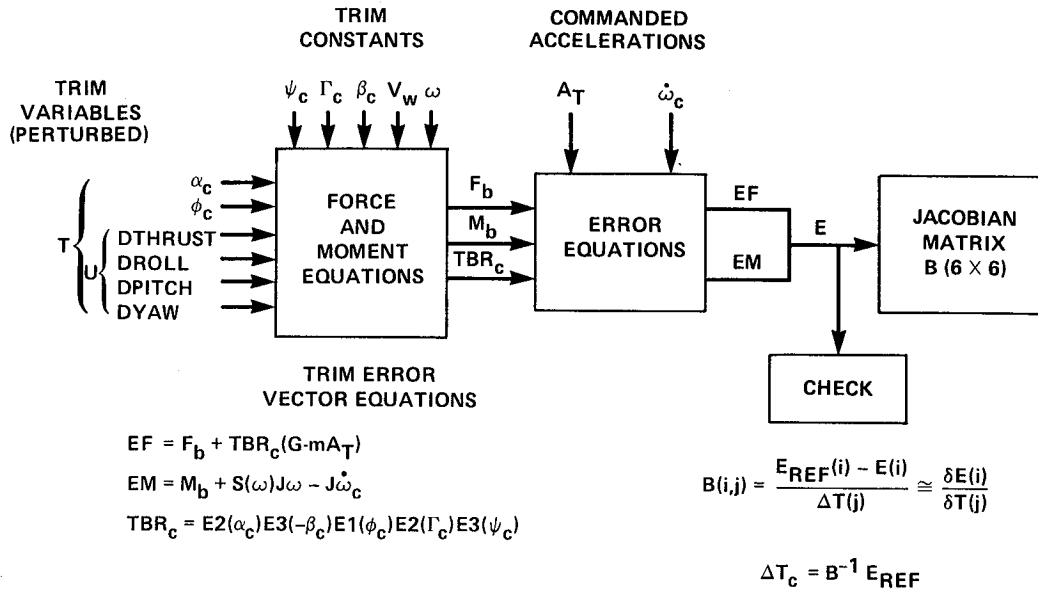


Figure 4.- Model inversion process.

commanded acceleration which are in Earth-reference axes must be transformed by the rotation matrix,  $TBR_c$ .

The force and moment calculations in the trim procedure of figure 4 are essentially the same as those used to compute the forces and moments acting on the aircraft model (plant) in the simulation with the exception that actuator dynamics and limits are ignored and some aerodynamic and propulsion system refinements are neglected. These calculations determine  $F_b$ ,  $M_b$ , and  $TBR_c$  which are three of the quantities needed by the trim error equations. Since this is the trim of the model of the aircraft that is imbedded in the control system, many quantities are indicated as commanded values with subscript  $c$ . A complete trim would be carried out at each airborne computer-loop-cycle time, that is, every 0.05 sec. During the 0.05-sec computer cycle, several quantities remain constant in the computer although they are updated at each computer-loop-cycle time. These constant quantities include commanded heading and flightpath angles,  $\psi_c$  and  $\Gamma_c$  (which are determined by the components of the commanded velocity vector), and the commanded sideslip angle,  $\beta_c$ , which must be specified (usually zero). The velocity with respect to the air in Earth-reference axes,  $V_w$ , and the aircraft angular velocity,  $\omega$ , remain constant at their estimated or measured values. Also the commanded linear acceleration,  $A_T$ , and angular acceleration,  $\dot{\omega}_c$ , remain constant during the 0.05-sec computer cycle. The trim variables are adjusted during the trim cycle in order to balance the error equations.

As will be more fully explained later, the trim process is actually carried out twice during a computer cycle; the first time is for six degrees of freedom with

angular acceleration and angular velocity taken as zero, and the second time for only four degrees of freedom but with nonzero angular acceleration and angular velocity inputs.

The objective of the first trim is to adjust the six trim variables so that the trim error equations will balance to within a small specified tolerance, typically 0.0015 g (20 lb) for the force equations, and 0.0015 rad/sec (80 ft·lb) for the moment equations. Sometimes more than one cycle of the trim procedure must be executed during a single computer cycle time. At the start of a trim cycle the trim variables (which are angle of attack  $\alpha_c$ , roll angle  $\phi_c$ , and Dthrust, Droll, Dpitch and Dyaw commands) retain the values from the previous trim cycle. Using these trim quantity values and the current values of the quantities that remain constant during a computer cycle, the forces and moments in body axes,  $F_b$  and  $M_b$ , are now computed in addition to the attitude transformation matrix,  $TBR_c$ . This matrix is calculated as the product of five elementary direction cosine matrices which correspond to the five angles through which the aircraft is rotated from Earth-reference axes. The expression for the matrix is:

$$TBR_c = E2(\alpha_c)E3(-\beta_c)E1(\phi_c)E2(\Gamma_c)E3(\psi_c)$$

This matrix represents two rotations,  $\psi_c$  and  $\Gamma_c$ , to define the velocity vector; and three more rotations,  $\phi_c$ ,  $-\beta_c$ ,  $\alpha_c$ , to establish the complete aircraft attitude. All of the quantities on the right side of the trim equations are now available so that the three-dimensional error vectors,  $EF$  and  $EM$ , can be calculated.

If all six scalar errors are within their specified tolerances, the aircraft model is said to be trimmed since the values of the six trim variables would produce the commanded path accelerations. If any errors exceed their tolerance, a perturbation procedure is initiated for which the six errors just calculated are taken as a six-dimensional reference error vector,  $E_{REF}$ . One trim variable,  $T(j)$ , is perturbed by a small amount,  $\Delta T(j)$ , and the forces and moments are recalculated to give six new errors,  $E$ . A column of the Jacobian matrix,  $B$ , is then calculated where each entry is approximately the partial derivative of a force or moment with respect to the perturbed variable.

$$B(i,j) = \frac{E_{REF}(i) - E(i)}{\Delta T(j)} \approx \frac{\partial E(i)}{\partial T(j)} \quad (1)$$

Similarly, the other five trim variables are individually perturbed to calculate the other columns of the six-by-six  $B$  matrix. The rows of the  $B$  matrix correspond to the six error equations in the order of the forces and moments along, and about, the aircraft axes. The columns correspond to the six trim variables in the order thrust, roll, pitch, yaw, angle of attack, roll angle. For example, the second row, first-column entry is aircraft, lateral-axis, force reference error minus lateral-axis, force error when thrust is perturbed all divided by the thrust perturbation. Note that a perturbation of the angle of attack or roll angle requires recalculation of the attitude matrix,  $TBR_c$ .

The Newton-Raphson procedure essentially inverts the B matrix by a Gaussian elimination to determine incremental corrections to the trim variables,  $\Delta T_c = B^{-1}E_{REF}$ . If the model was linear, the corrected trim variables would give zero error values in the trim equations. A calculation of the forces, moments, and the transformation matrix is made using the corrected trim variables so that the resulting errors can be checked. If the errors are within the tolerance limits, the trim process is terminated. Otherwise, the trim cycle is repeated still at the same computer cycle time until a satisfactory solution is achieved. For most flight conditions, a single trim cycle is sufficient and often the perturbation portion of the trim cycle is not required as the trim equation errors are found to be within their tolerance limits at the start of the trim cycle. However, for this condition, the previous Jacobian matrix is still used with the current error to calculate a trim variable correction. On the other hand, when commanded accelerations are changing rapidly or severe disturbances are encountered, two or more trim cycles may be required.

The general outline of the control concept and the Newton-Raphson trim procedure is now complete. However, before examining the results of the simulation runs, two other important features should be described. First, recall that the attitude transformation matrix TBR expresses the aircraft attitude with respect to an inertial axis system (the Earth-reference system with axes north, east, and down). In the vertical-attitude hover mode, the aircraft is at a singularity of the Euler angle representation of this transformation, and furthermore, velocity may be zero so that angle of attack is undefined. This causes problems for the attitude perturbations; therefore, a second inertial system that is rotated 90° about the east-reference axis and called the perpendicular system with axes up, east, and north, respectively, is used to express the aircraft attitude when the pitch angle above the horizontal is greater than approximately 50°. Switching between the two axis systems is accomplished with no noticeable transient effects.

For trim with the perpendicular axis system, the angle of attack is not used as a trim variable; instead the attitude matrix, TBP, represents the transformation from the perpendicular system to body axes and is expressed by the three conventional Euler angles with pitch and yaw taken as trim variable. Roll about the vertical axis is taken as the first Euler angle and is specified as a commanded heading direction for the aircraft landing gear. The perpendicular transformation matrix is expressed as:

$$TBP = E3(\psi_{pc})E2(\theta_{pc})E1(\phi_{pc}) \quad (2)$$

where  $\theta_{pc}$  and  $\psi_{pc}$  are trim variables and are angles about the aircraft pitch and yaw axes, respectively. The commanded roll angle is  $\phi_{pc}$ . The pitch angle at which switching occurs is not critical and could be anywhere between 50° and 80° above the horizontal so a hysteresis loop with 10° of displacement is used in the switching circuit to prevent chatter at the switching point.

The second additional feature is shown in figure 5 which is a more detailed diagram of the complete control system. It includes several details which are not

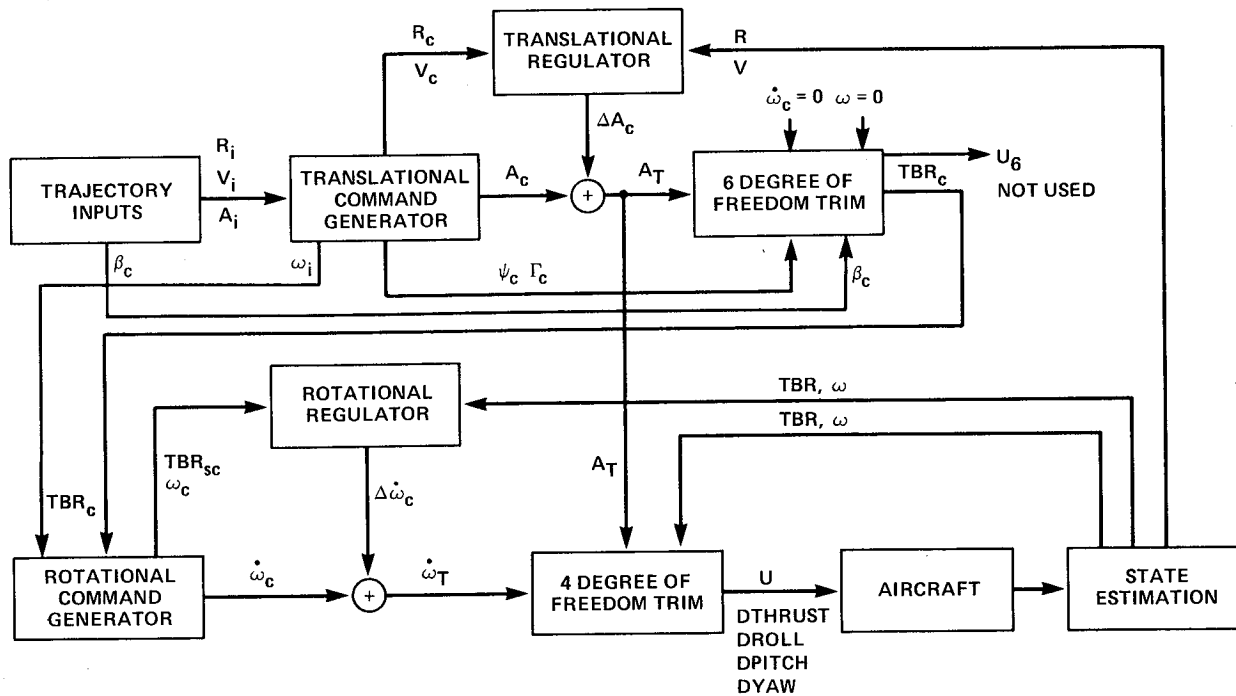


Figure 5.- Complete control system concept.

completely described in the introductory discussion of the control-system concept. For example, the canonical model in the translational command generator actually has four integrators in each channel in order to represent the attitude dynamics which were ignored in the introductory discussion of figure 2. We have so far considered only the first part of the system from the trajectory inputs through the translational command generator, and regulator and the six-degree-of-freedom trim. The six-degree-of-freedom trim is carried out with commanded angular acceleration and angular velocity set to zero. The commanded attitude matrix,  $TBR_c$  (or  $TBP_c$ ) is sent to the next part of the control system, but the other trim variables  $U_6$  from this trim are not used. Instead, another Newton-Raphson trim with only four degrees of freedom is performed. The rotational command generator, described more fully in appendix A, is similar to the translational command generator except that its canonical model has only two integrators in each of three channels which correspond to the three aircraft body axes. It is used with the commanded attitude matrix,  $TBR_c$  (or  $TBP_c$ ), and the rough commanded trajectory angular velocity,  $\omega_i$ , to compute a smooth-commanded angular acceleration vector,  $\dot{\omega}_c$ . This is combined with a feedback correctional acceleration from the rotational regulator,  $\Delta\dot{\omega}_c$ , to form the total commanded-angular acceleration vector,  $\dot{\omega}_T$ , which is input to the four-degree-of-freedom trim. Other inputs to this trim are the same commanded-linear acceleration,  $A_T$ , that is used for the six-degree-of-freedom trim and the measured aircraft attitude,  $TBR$  (or  $TBP$ ), and angular velocity,  $\omega$ . The four-degree-of-freedom trim uses the three moment trim error equations and the one force trim error equation for the aircraft longitudinal axis. The trim variables are the four commands Dthrust, Droll, Dpitch, and Dyaw and they are scaled and sent to the actual aircraft actuators. The four-degree-of-freedom trim switches to the perpendicular axis system at

the same time that the six-degree-of-freedom trim switches. The reason for using two trim sections is the desire to separate the trajectory and attitude portions of the control system. The first (six-degree-of-freedom) trim is done with zero angular acceleration and angular velocity and gives the steady state attitude necessary to provide the commanded trajectory accelerations which are primarily due to aerodynamic forces produced by angle of attack. Nulling the angular acceleration and velocity removes the zeros in the transfer function caused by these quantities. The second (four-degree-of-freedom trim) has the angular acceleration consistent with this attitude (developed by the rotational command generator) as an input in addition to the same commanded-linear acceleration used for the six-degree-of-freedom trim. The second trim determines the controls that are needed to produce this angular acceleration. The second trim is part of the aircraft attitude control loop which is similar to a conventional automatic pilot-attitude control loop. The angular acceleration inputs to the four-degree-of-freedom trim will produce zeros in the transfer function, and in fact, they are right-half-plane zeros or nonminimum phase zeros. Their effect is clearly seen in the response of the actual aircraft, but their effect is suppressed in the four-degree-of-freedom trim as will be explained later.

#### SIMULATION DATA

An extensive series of simulation runs was made using the VATOL aircraft and the trajectory control system just described. These tests covered operation over a large part of the flight envelope. The simulations were run in the completely automatic mode with no pilot interaction so no displays were involved, and all data was collected as time-history plots of system variables. For each run 240 variables were recorded at each computer cycle time, 0.05 sec. Only a selected number of these runs (8) are presented, and only a limited number of variables are shown. Over 60 variables are shown for the first run to illustrate the system features, but many variables of minor importance or those whose behavior is essentially the same for all runs are not included in subsequent runs with the understanding that their performance can be inferred from the prior runs or from other variables that are displayed. The choice of scales was made to permit easy comparison of related quantities rather than to maximize the fine detail by setting full-scale equal to the maximum excursion. The maximum and minimum values achieved by each variable are recorded in the upper right-hand corner of each plot. Trajectory data for conventional flight are calculated in an inertial system with axes north, east, and down as positive directions. For ease of interpretation, the sign of vertical axis data is reversed so that upward acceleration, velocity, and displacement are plotted as positive quantities.

Each page of time-history data contains up to 8 separate plots which are numbered at the right margin consecutively from the top to facilitate identification in the discussion. Some plots contain two or more variables plotted as solid, dashed, and dotted lines. In some cases, the ordinate scale has two dimensions with the same numerical values; for example, both angle and angular rate, or both

acceleration and acceleration rate. All runs start in a steady-flight condition which is maintained for the first 5 sec. Trajectory commands are then given to establish accelerations along various space or flightpath axes. Usually the input commands are steps of acceleration rate so that ramp acceleration commands result which are then integrated to give the corresponding velocity and displacement commands. These inputs were chosen because they were easy to implement, gave a less severe input than did acceleration steps, and are somewhat similar to what a pilot might use for a maneuver. Many other methods of generating trajectory commands would be satisfactory, and in fact, steps of acceleration modified by a low-pass filter were used as a matter of convenience for the vertical attitude maneuvers in the sixth and seventh runs of the simulation. The primary input commands are executed at preselected program times for these automatic trajectories, but could just as easily be input by a human pilot in real-time using a hand controller since there are only 4 fundamental inputs, three translational acceleration rates, and a heading rate. Accelerations are plotted in g units although the actual simulation commanded ft/sec/sec usually in whole numbers so when the discussion indicates "about 0.1 g or 0.4 g" the actual commands were 3 ft/sec/sec and 12 ft/sec/sec. All g levels are thus approximate in the discussions.

The time-history plots of variables for each run are preceded by a plot of the trajectory with way point numbers which refer to the way point data table at the beginning of the discussion of each run. The acceleration and acceleration rate commands at the way points are described in the text that follows. The resulting horizontal and vertical velocities and altitude or other pertinent variables at the way point times are given in the tables. For runs where the trajectory includes east-west excursions in addition to north-south, a plot of the ground track is shown in addition to a plot of altitude against time.

#### SUMMARY OF DATA RUNS

The following summary of data runs correlates the figure numbers with a particular trajectory:

1. Run 1 (table 1). Conventional flight accelerating trajectory from 400 ft/sec to 920 ft/sec with 5,600 ft of altitude gain and turns of 2 and 3 g. Curves of 70 variables are presented in 10 pages of figure 6.

2. Run 2 (table 2). Conventional flight decelerating trajectory from 800 ft/sec to 530 ft/sec with 2,200 ft of altitude loss and a 3-g turn. Curves of 52 variables are presented in 7 pages of figure 7.

3. Run 3 (table 3). Conventional flight at 500 ft/sec with initial path offsets and steady winds. Curves of 22 variables are presented in 3 pages of figure 8.

4. Run 4 (table 4). Transition from conventional flight at 180 ft/sec to hover in a vertical attitude at constant altitude. Curves of 27 variables are presented in 4 pages of figure 9.

5. Run 5 (table 5). Transition from hover in a vertical attitude to conventional flight at 530 ft/sec with an altitude gain of 3,700 ft. Curves of 19 variables are presented in 3 pages of figure 10.

6. Run 6 (table 6). Tail sitter simple maneuvering in a vertical attitude along the north and vertical axes with roll about the vertical. Curves of 45 variables are presented in 5 pages of figure 11.

7. Run 7 (table 7). Tail sitter complex maneuvering in a vertical attitude along each individual axis with roll about the vertical, then simultaneous maneuvering about all axes. Curves of 39 variables are presented in 5 pages of figure 12.

8. Run 8 (table 8). Tail sitter response to path offsets and steady winds. Curves of 22 variables are presented in 4 pages of figure 13.

DATA FOR RUN 1

TABLE 1.- WAY POINT TABLE FOR RUN 1

Way point, WP	Time	Trajectory desired			Next segment commands
		Velocity		Altitude	
		Horizontal	Vertical		
1	0	400	0	1000	Constant speed, level flight
2	5	400	0	1000	Horizontal path acceleration
3	23	570	0	1000	Constant speed
4	25	570	0	1000	2 g left turn
5	41	570	0	1000	Constant speed
6	45	570	0	1000	Accelerating climb
7	65	570	108	1985	Constant speed climb
8	69	570	108	2410	3 g right turn and constant speed climb
9	80	570	108	3680	Constant speed climb
10	84	570	108	4030	Path acceleration and constant speed climb
11	97	680	108	5444	Path acceleration and decelerating climb
12	117	800	0	6424	Path acceleration level flight
13	123	860	0	6424	Constant speed
14	140	860	0	6424	End of run 1

Run 1. Conventional Flight Trajectory

Data for the first run is presented in figure 6. The horizontal and vertical trajectories with way point numbers are shown in figure 6(a). The run starts in straight and level flight at an altitude of 1,000 ft and a velocity of 400 ft/sec north (WP1). After 5 sec (WP2), a path acceleration rate command of approximately 0.1 g/sec is applied as shown by the dashed curve in plot 1 of figure 6(b). This command is resolved through the flightpath-heading angle so that it always generates an acceleration rate along the instantaneous direction of the commanded flightpath, which is initially north. After 4 sec this input is removed and the commanded path acceleration shown in the solid line remains at 0.4 g until it is reduced to zero by 23 sec (WP3). The second plot in figure 6(b) shows the commanded centripetal acceleration rate for a left turn in the dashed curve and the resulting commanded

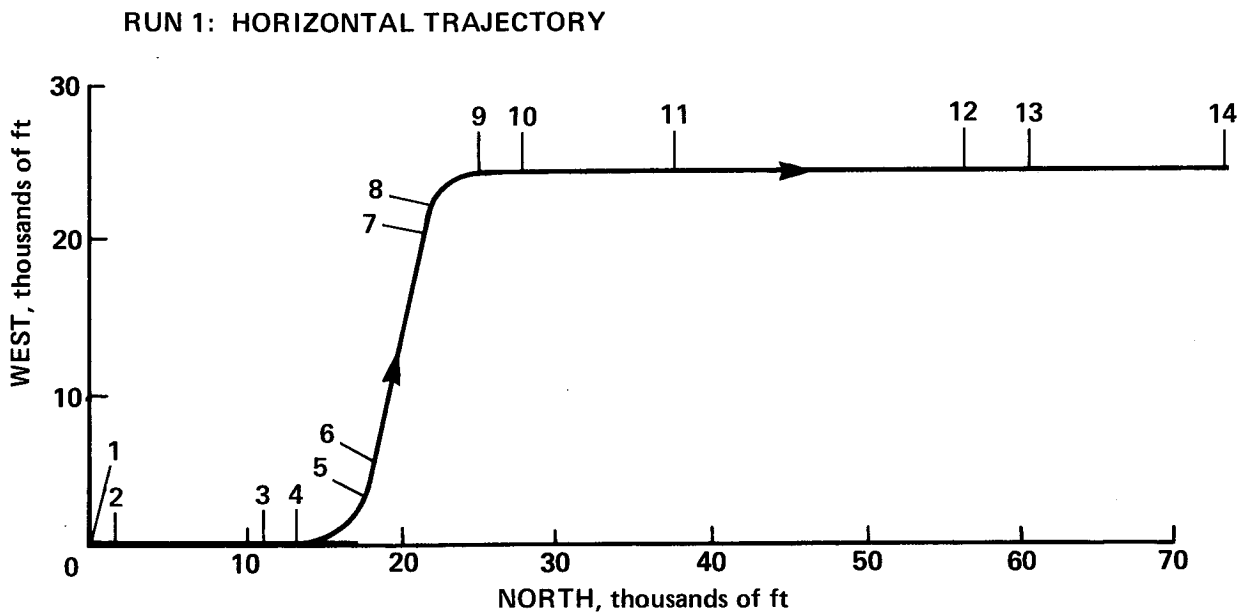
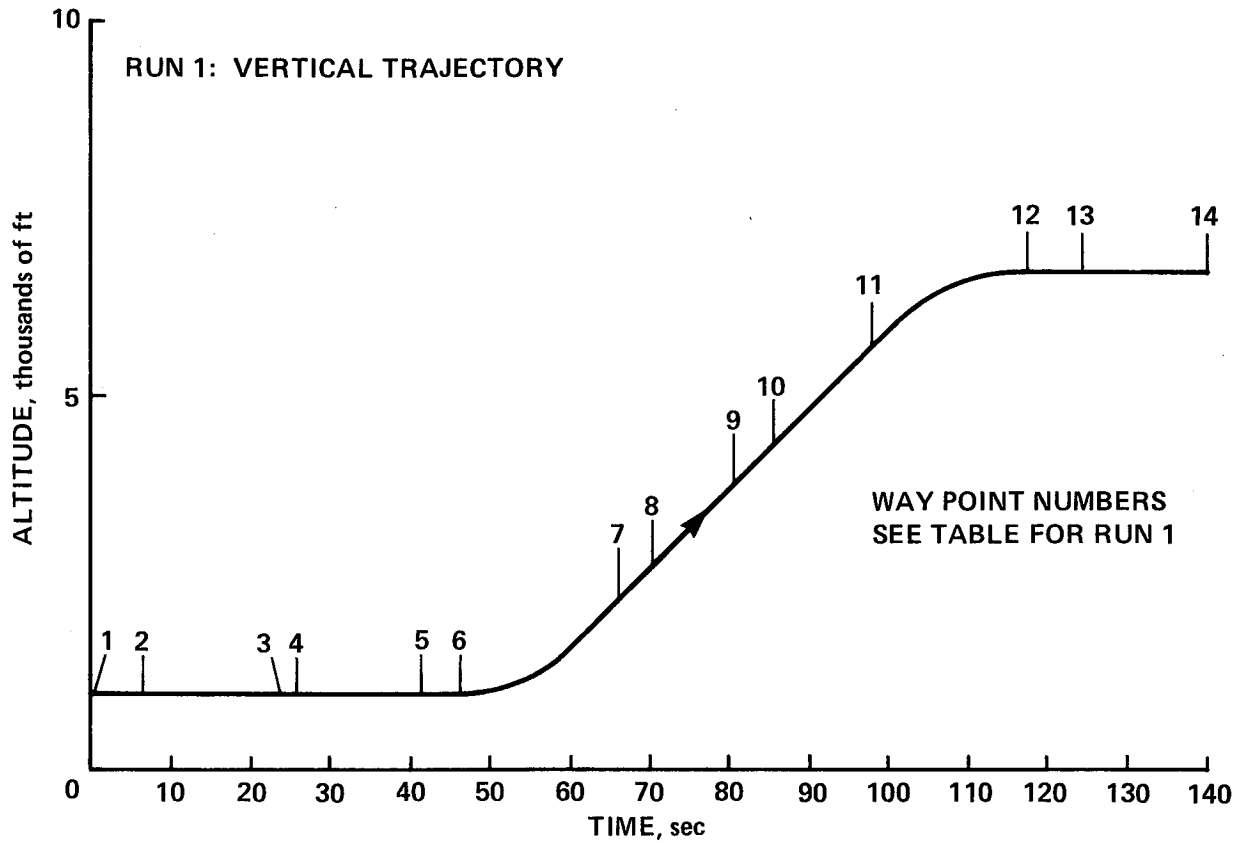


Figure 6(a).- Run 1. Conventional flight, accelerating trajectory.

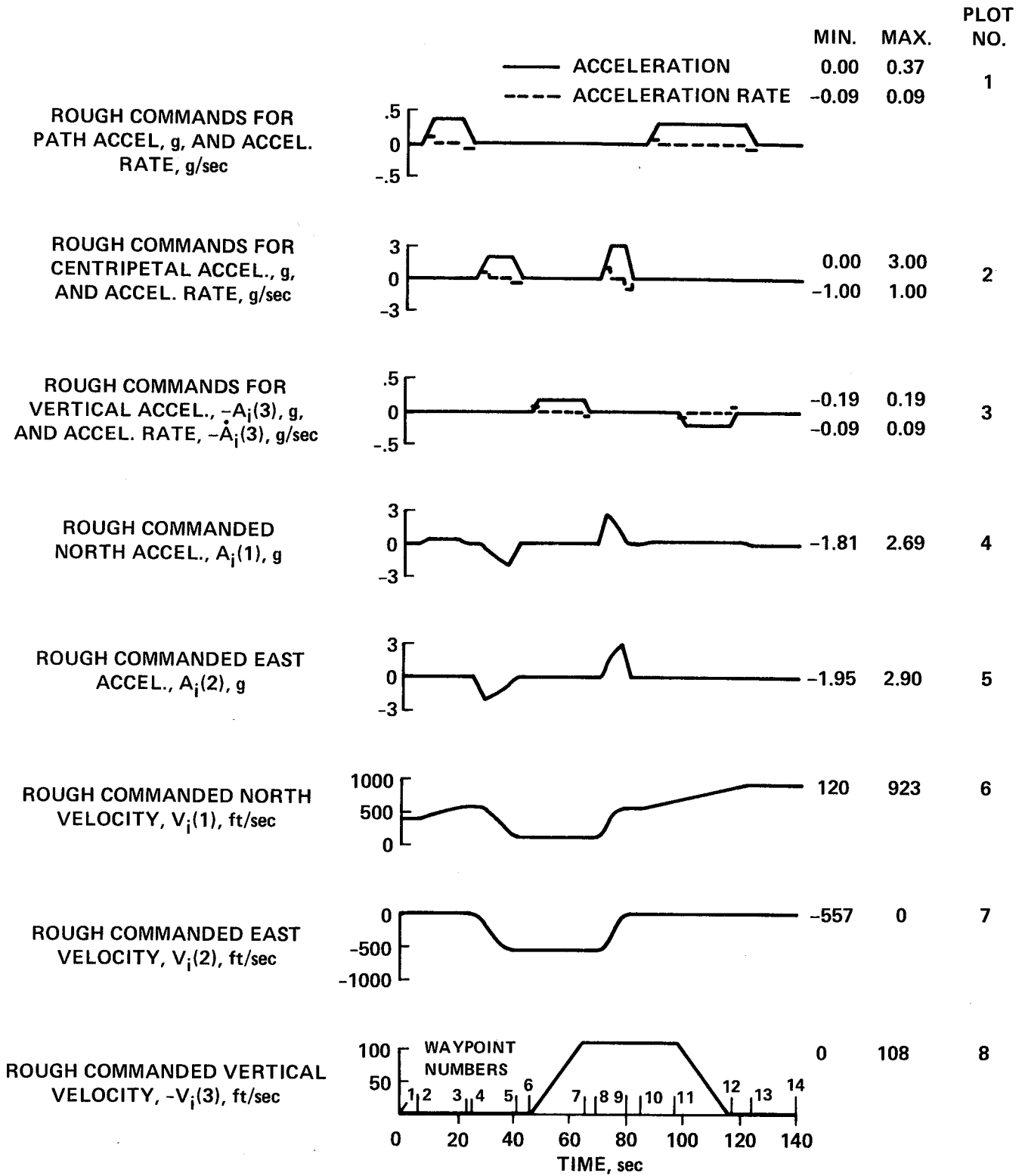


Figure 6(b).- Run 1. Continued.

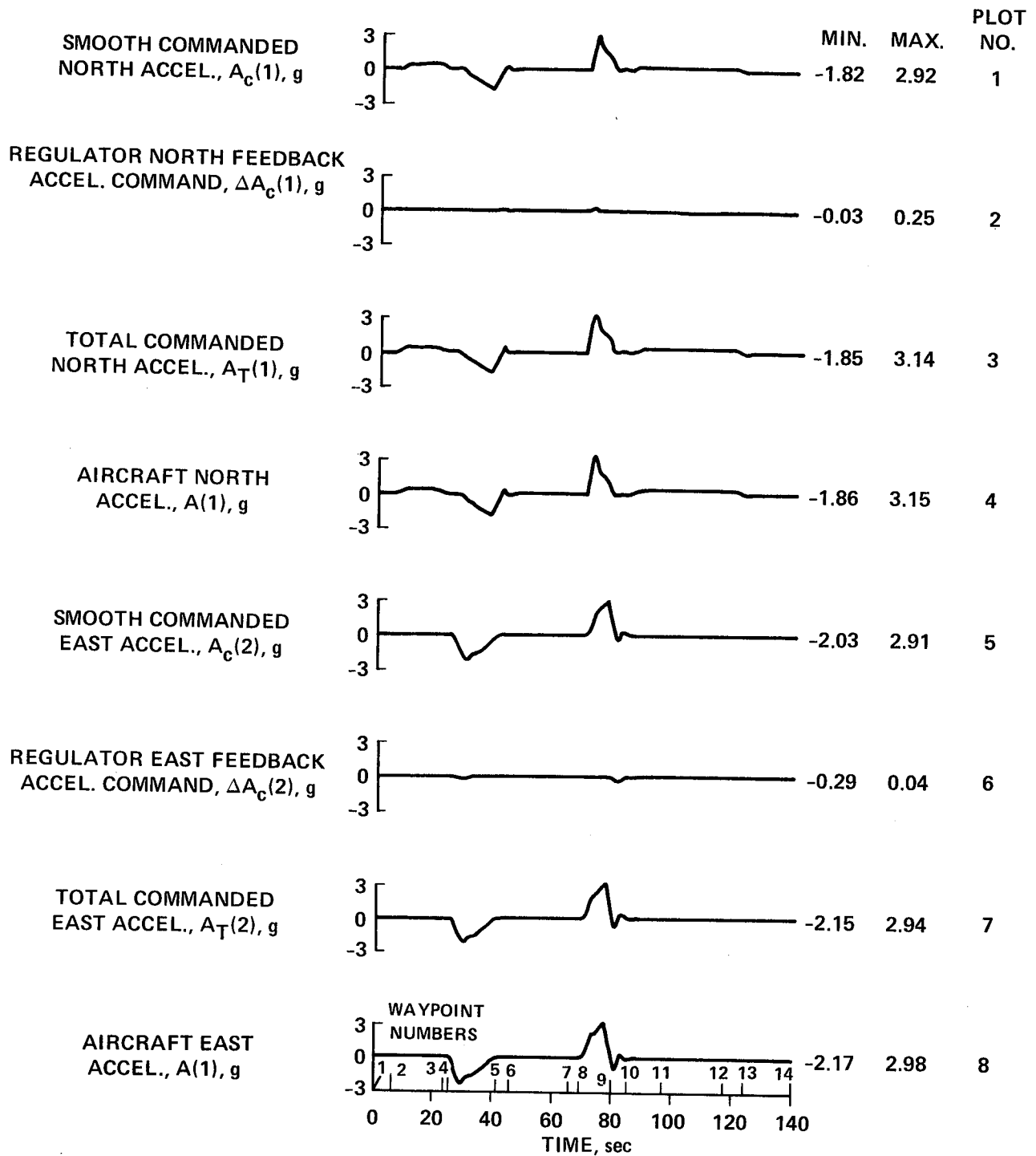


Figure 6(c).- Run 1. Continued.

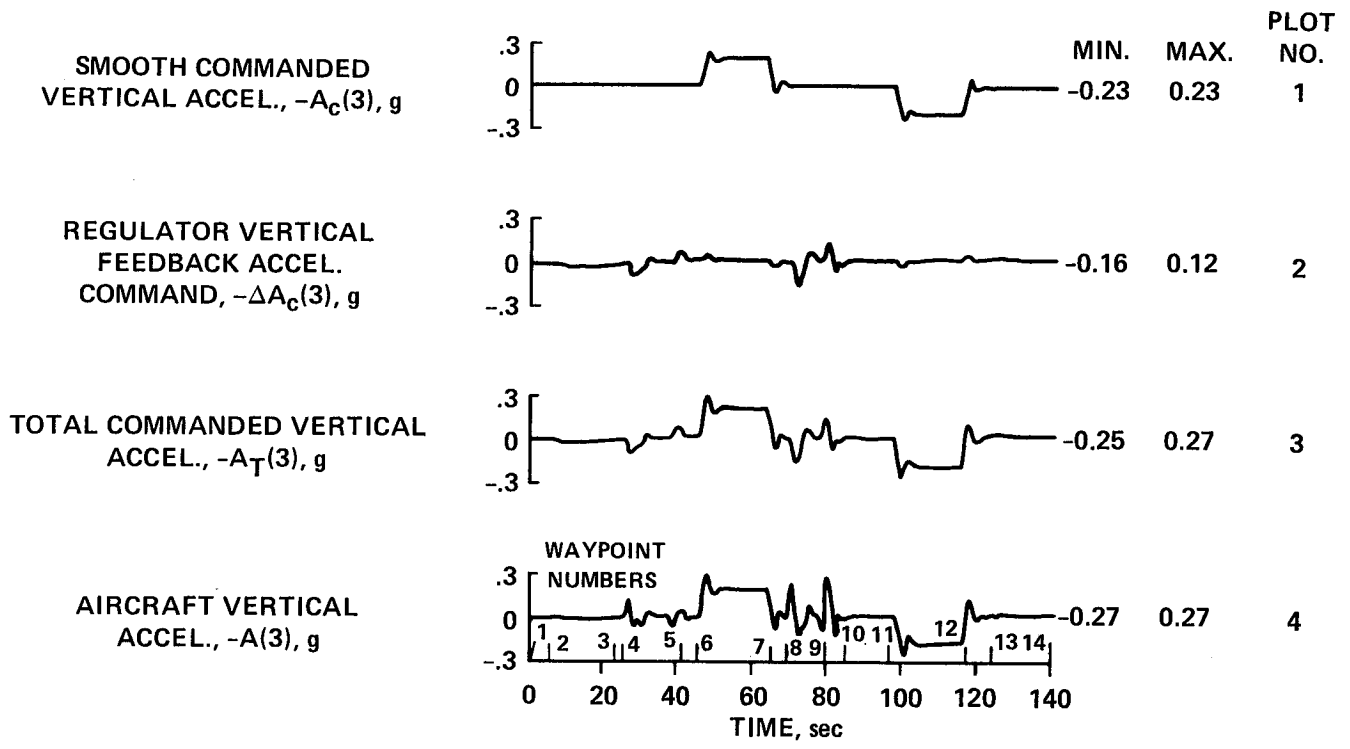


Figure 6(d).- Run 1. Continued.

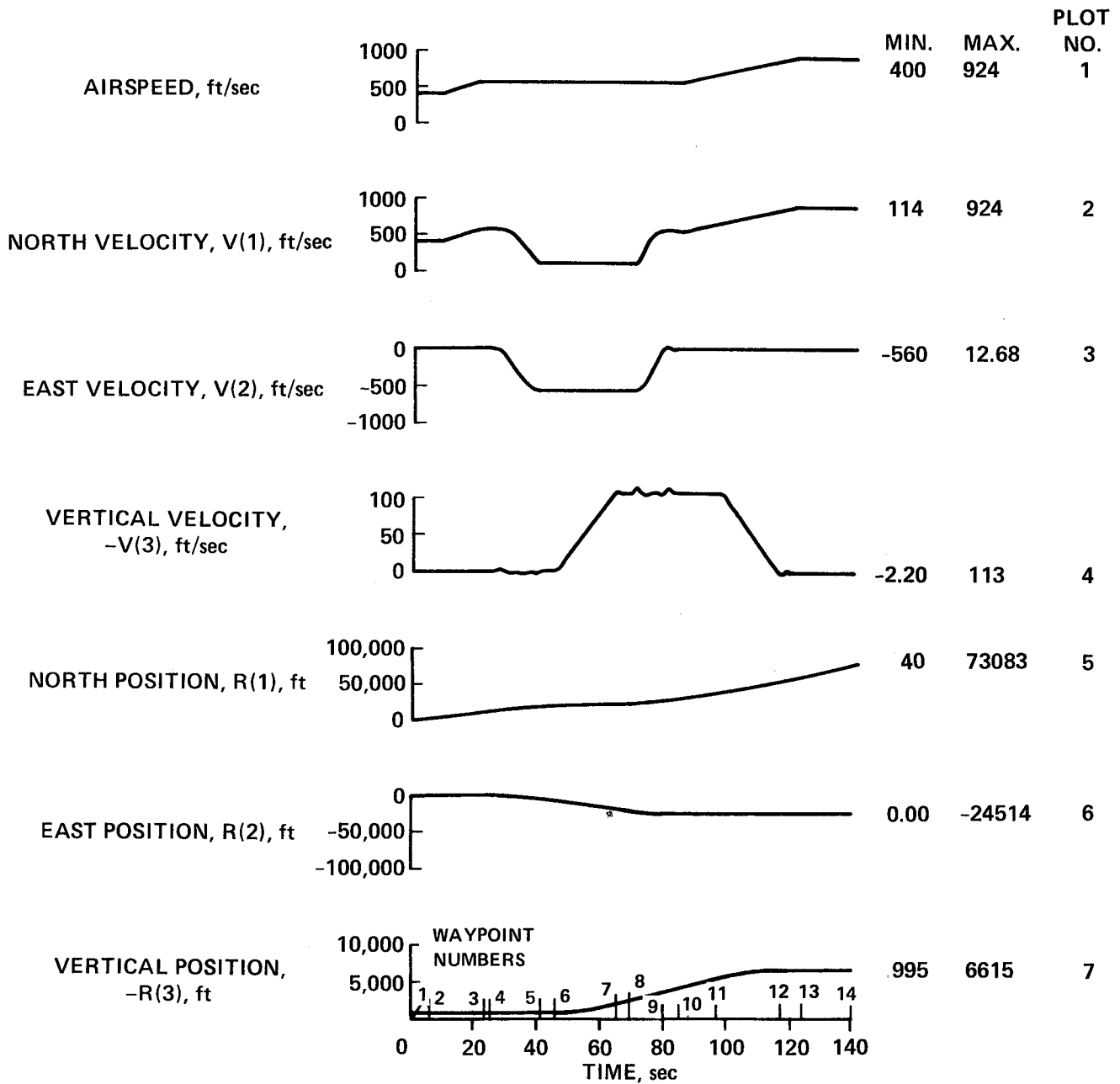


Figure 6(e).- Run 1. Continued.

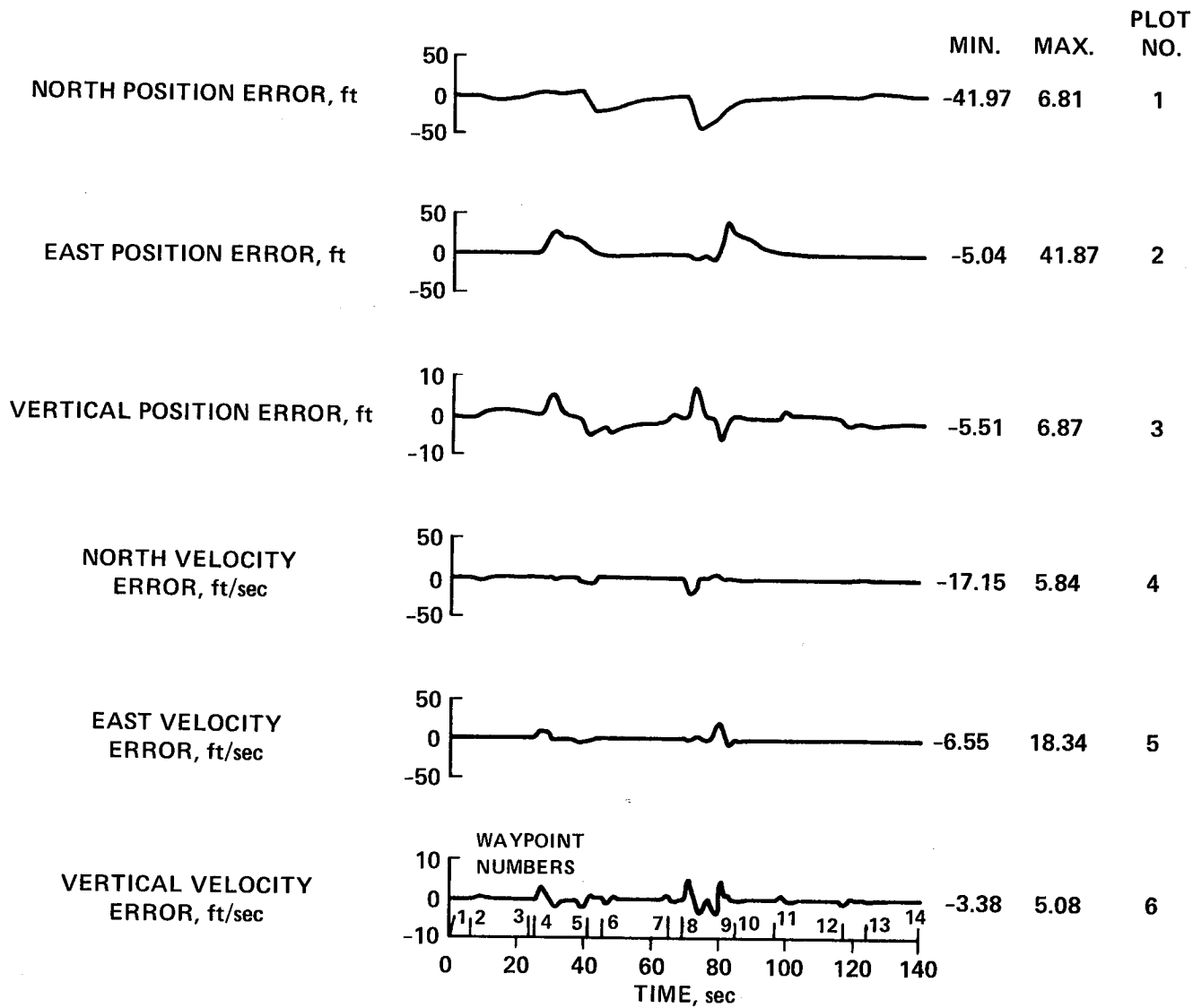


Figure 6(f).- Run 1. Continued.

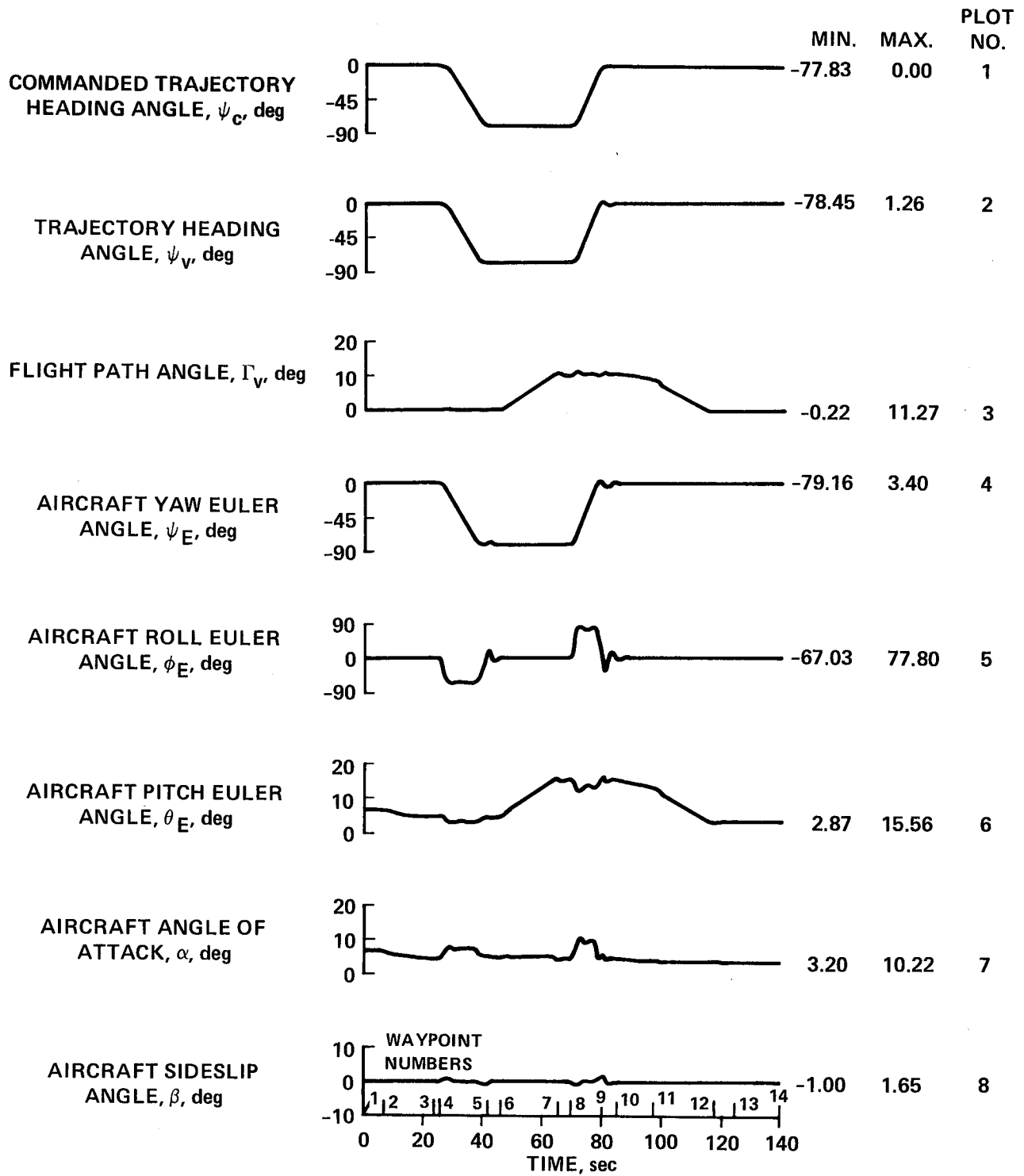


Figure 6(g).- Run 1. Continued.

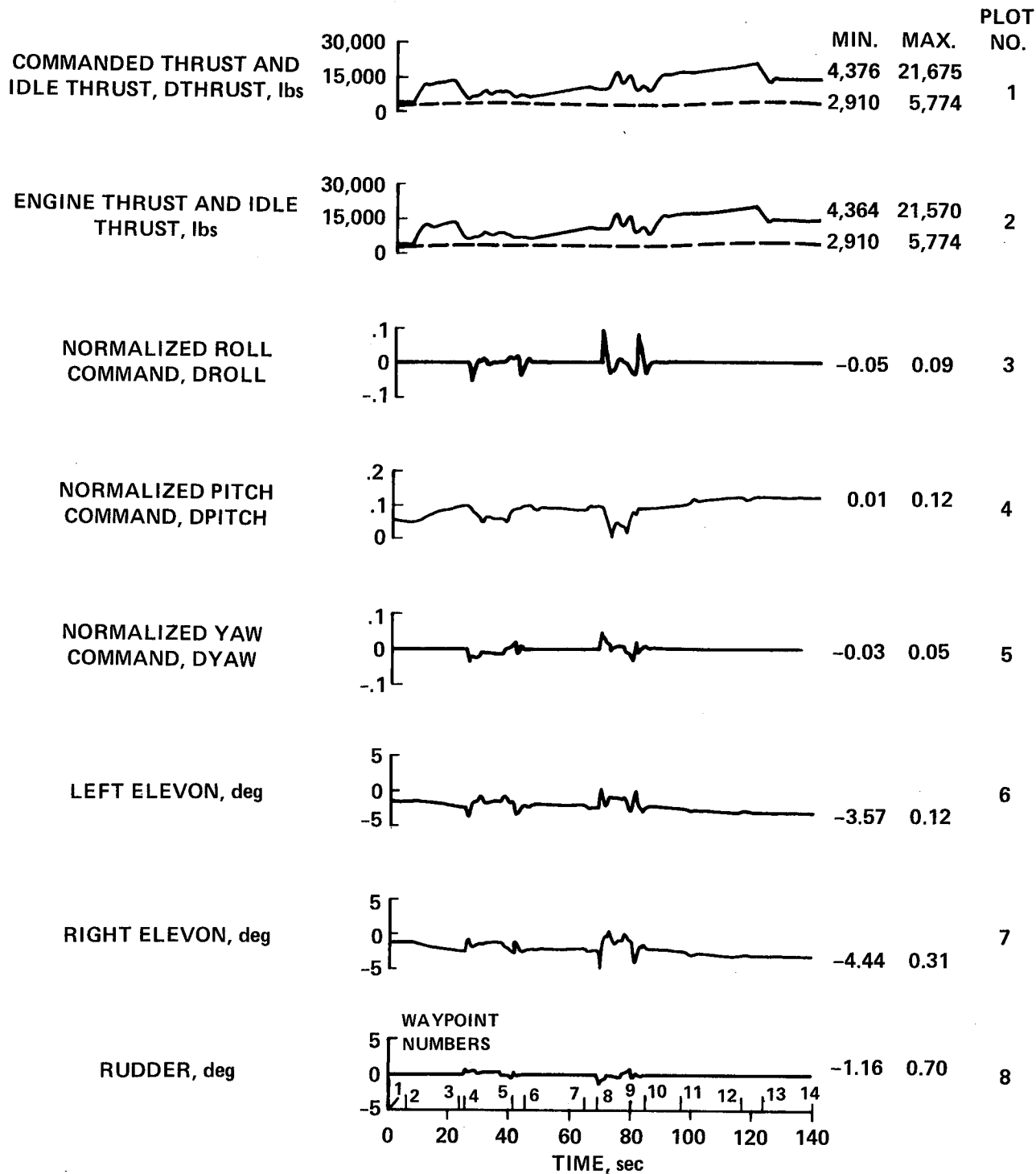


Figure 6(h).- Run 1. Continued.

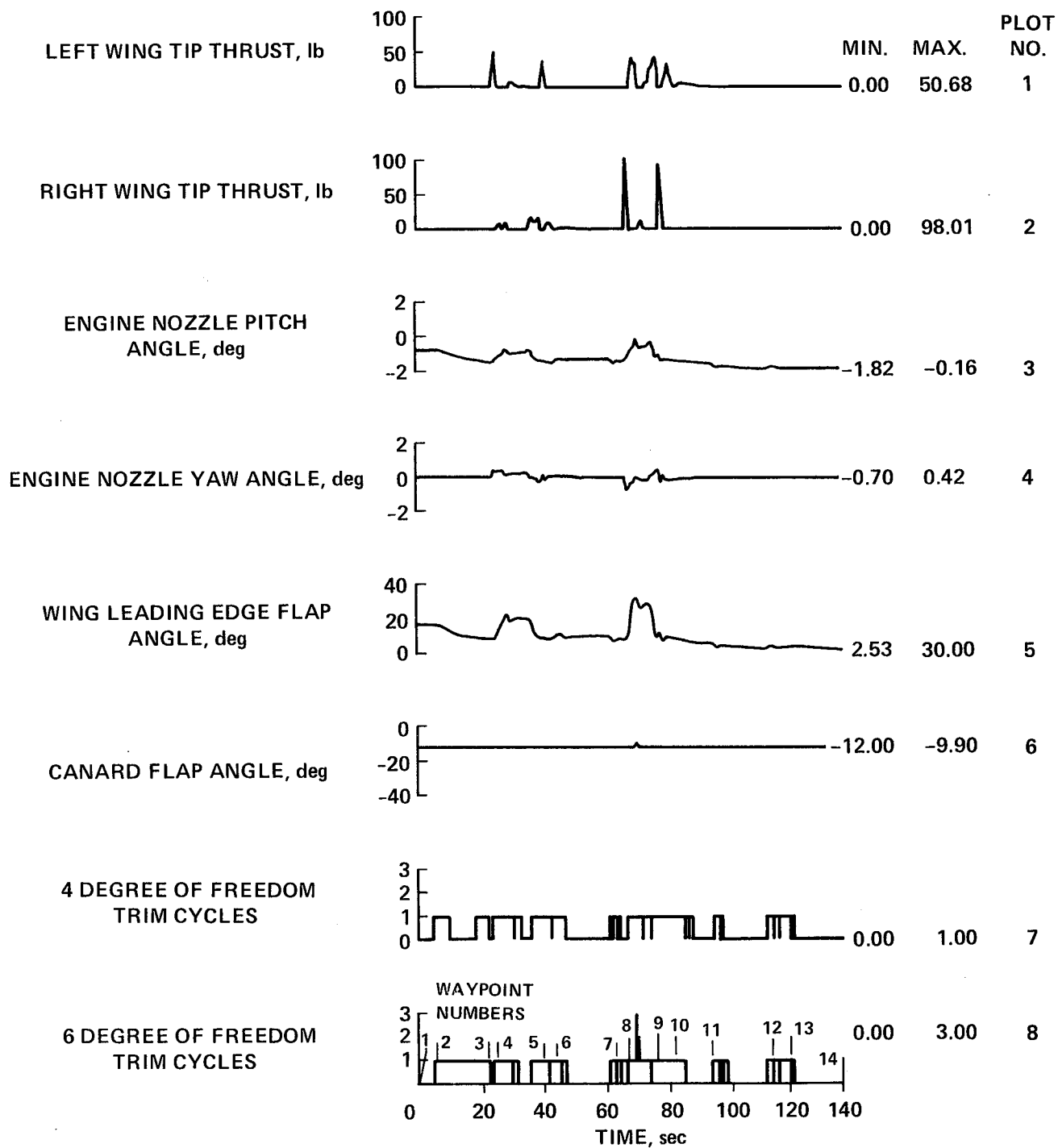


Figure 6(i).- Run 1. Continued.

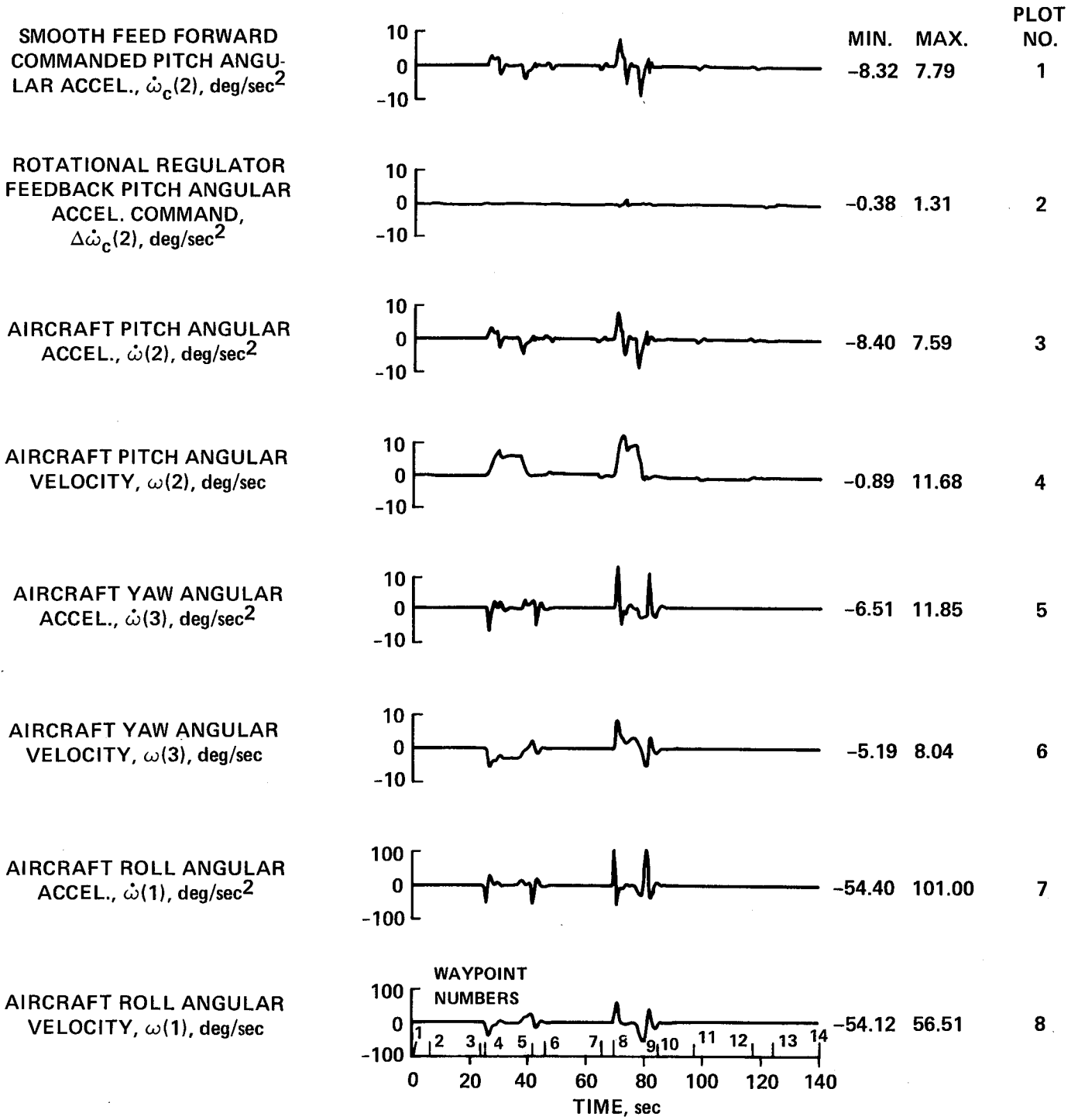


Figure 6(j).- Run 1. Concluded.

centripetal acceleration in the solid curve. This acceleration command is always perpendicular to the commanded velocity vector in a horizontal plane. Acceleration is always input as a positive quantity and the turn sense is determined by a left or right specification. The command for a left turn with an acceleration rate of 0.5 g/sec for 4 sec in plot 2 results in a 2-g left turn which is terminated after the heading angle reaches approximately  $78^\circ$  at 41 sec (WP5). The third plot in figure 6(b) shows the vertical acceleration rate command in the dashed line and the resulting vertical acceleration command in the solid line. The vertical acceleration rate command of 0.1 g/sec at 45 sec (WP6) produces a 0.2 g vertical acceleration command at 47 sec which is maintained until it is reduced to zero at 65 sec (WP7). This command is in the inertial vertical direction. Examination of the remaining parts of the first three plots shows a commanded 3-g right turn at 69 sec (WP8), until the heading angle reaches almost zero degrees at 80 sec (WP9) followed at 84 sec (WP10), by a path acceleration command of 0.3 g until time reaches 123 sec (WP13). A vertical deceleration of 0.2 g is commanded at 97 sec (WP11) until vertical velocity is reduced to zero at 117 sec (WP12). Straight- and level-flight at constant velocity is then commanded until 140 sec (WP14). The remaining plots for this run display the response of the aircraft and its control system to the three primary input commands just described, which are shown as dashed lines in the first three plots.

This is essentially an acceleration control system so that attention will first be directed to the acceleration commands and responses in various parts of the system. The input commands just described were applied in instantaneous trajectory-axes coordinates. The control system first resolves these commands into the reference inertial-axis system (north, east, down) to give the rough acceleration commands in inertial axes. The resulting vertical command is the solid curve in the third plot, the north command is the fourth plot, and the east command is the fifth plot. These are the three components of the rough acceleration command vector,  $A_i$ , in figure 5. The shape of the north and east curves can be derived from the solid line curves of the first two plots of the figure by considering the effect of resolving the commands along, and perpendicular to, the path into north and east as the heading changes through almost  $90^\circ$ . These rough acceleration commands are then integrated to give the three rough velocity commands which are shown in the last three plots of the figure. They are the components of the vector,  $V_i$ , in figure 5. Figure 5 shows (1) that the translational command generator processes these rough input commands to give a smooth, executable feed-forward, acceleration-command vector,  $A_c$ , and (2) that the regulator provides an acceleration command,  $\Delta A_c$ , which is added to it, to yield the total acceleration command vector,  $A_T$ .

The first three plots of figure 6(c) show these acceleration command signals for the north channel, and the fourth plot shows the resulting aircraft acceleration. It will be noted that the closed-loop correction signal in the second plot is a small percentage of the feed-forward signal so that the total command is close to the smooth open-loop command. A most important criterion for evaluating the system performance is the fidelity with which the aircraft response follows the total command. This indicates how well the model inversion is performed. Although it has slightly more transient overshoot than the total command does, the aircraft

acceleration response is smooth and satisfactory. The minimum and maximum values for the total commanded and actual aircraft acceleration agree well as indicated by the numerical data displayed in the upper-right corner of each plot. A similar set of curves for the east channel is presented in the last four plots of figure 6(c) and the same comments generally apply.

The same acceleration data for the vertical channel is shown in figure 6(d). The vertical channel differs from the other two channels in that the acceleration values are much smaller, the rough input command shown as the solid line in the third plot of the prior figure 6(b) is already in the vertical axis so it does not have to be resolved, and the sign of the data is reversed so that vertical accelerations are shown positive-up. The closed-loop regulator signal, plot 2, figure 6(d), is more significant than for the other channels and shows cross-coupling effects when large accelerations are applied to the other channels. This effect is evident in the aircraft response of the fourth plot which, however, is still seen to be satisfactory when the magnitudes of the accelerations are considered.

The curves of figure 6(e) show the aircraft velocity and displacement responses in the three inertial axes as well as the airspeed in the first plot which increases from 400 to 925 ft/sec. The inertial axes responses should again be interpreted by correlating them with the change of heading angle.

The curves of figure 6(f) display the velocity and position errors between the smooth commanded values,  $V_c$  and  $R_c$ , in figure 5, and the actual aircraft responses,  $R$  and  $V$ . It will be seen that the vertical channel errors are small. The horizontal channels develop larger errors in response to the abrupt commands to execute the 2-g and 3-g turns. If these trajectory transients were considered excessive, a more gradual turn-entry command could be employed.

Angular data for the trajectory is presented in figure 6(g). The first plot is the trajectory heading-command angle generated by the effect of the centripetal acceleration commands. The second and third plots are the actual trajectory heading angle and flightpath angle; both of these plots are computed from the aircraft velocity vector components. The next three curves are the actual aircraft Euler angles between the body axes and the inertial reference axes. The roll angle during the turns, shown in the fifth plot, reaches approximately  $80^\circ$ . The aircraft angle of attack and sideslip are shown in the last two curves. The angle of attack increases significantly in the steep turns but remains nearly constant during the straight portions of the trajectory when the aircraft attitude is equal to the flightpath angle plus the angle of attack.

The aircraft command and control variables are shown in figure 6(h). The solid-line curve of the first plot is the thrust command which is sent to the aircraft from the four-degree-of-freedom trim in figure 5. It is the first perturbation variable for that trim. The dotted curve is the engine-idle, thrust-level limit. Commands may go below this value, but the total generated thrust may not. The solid curve in the second plot is actual effective engine thrust which is seen to follow the command closely. The total available thrust is approximately 32,000 lb, whereas a nominal aircraft weight is 16,400 lb. The next three plots are

the normalized roll, pitch, and yaw commands sent to the aircraft control system. They are the remaining perturbation variables from the four-degree-of-freedom trim. They are scaled by the control system and are sent in various combinations to the aircraft control surface and nozzle actuators. The right and left elevons receive the negative scaled sum and difference of the pitch and roll commands and the rudder is a scaled negative copy of the yaw command. The control surface deflections for this run are small when compared to the elevon limits of  $\pm 60^\circ$  and the rudder limits of  $\pm 25^\circ$ .

The first two plots of figure 6(i) display the thrust that is generated by the left- and right-wing-tip, engine-bleed air jets which are located on the upper wing surfaces. They are seen to be a scaled version of the roll command, but because they cannot generate negative thrust, the left wing jet responds to negative roll commands and the right wing jet responds to positive roll commands. The torque produced by these jets depends on the fact that they are at a lever arm of 13 ft from the aircraft centerline, and are 11 ft behind the aircraft center of gravity. The third plot in figure 6(i) is the engine-nozzle, pitch-angle deflection which is a negative-scaled version of the pitch command. The fourth plot is the engine-nozzle, yaw-angle deflection and is a negative-scaled version of the yaw command. These nozzle angles are a small percentage of the total available nozzle angles of  $\pm 15^\circ$ .

The wing leading-edge flap and the trailing-edge canard flap deflections are shown on the fifth and sixth plots, respectively. They are deflected as a linear function of the angle of attack and are limited about a nominal angle of attack. The wing flap goes from  $0^\circ$  to  $30^\circ$  as the angle of attack goes from  $2.6^\circ$  to  $9.8^\circ$ . The canard flap goes from  $-12^\circ$  to  $25^\circ$  as the angle of attack goes from  $9.8^\circ$  to  $16.5^\circ$ . The last two curves in this figure are the number of trim cycles required for the four-degree-of-freedom trim and the six-degree-of-freedom trim. For this trajectory, the four-degree-of-freedom trim never requires more than one trim cycle and does not require any trim cycles for approximately half the run. It will be recalled that for each trim cycle, the previous control variables are first used with the aircraft model to determine the errors between commanded acceleration and the acceleration that would be generated by those controls. If the errors are less than the tolerance values, a trim cycle is not initiated; however, the new errors are then used with the previous Jacobian matrix to determine new control variables so that the controls may be adjusted at each computer cycle time even though no trim perturbation cycle is needed. The six-degree-of-freedom trim requires two, and even three, trim cycles during the entry into the 3-g right turn at way point 8. The trim cycle number plots reflect the severity of the commands, the effect of system nonlinearities, and indicate the required computer capacity and speed.

Although this control scheme is computationally intensive, it is believed that future airborne digital computers will have adequate speed and capacity so that the required calculations can be easily performed even when several trim cycles are required. This simulation, which included calculation and collection of a considerable amount of data, was carried out on a VAX model 11/750 computer and required a

computational time of approximately three times simulated run time, i.e., 30 sec of computer time for a 10-sec trajectory.

The angular acceleration data of figure 6(j) is analogous to the linear acceleration variables shown in figure 6(c), etc. The pitch channel data is shown in detail in the first four plots. The smooth, open-loop pitch-acceleration command in the first plot ( $\dot{\omega}_c(2)$  in fig. 5) shows major transient activity at entry and exit for the two turns. The closed-loop feedback correction,  $\Delta\dot{\omega}_c(2)$ , in the second plot is small and the actual aircraft pitch acceleration,  $\dot{\omega}(2)$ , in the third plot can be seen to closely follow the total command,  $\dot{\omega}_T(2)$  (the sum of the first two plots but not shown explicitly). The aircraft pitch-angular velocity,  $\omega(2)$ , is shown in the fourth plot. The next two plots show the angular acceleration and angular velocity about the aircraft yaw axis, and again the aircraft exhibits transient behavior during the turns. The last two plots on this figure show the aircraft roll-axis, angular acceleration and angular velocity, and as much higher values are reached in the turns these values are plotted to a scale ten times that of the previous variables.

These plots for the system variables show a generally satisfactory operation of the control system over this trajectory and display the transient behavior of a number of internal system variables. Similar time-history plots will be presented for the other test trajectories, but with fewer plots to show only the most important trajectory variables and certain other quantities of particular interest for the specific trajectory.

DATA FOR RUN 2

TABLE 2.- WAY POINT TABLE FOR RUN 2

Way point, WP	Time	Trajectory commands			Next segment commands
		Velocity		Altitude	
		Horizontal	Vertical		
1	0	800	0	5000	Constant speed
2	5	800	0	5000	Horizontal path deceleration
3	20	715	0	5000	3 g right turn and path deceleration
4	35	640	0	5000	Path deceleration
5	38	620	0	5000	Constant speed
6	42	620	0	5000	Accelerating descent
7	58	620	75	4400	Constant speed descent
8	70	620	75	3200	Decelerating descent
9	86	620	0	2816	Constant speed level
10	90	620	0	2816	Path deceleration
11	140	565	0	2816	End of run 2

Run 2. Conventional Flight Trajectory

Data for the second run is presented in figure 7. The horizontal and vertical trajectories with way point numbers are shown in figure 7(a). This is a decelerating descending run that starts at an altitude of 5000 ft and a velocity of 800 ft/sec north (WP1). After 5 sec (WP2), a path-deceleration rate command of approximately 0.1 g/sec is given for 2 sec (fig. 7(b) plot 1), and the resulting deceleration of 0.2 g is maintained until it is reduced to zero at 35 sec (WP4) when the velocity has been reduced to 620 ft/sec. This velocity is held until another deceleration rate command at 90 sec (WP10) gives a deceleration of 0.1 g for the remainder of the trajectory. The second plot shows the centripetal acceleration commands for a right turn of approximately 82°. A descending vertical acceleration rate at 42 sec (WP6) shown as the dashed curve in the third plot gives a downward acceleration command of 0.2 g until 58 sec (WP7). The resulting descent velocity of 75 ft/sec is held until 70 sec (WP8), followed by an upward acceleration which brings the commanded vertical velocity to zero at 86 sec (WP9).

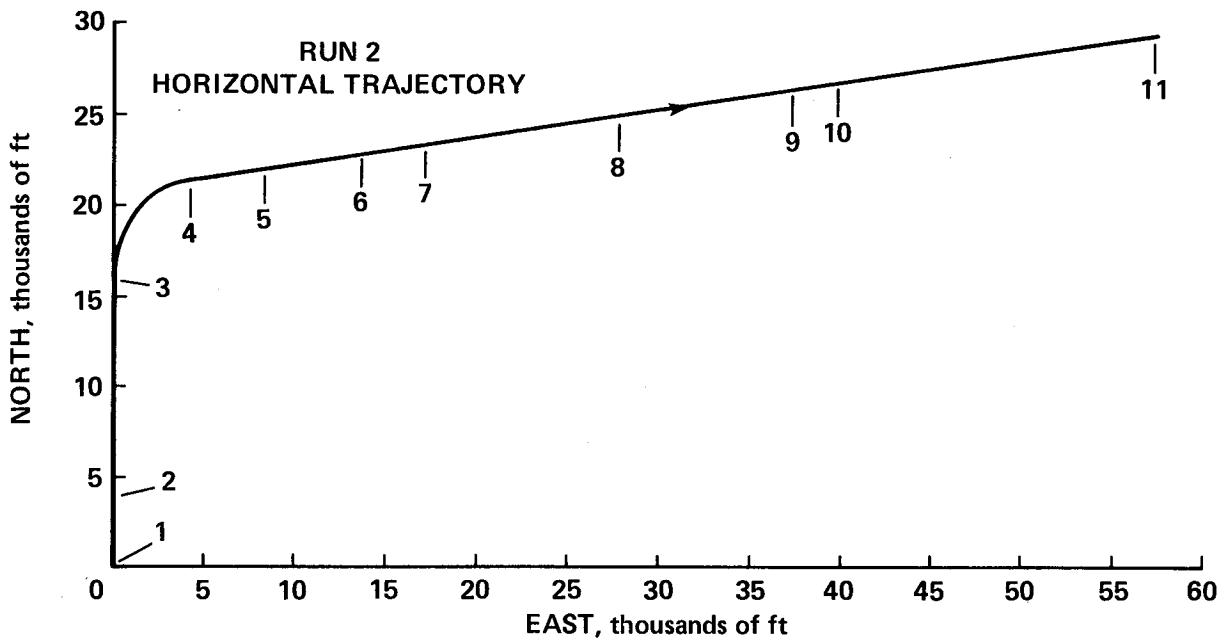
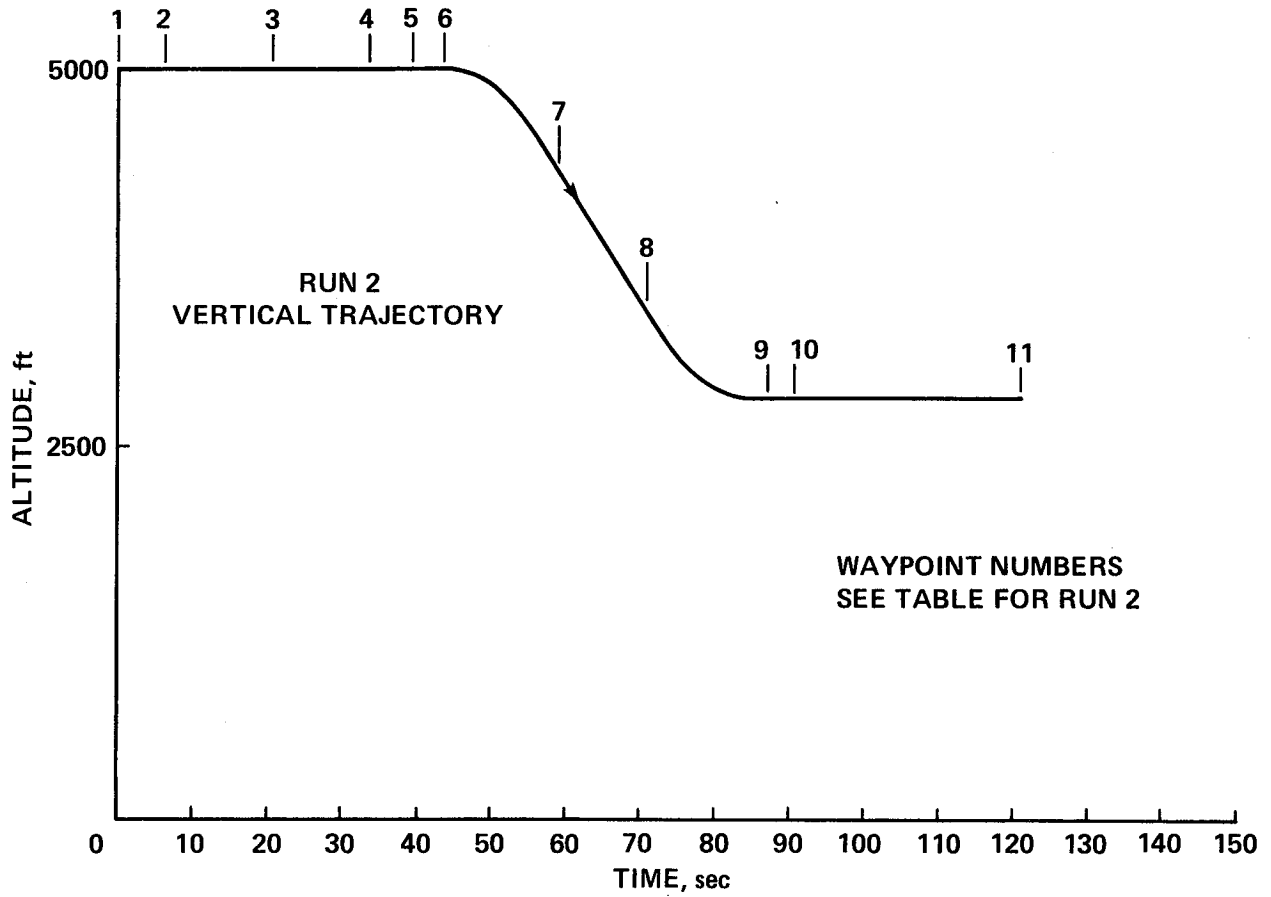


Figure 7(a).- Run 2. Conventional flight, decelerating trajectory.

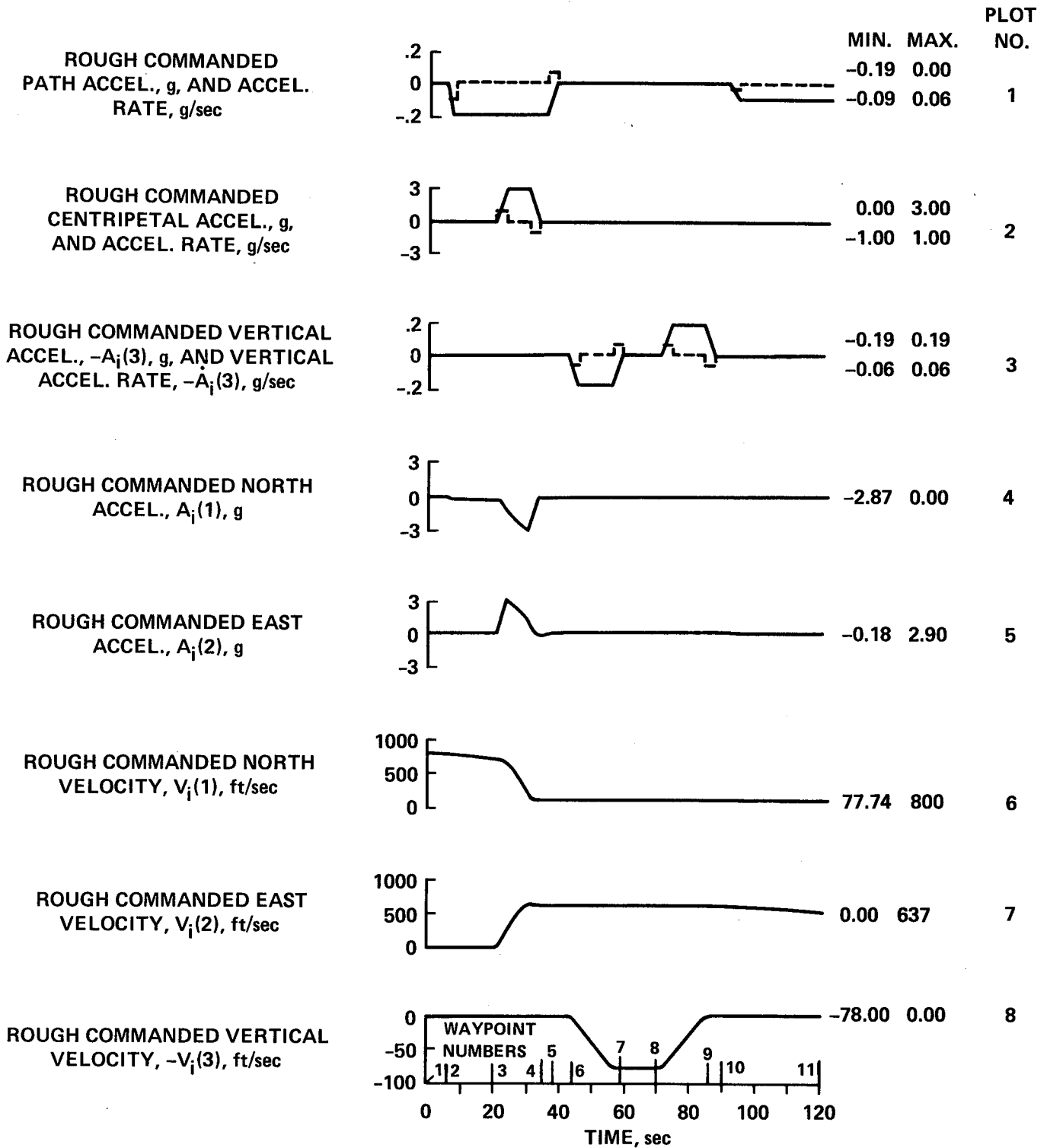


Figure 7(b).- Run 2. Continued.

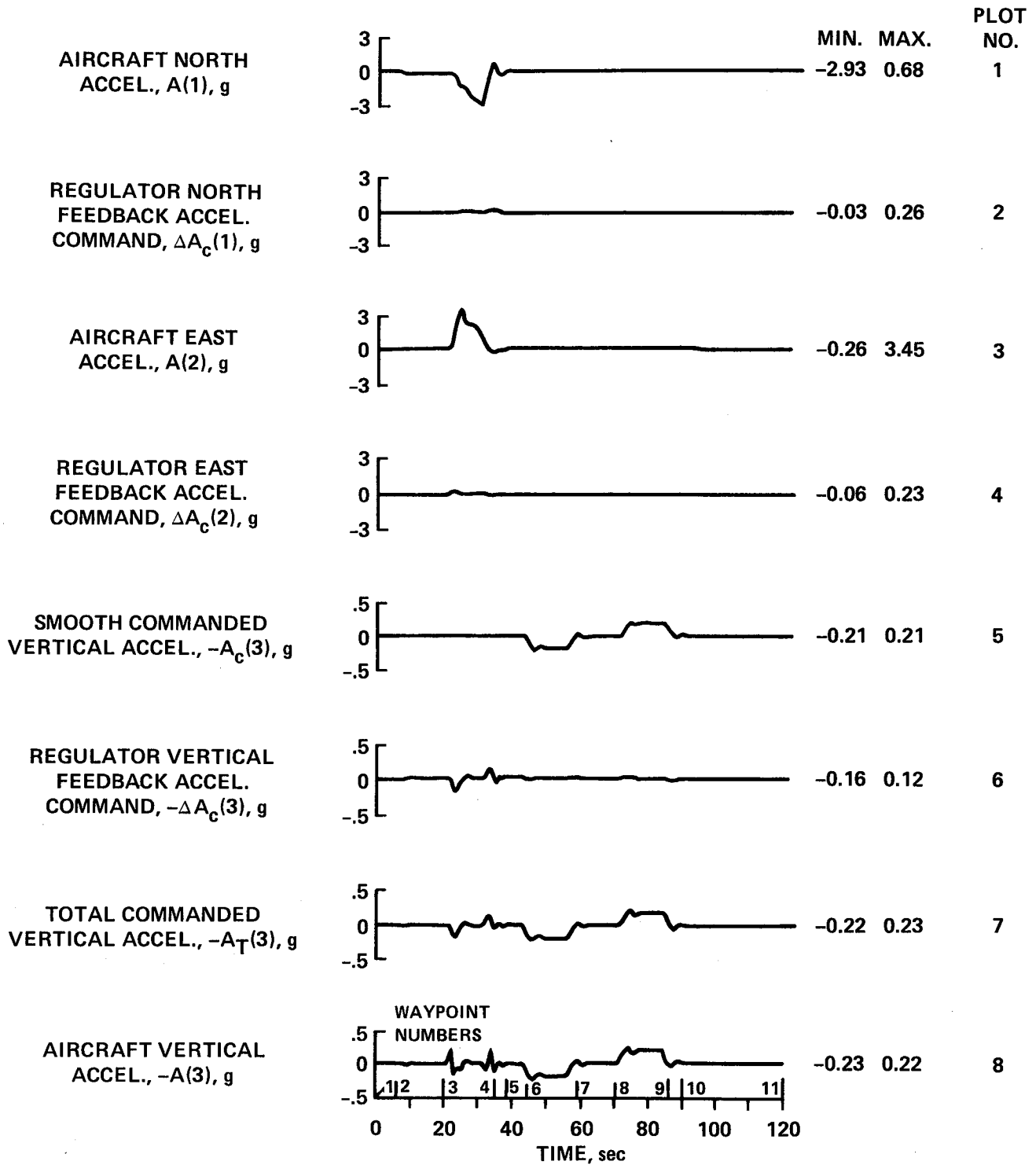


Figure 7(c).- Run 2. Continued.

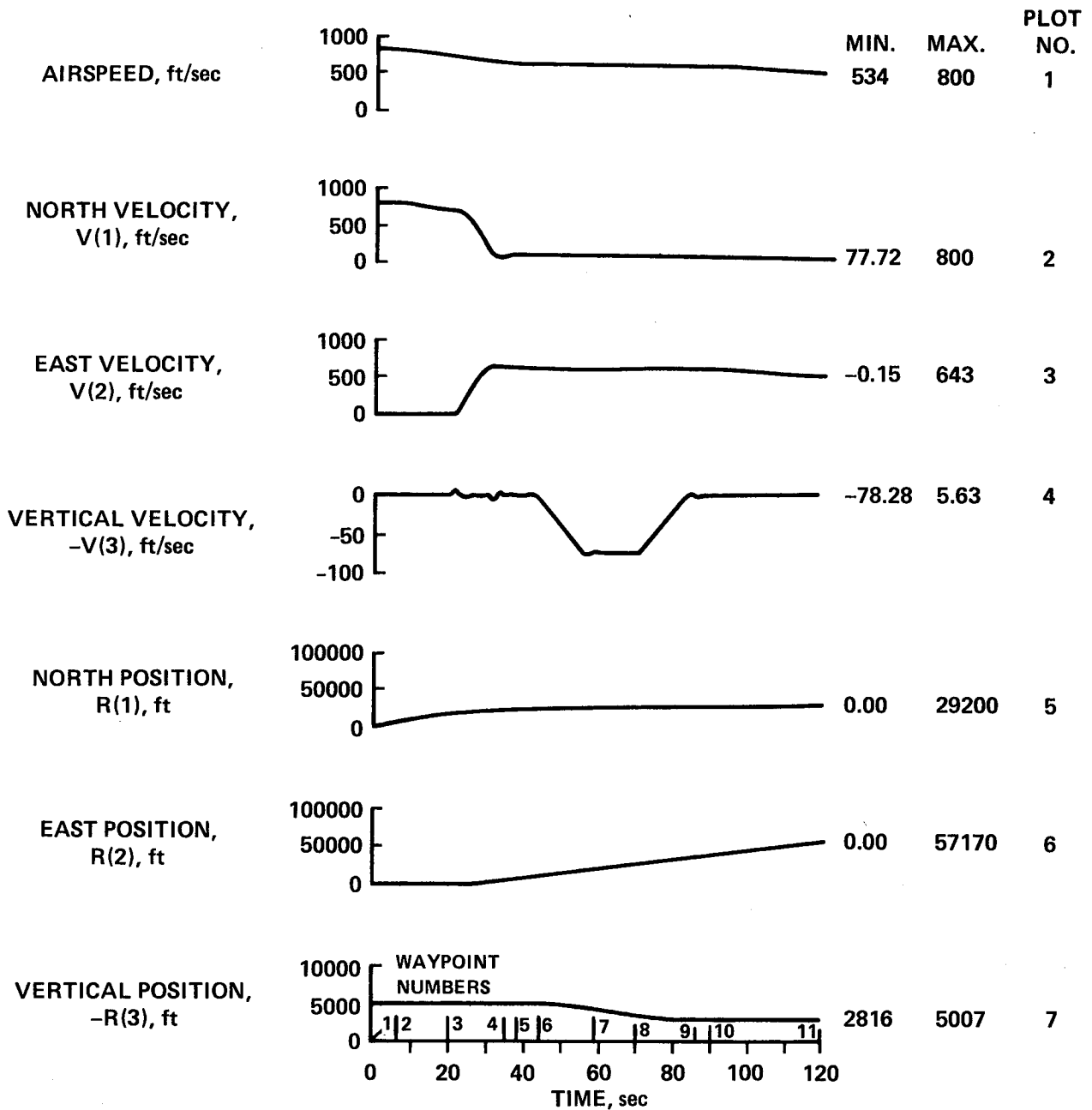


Figure 7(d).- Run 2. Continued.

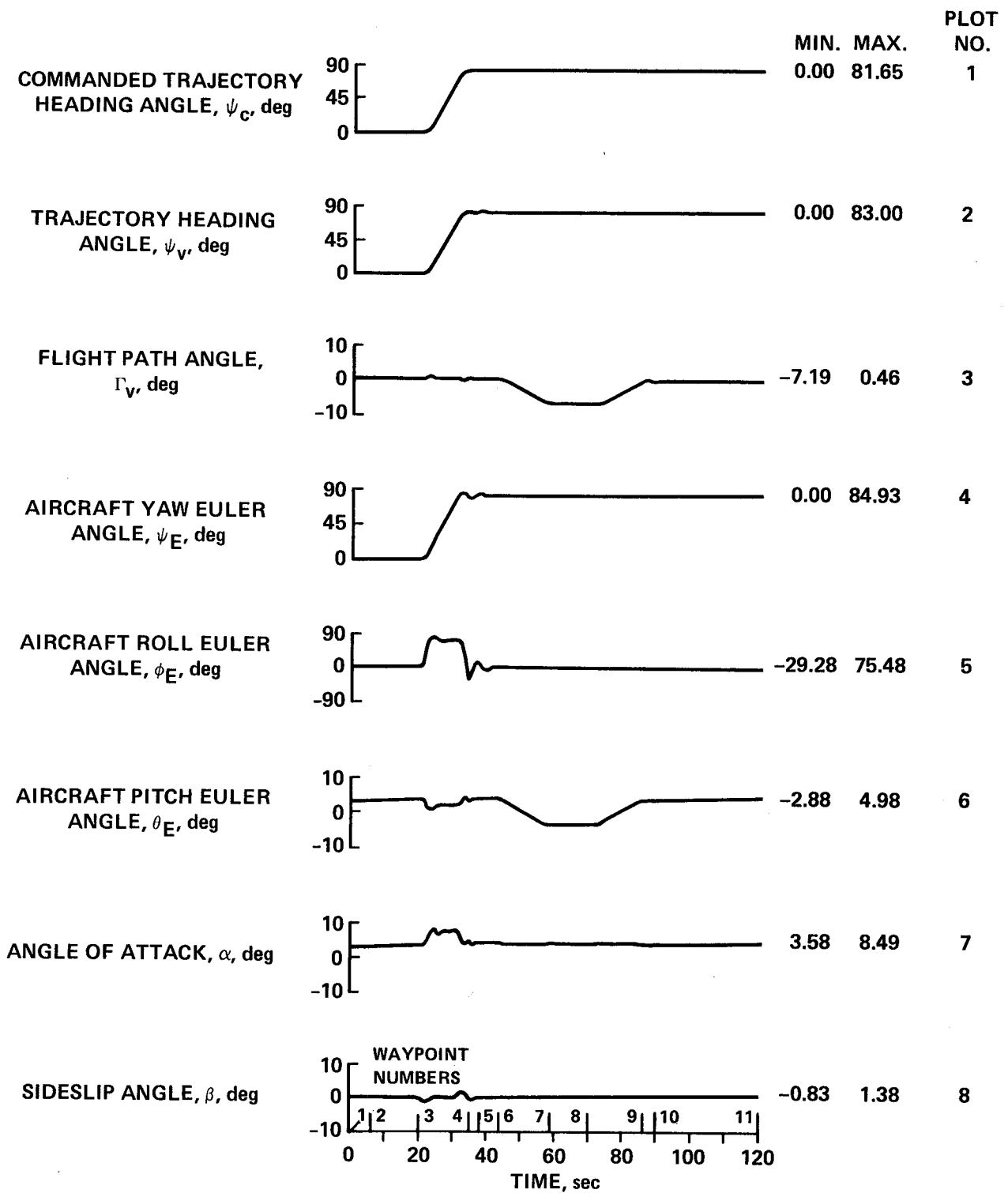


Figure 7(e).- Run 2. Continued.

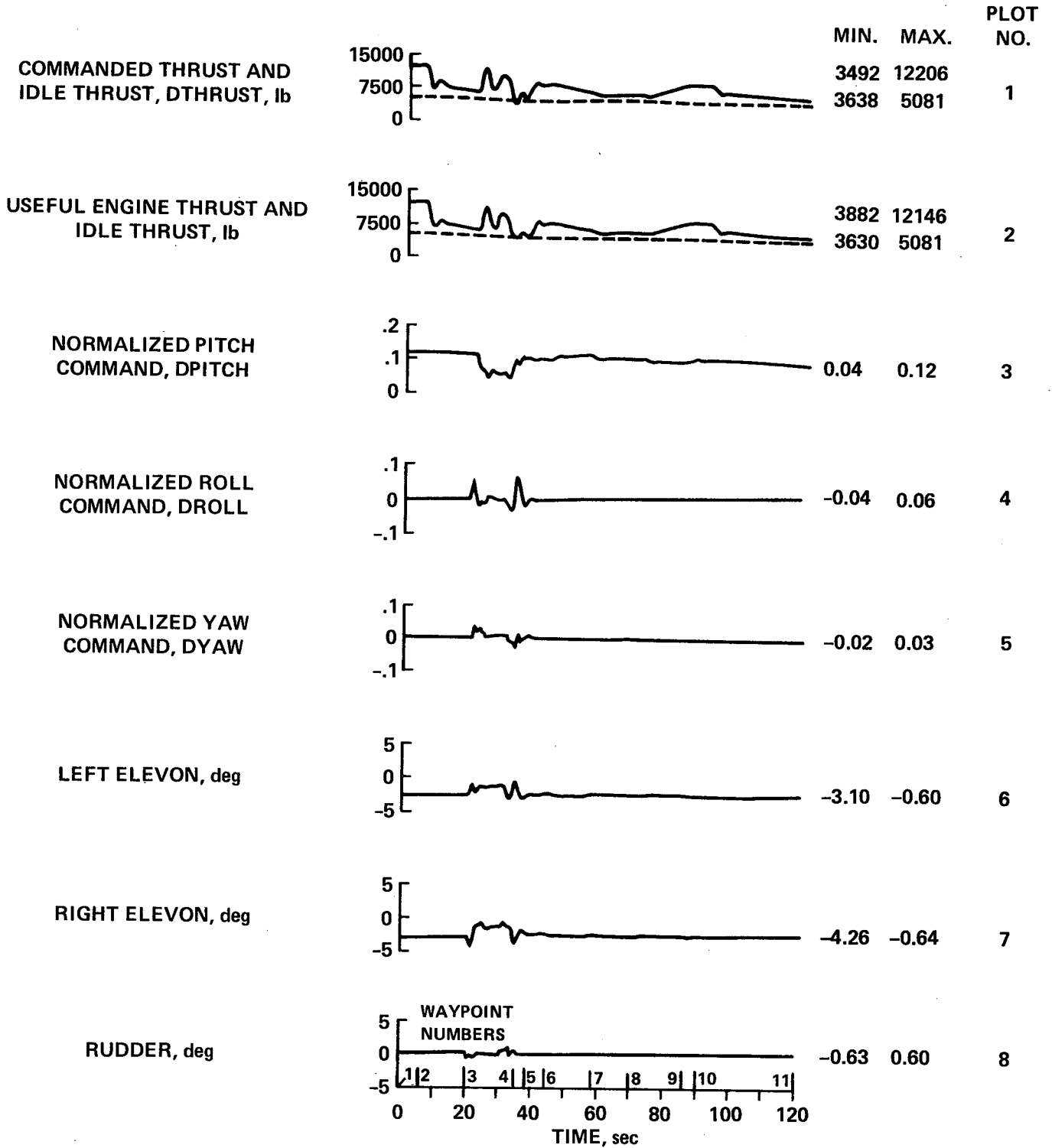


Figure 7(f).- Run 2. Continued.

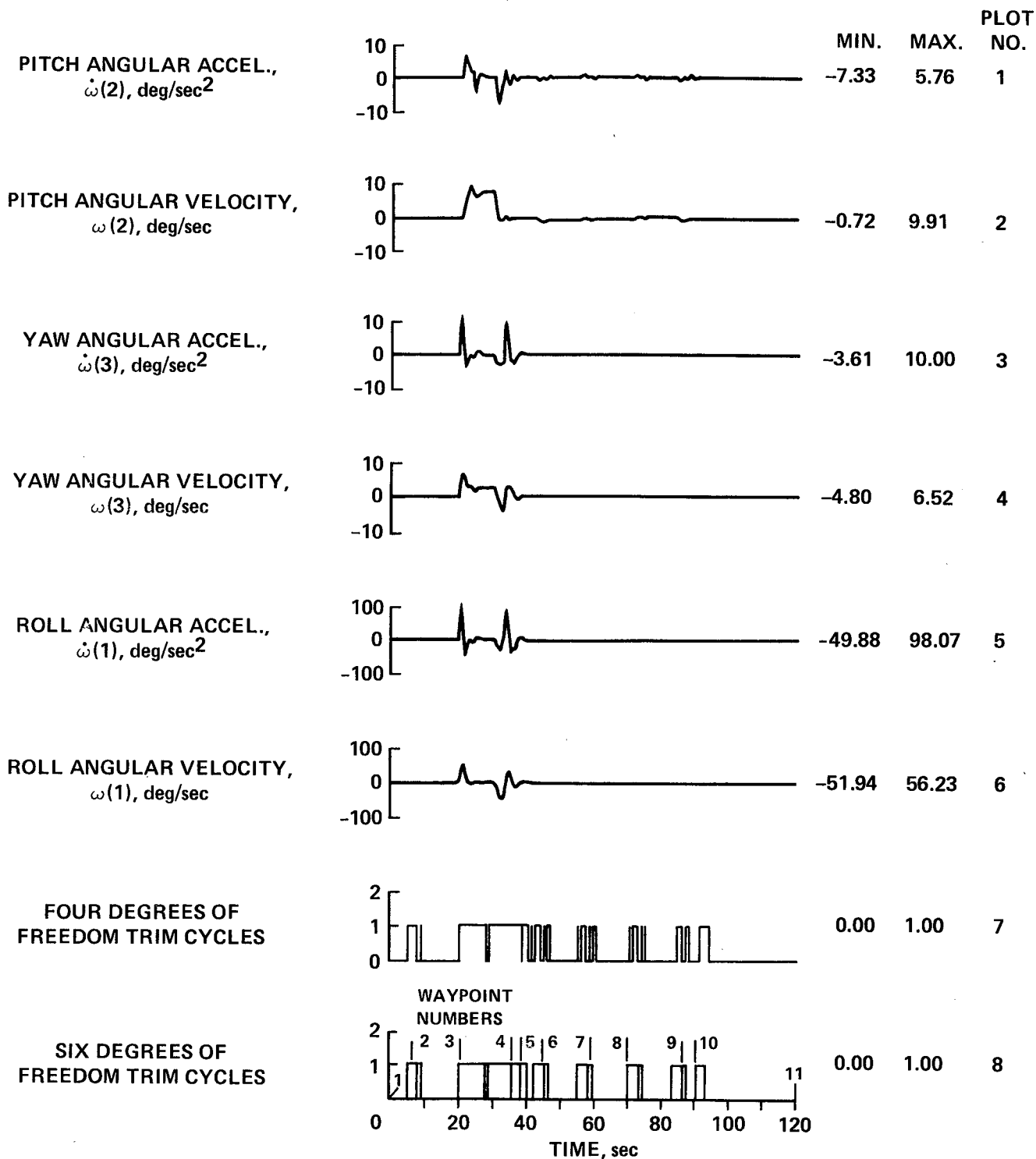


Figure 7(g).- Run 2. Concluded.

The three primary commands are shown by dashed lines in the first three plots and all remaining plots for this run show the aircraft and control system responses. The rough horizontal acceleration commands resolved into inertial reference axes ( $A_i$ , in fig. 5) are shown in the fourth and fifth plots and the corresponding rough velocity commands,  $V_i$ , are shown in the final three plots of figure 7(b). As with the previous accelerating trajectory of figure 6, the horizontal components of aircraft acceleration closely follow the total commanded acceleration,  $A_T$ . Therefore, the first four plots of figure 7(c) show only the horizontal components of actual aircraft acceleration and the corresponding horizontal components of the closed-loop feedback commands,  $\Delta A_c$ , which give an idea of how much correction must be supplied by the regulator. The vertical accelerations are at a much lower level and the internal smooth, feedback, and total-acceleration commands as well as the aircraft vertical-acceleration are shown in the final four plots of figure 7(c). The aircraft vertical acceleration in the last plot shows some interaction at 20 sec (WP3) when the turn is made even though no smooth command is present in the fifth plot. Note that the feedback signal in the sixth plot responds to vertical velocity and position errors through the regulator to give a total acceleration command in plot 7 in a direction to correct the disturbance.

The aircraft velocity and position responses are shown in figure 7(d). Airspeed decreases from 800 to 530 ft/sec while altitude decreases from 5000 to 2800 ft. All responses are smooth.

The angular responses in figure 7(e) show the commanded heading angle in the first plot and the actual heading and flightpath angles in the next two plots. The aircraft Euler angles are shown in the fourth, fifth, and sixth plots. The angle of attack in the seventh plot shows an increase during the turn, and small values of sideslip are shown in the last plot.

The controls and control commands are shown in figure 7(f). The first plot of thrust shows that the command is reduced below the engine idle thrust at approximately 30 sec. This reflects the difficulty that the aircraft has in decelerating since no speed brakes are available; thus, deceleration depends on thrust reduction. A thrust command below idle is merely limited in the aircraft actuator so that the generated idle thrust is maintained. Many successful simulation runs have been made where a large commanded deceleration led to a commanded thrust well below idle. The only effect was a lag behind the commanded trajectory and a corresponding buildup in the regulator error signal which was then limited so that the trim inversion routine functioned satisfactorily. It will be noted that the aircraft useful thrust in the second plot goes slightly below the idle thrust level. This is due to thrust losses from nozzle turning angles and bleed air extraction after the total generated thrust is established at the idle level by the throttle position. The pitch, roll, and yaw commands are shown in the next three plots, and the elevon and rudder deflections determined by them, as explained previously, are shown in the final three plots.

The aircraft angular accelerations and angular rates are shown in figure 7(g). Significant transient activity occurs only at the turn. Again the roll responses are much greater and are plotted to a ten-times higher scale in the

fifth and sixth plots. The two final plots show the trim counts. For this trajectory neither count exceeds one.

DATA FOR RUN 3

TABLE 3.- WAY POINT TABLE FOR RUN 3

Velocity 500 ft/sec North				
Way point, WP	Time	Position East	Altitude	Trajectory situation
1	0	0	1000	Constant speed
2	5	100	900	Path displacements
3	30	5	997	Wind gusts
4	50	63	931	Wind gusts
5	100	49	946	Wind gusts. End of run

Run 3. Conventional Flight with Disturbances

Data for the third run is presented in figure 8. The commanded flightpath is only north so the horizontal and vertical trajectories are both plotted against time and are shown with way point numbers in figure 8(a). The run starts at 1000 ft altitude and velocity of 500 ft/sec north (WP1). All acceleration commands are zero throughout the run. At 5 sec (WP2) the aircraft is assumed to be suddenly offset by 100 ft west of, and below, the commanded trajectory. These displacements and the resulting time-histories of aircraft position are shown by the solid-line curves of the third and fourth plots of figure 8(b) where the commanded position is shown by the dashed lines. At 30 sec (WP3) step-wind gusts of 10 ft/sec are applied in the westward and downward directions as shown by the solid-line curves of the first two plots. The aircraft instrumentation system is assumed to estimate these gusts by a first-order filter with a 25 sec time constant as shown by the dashed curves. The displacement response to the disturbances is shown in the third and fourth plots. The gust response excursion is well checked within 20 sec (WP4) and starts to return to the commanded trajectory. Approximately half the displacement has been corrected to within 70 sec (WP5). The velocity responses are shown in the fifth and sixth plots and the aircraft acceleration responses are shown in the last two plots of figure 8(b). Note that the aircraft responds with a steep buildup of acceleration to the initial offsets; however, an instantaneous step of acceleration results from the step-wind gust. All transient responses are satisfactorily smooth.

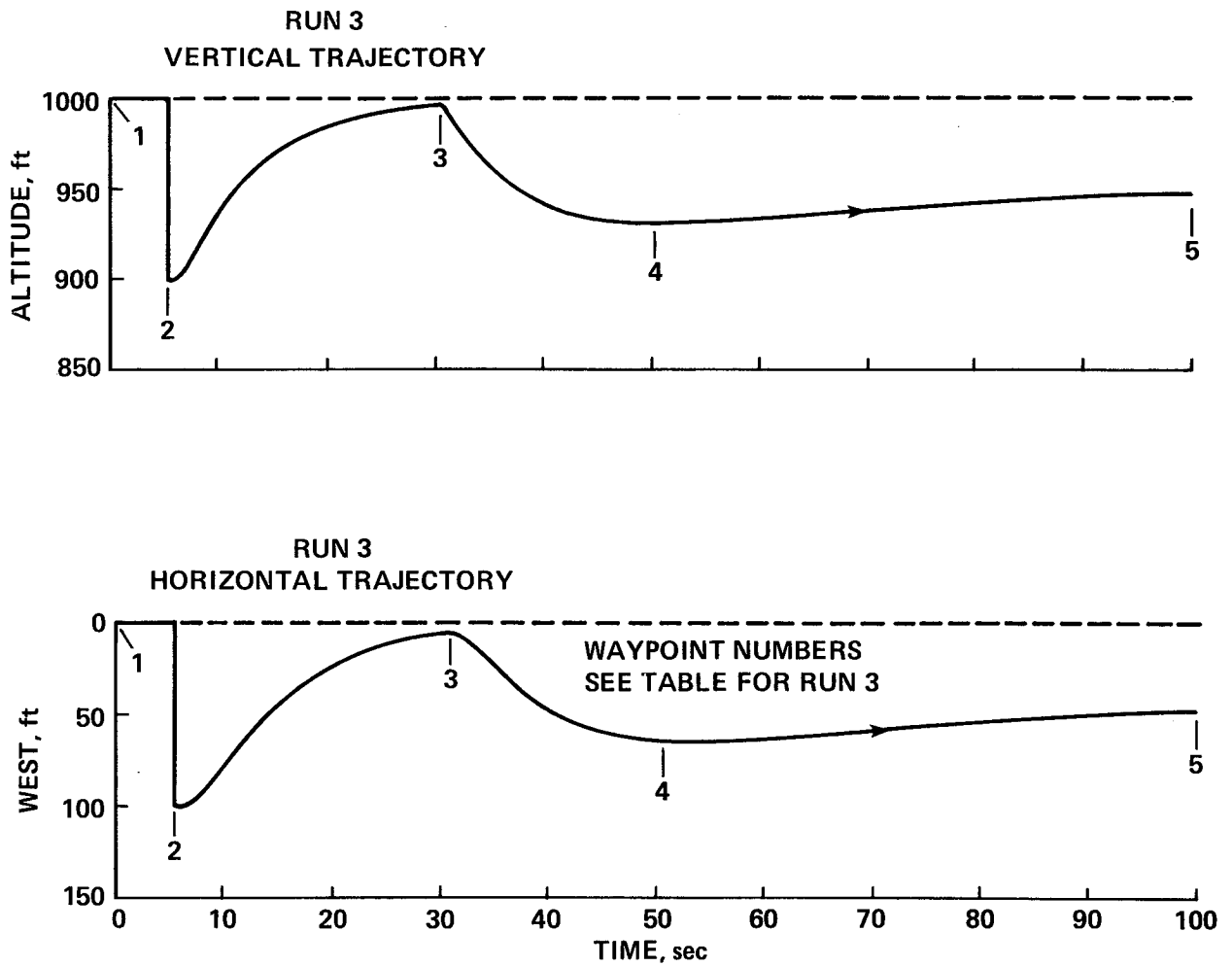


Figure 8(a).- Run 3. Conventional flight with disturbances.

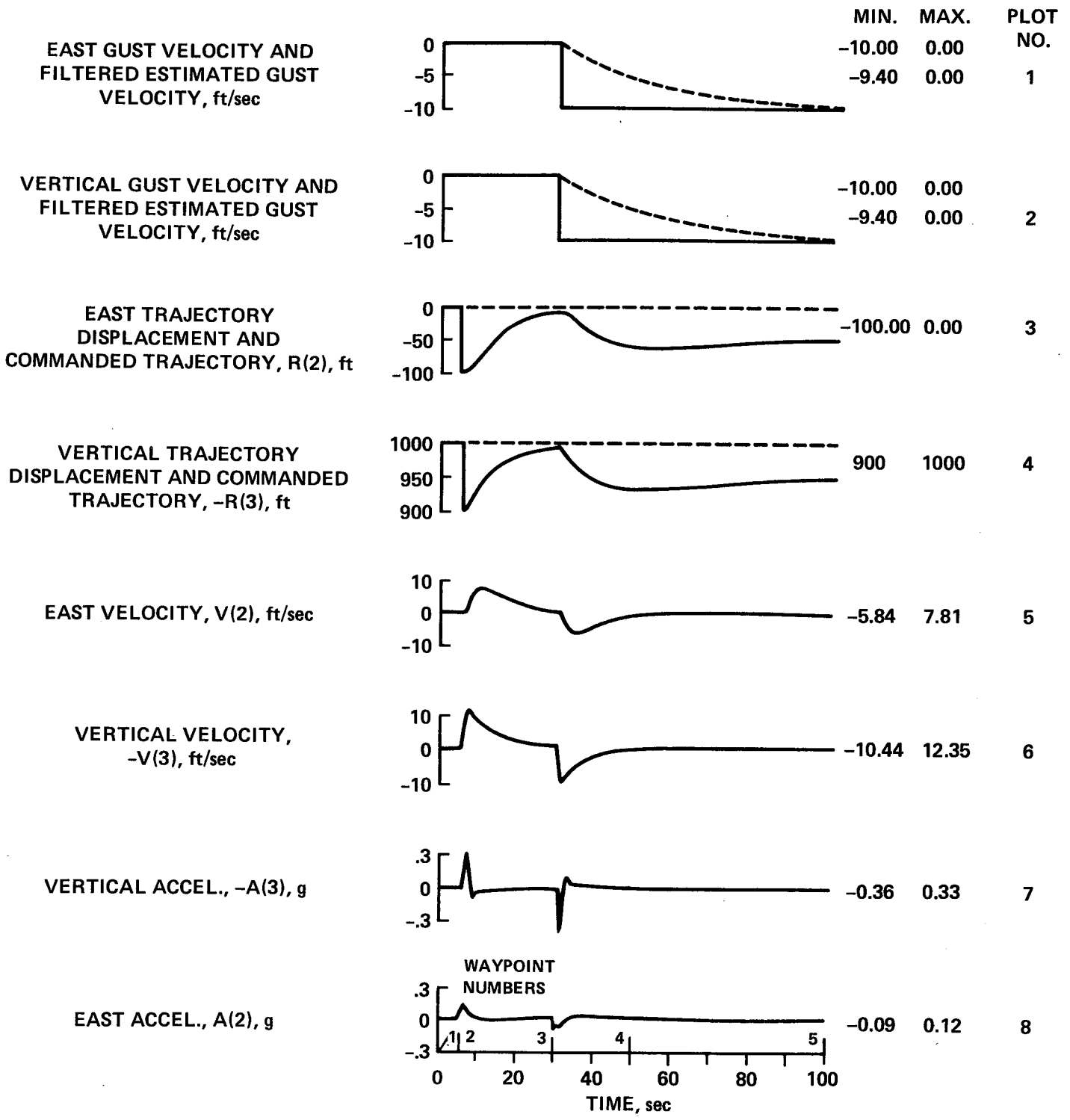


Figure 8(b).- Run 3. Continued.

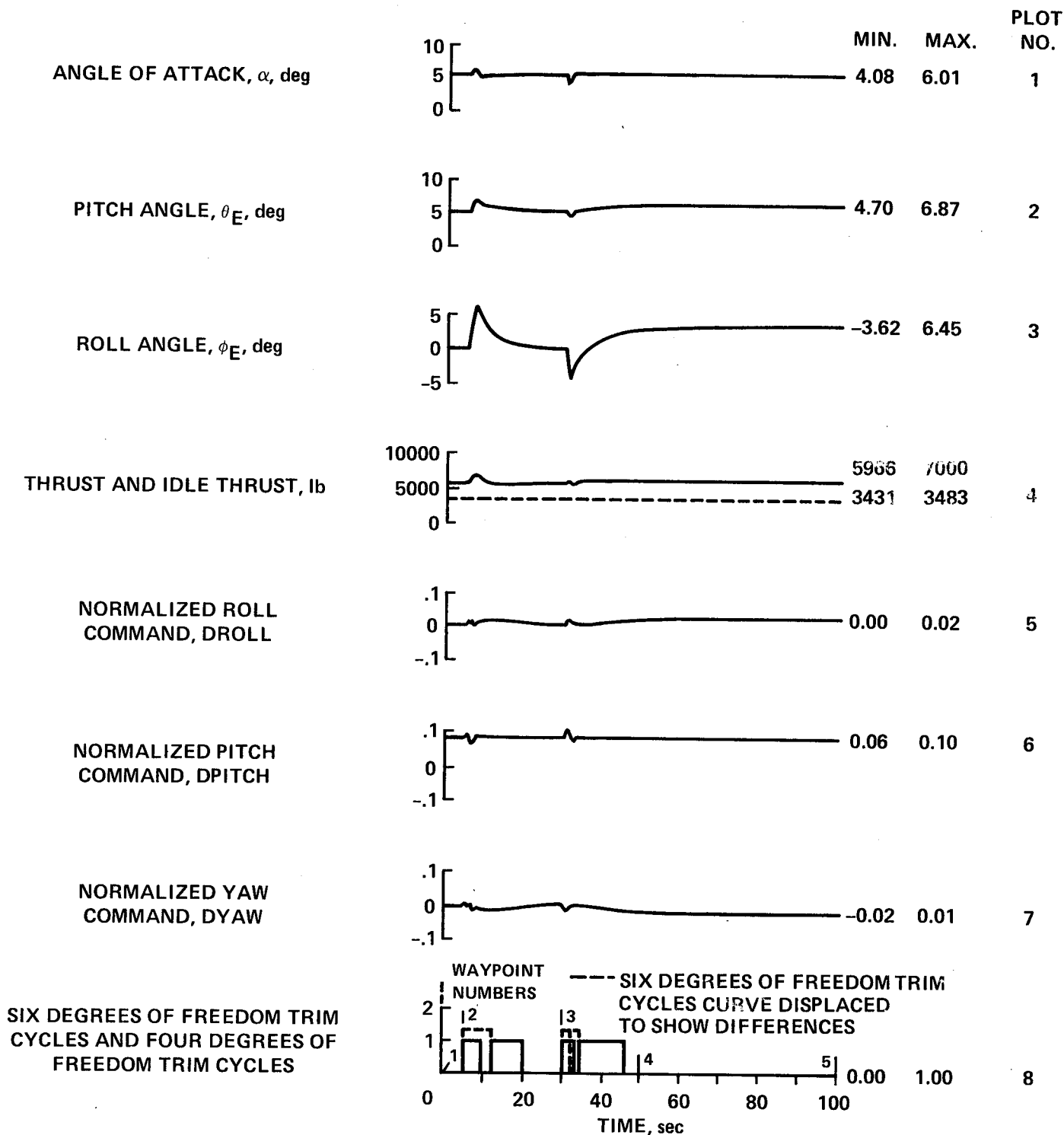


Figure 8(c).- Run 3. Concluded.

Figure 8(c) shows the other variables of interest for this run. The angle of attack in the first plot shows an instantaneous step when the gust is applied; however, recovery is smooth. Aircraft pitch angle is shown in the second plot and roll angle is shown in the third plot. Both responses are smooth. The thrust in the fourth plot remains well above the idle limit. The roll, pitch, and yaw commands generated in response to the disturbances are shown in the next three plots. Note that roll and yaw commands are zero for level flight while pitch has an average value of approximately 8% of maximum. The trim cycle counts for the six- and four-degree-of-freedom trims never exceed one, and are shown by the dashed and solid lines, respectively, in the last plot.

This run with disturbances was made only to show the character of the system response. No particular design effort was made to cope with wind gusts by introducing trajectory-error integrators or adjustments to the regulator limits. Tighter trajectory control could be maintained if a better estimate of wind conditions was available. Satisfactory operation under wind gust conditions was achieved in the recent flight tests of this type of system in a helicopter (ref. 6).

DATA FOR RUN 4

TABLE 4.- WAY POINT TABLE FOR RUN 4

Way point, WP	Time	Velocity	Angle of attack	Trajectory situation
1	0	180	19	Constant speed
2	5	180	19	Path deceleration
3	22	134	35	Lift curve slope reversal
4	30	109	54	Switch to perpendicular reference system
5	33	101	61	Increase path deceleration
6	42	11	--	Command zero acceleration
7	62	0	--	End of run 4

Run 4. Decelerating Transition Run

This run started in conventional flight at an altitude of 1000 ft and a velocity of 180 ft/sec north (WP1). The objective was to bring the aircraft to rest in a vertical-attitude-hover position while holding altitude. The only command input was path deceleration rate as shown by the dashed line in the first plot of figure 9(b). A deceleration rate command of approximately 0.03 g per sec (WP2) gave a deceleration of 0.1 g until 33 sec when it was increased to 0.4 g and then reduced

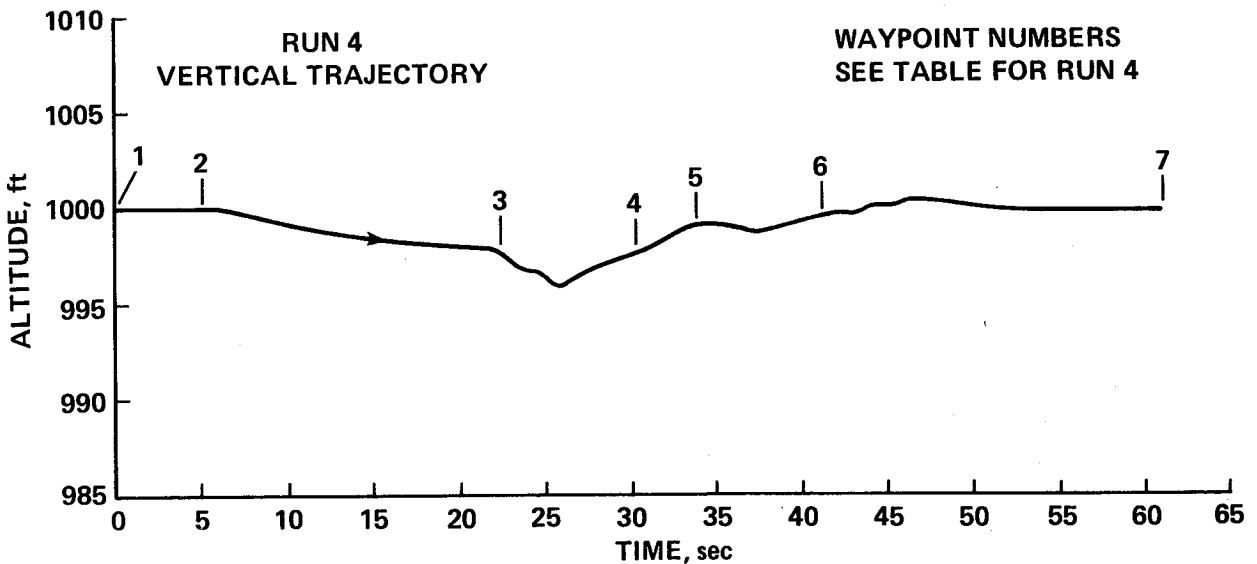


Figure 9(a).- Run 4. Transition from conventional flight to hover.

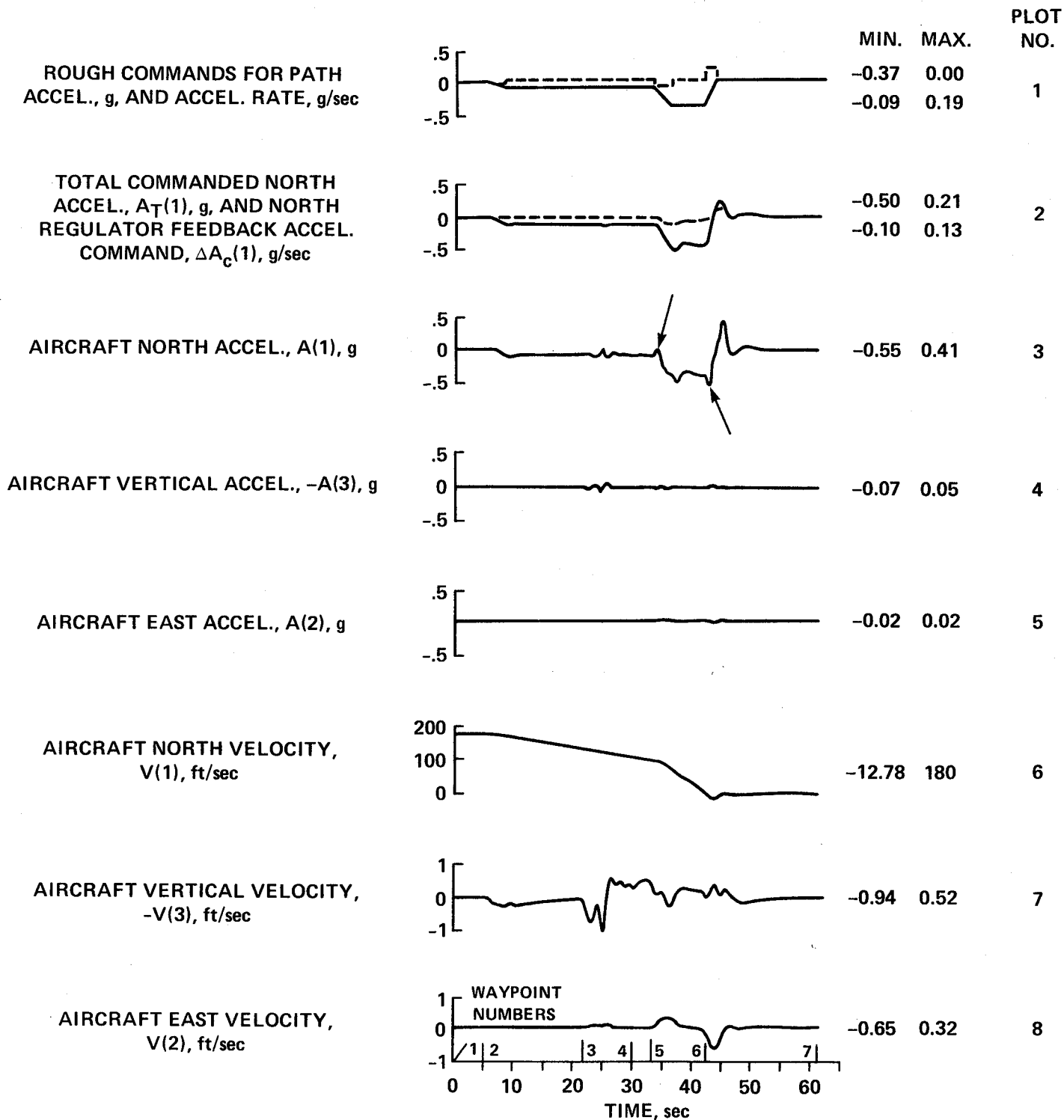


Figure 9(b).- Run 4. Continued.

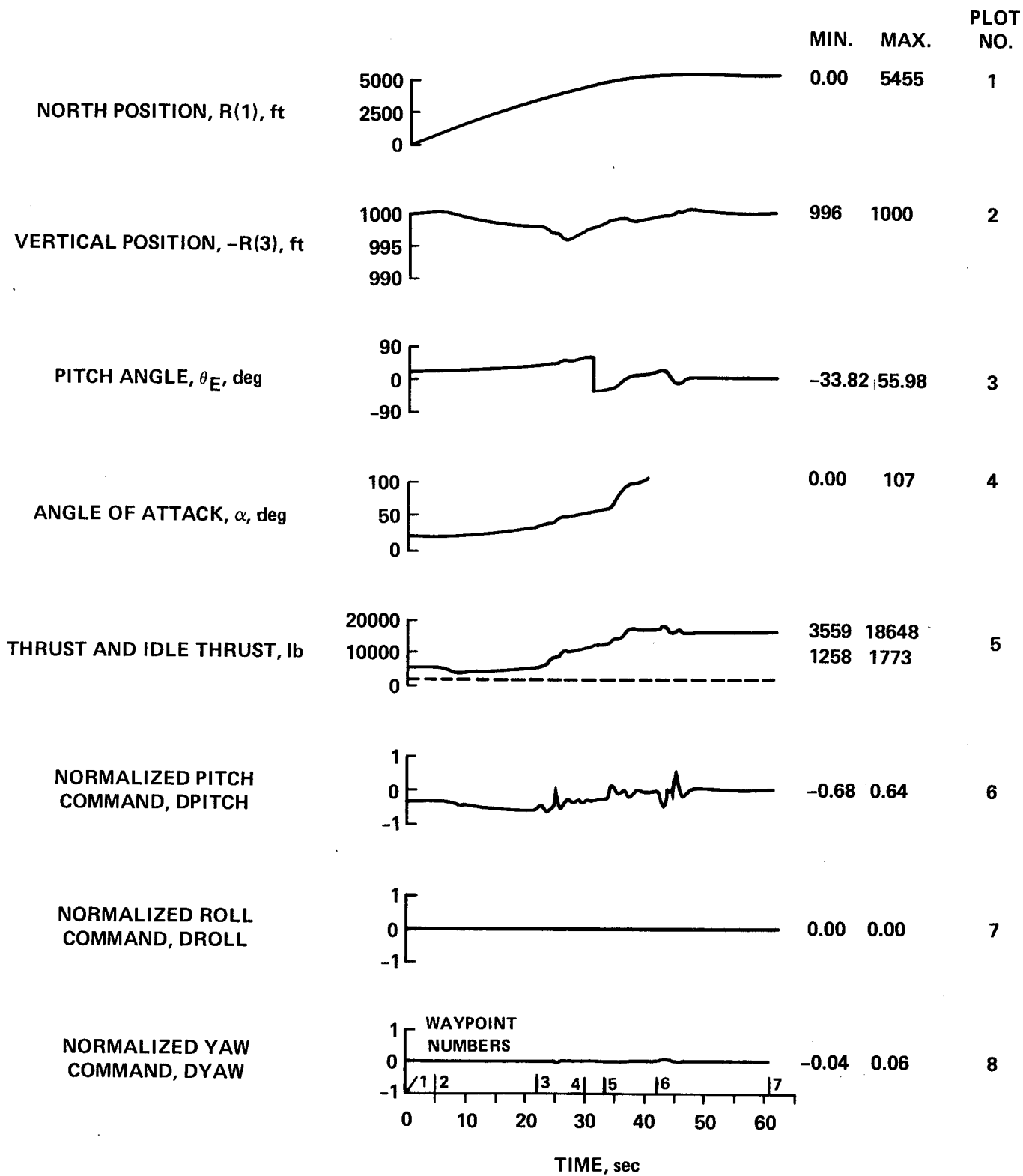


Figure 9(c).- Run 4. Continued.

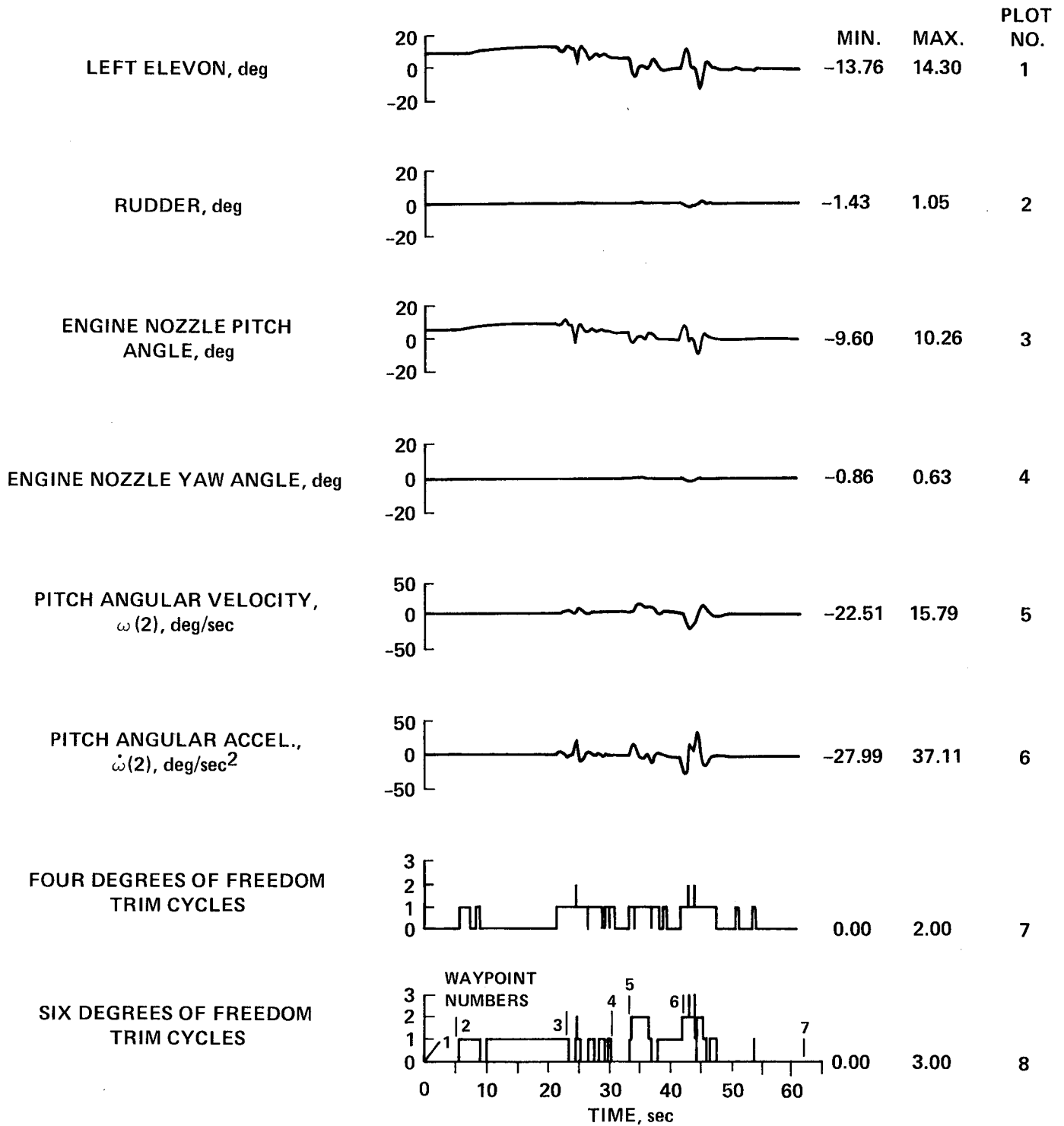


Figure 9(d).- Run 4. Concluded.

to zero at 42 sec (WP6) as shown by the solid curve in the first plot. The second plot shows the north-axis feedback, acceleration-correction signal in the dashed line and the total commanded acceleration in the solid plot. The trajectory command is so abrupt that a considerable transient overshoot occurs in the total command. This feature should be kept in mind when examining the aircraft acceleration response which is evaluated by its departure from this total command.

Several interesting features should be noted in this run which is a severe test of the control system's ability to maintain a desired trajectory over a large portion of the flight envelope while strong nonlinear effects are encountered in the aerodynamic and propulsion characteristics. The aircraft experiences lift-curve slope reversal at approximately 22 sec (WP3) as the angle of attack reaches approximately  $35^\circ$  and thrust and attitude must be increased rapidly to hold altitude (fig. 9(c)). Then as attitude continues to increase and reaches  $54^\circ$  at 30 sec (WP4), the attitude reference system is switched to the perpendicular axis system as previously discussed. Finally, as the aircraft assumes a nearly vertical attitude where maneuvering depends almost entirely on engine nozzle-angle displacements, the nonminimum phase effect of the right-half plane zero in the aircraft transfer function becomes apparent. The concluding remarks mention the nonminimum phase effect and explain why it is not modeled in the dynamics of the inverse model. The aircraft acceleration north is shown in the third plot of figure 9(b). A transient effect is seen between 22 and 26 sec as lift-curve slope reversal occurs over the various lifting surfaces. However, no disturbance is seen when the coordinate system switches at 30 sec. This switch in angle reference does not affect the trajectory variable displays which are still resolved into Earth-reference axes. The nonminimum phase effect is seen in the aircraft acceleration response at 33 sec (small arrow on plot 3) where it is initially in a direction opposite to the command. The same effect occurs when acceleration is reduced at 42 sec (small arrow).

The aircraft vertical acceleration in the fourth plot of figure 9(b) should remain at zero, but it shows a coupling effect at lift-curve slope reversal. The side acceleration in the next plot shows almost no deviation from its zero value. The north velocity in the sixth plot shows the reduction of speed-to-zero with various slopes and some overshoot at hover. The vertical and side velocities in the last two plots are shown at a magnified scale, but they actually represent good control of variables that should remain at zero.

The first two plots of figure 9(c) show the aircraft displacements in the vertical plane. While a total range of 5500 ft is covered, the vertical displacement is held to less than 5 ft during lift-curve slope reversal. The pitch attitude in the third plot shows the switch in axis-reference system at 30 sec when it changes from  $56^\circ$  above the horizontal to  $34^\circ$  below the vertical. The angle of attack in the fourth plot shows an increase at lift-curve slope reversal, and again as the vertical attitude is approached. The angle of attack becomes unimportant and erratic during the transients at hover so it is deleted there. The thrust in the fifth plot shows a sharp increase at lift-curve slope reversal and rapidly increases to support the entire weight of the aircraft in hover. The afterburner came on at approximately 37 sec. Only the pitch command shows significant activity among the

control commands of the last three plots. This pitch command is followed, scaled, and reversed in sign, by the elevon deflection in the first plot and by the engine nozzle-pitch angle in the third plot of figure 9(d).

The slight yaw command in the last plot of figure 9(c) shows up in the rudder and engine nozzle-yaw angles in the second and fourth plots of figure 9(d). The pitch angular acceleration in the sixth plot follows the engine nozzle-pitch angle with a sign reversal. The trim counts in the final two plots show the severity of the maneuver. The six-degree-of-freedom trim requires three cycles when the large acceleration signal is applied at 43 sec.

DATA FOR RUN 5

TABLE 5.- WAY POINT TABLE FOR RUN 5

Way point, WP	Time	Velocity		Angle of attack	Trajectory situation
		Horizontal	Vertical		
1	0	0	0	---	Stationary hover
2	5	0	0	---	Vertical acceleration
3	12	0	33	0	North acceleration
4	28	87	130	10	Switch to runway reference system
5	30	99	141	9.6	Increase north acceleration and decrease vertical acceleration
6	57	420	1	6.5	Path acceleration, level flight
7	68	530	0	5	Constant speed level flight
8	80	530	0	5	End of run 5

Run 5. Accelerating Transition Run

The vertical flight profile for the first 50 sec of the run is shown in figure 10(a) with way point numbers. This plot is with displacement shown on both axes to display the true flightpath angle. This run started in hover in a vertical attitude with the aircraft landing gear pointing north (WP1). After 5 sec (WP2) a vertical acceleration rate command was applied until a vertical acceleration command of approximately 0.2 g was achieved at 8 sec as shown in the second plot of figure 10(b). At 12 sec (WP3) a north acceleration rate command in the first plot resulted in commanded accelerations of 0.2 g in both the north and vertical axes until 30 sec (WP5). At 30 sec the north acceleration was increased to 0.4 g and a

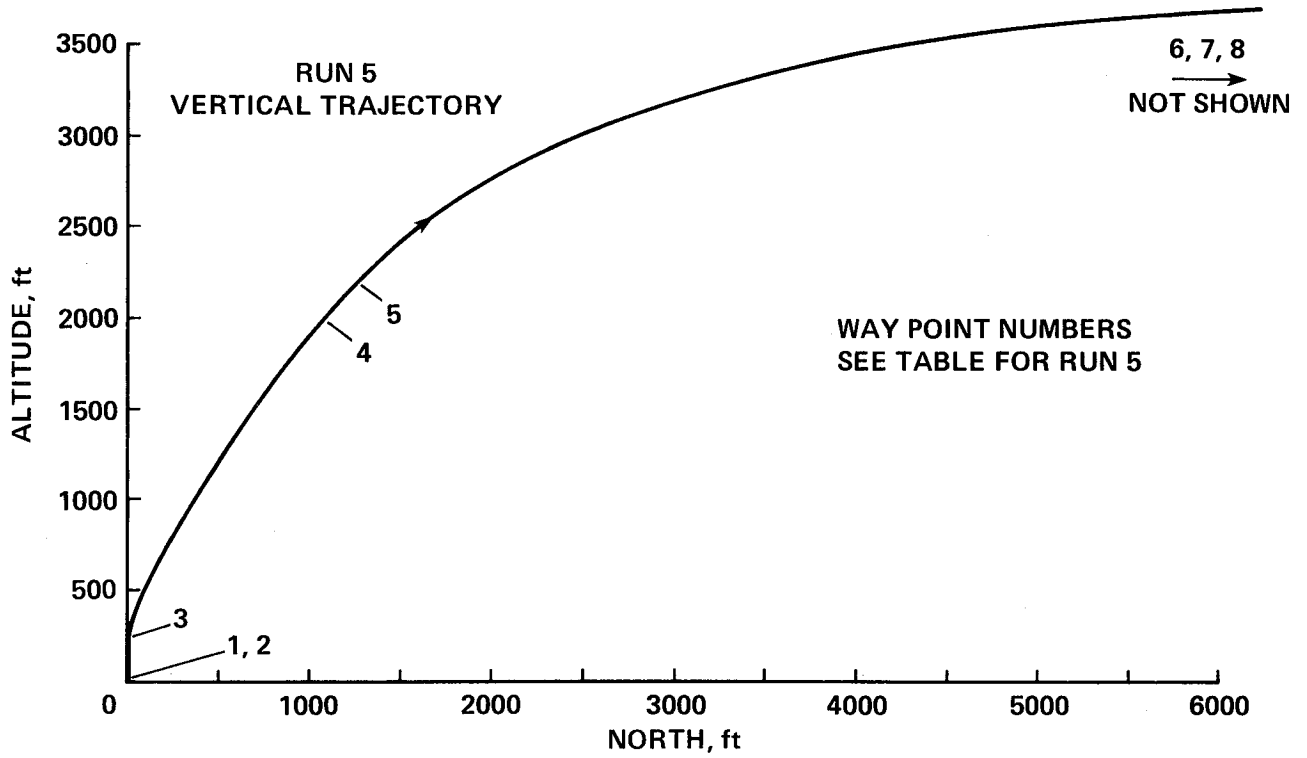


Figure 10(a).- Run 5. Transition from hover to conventional flight.

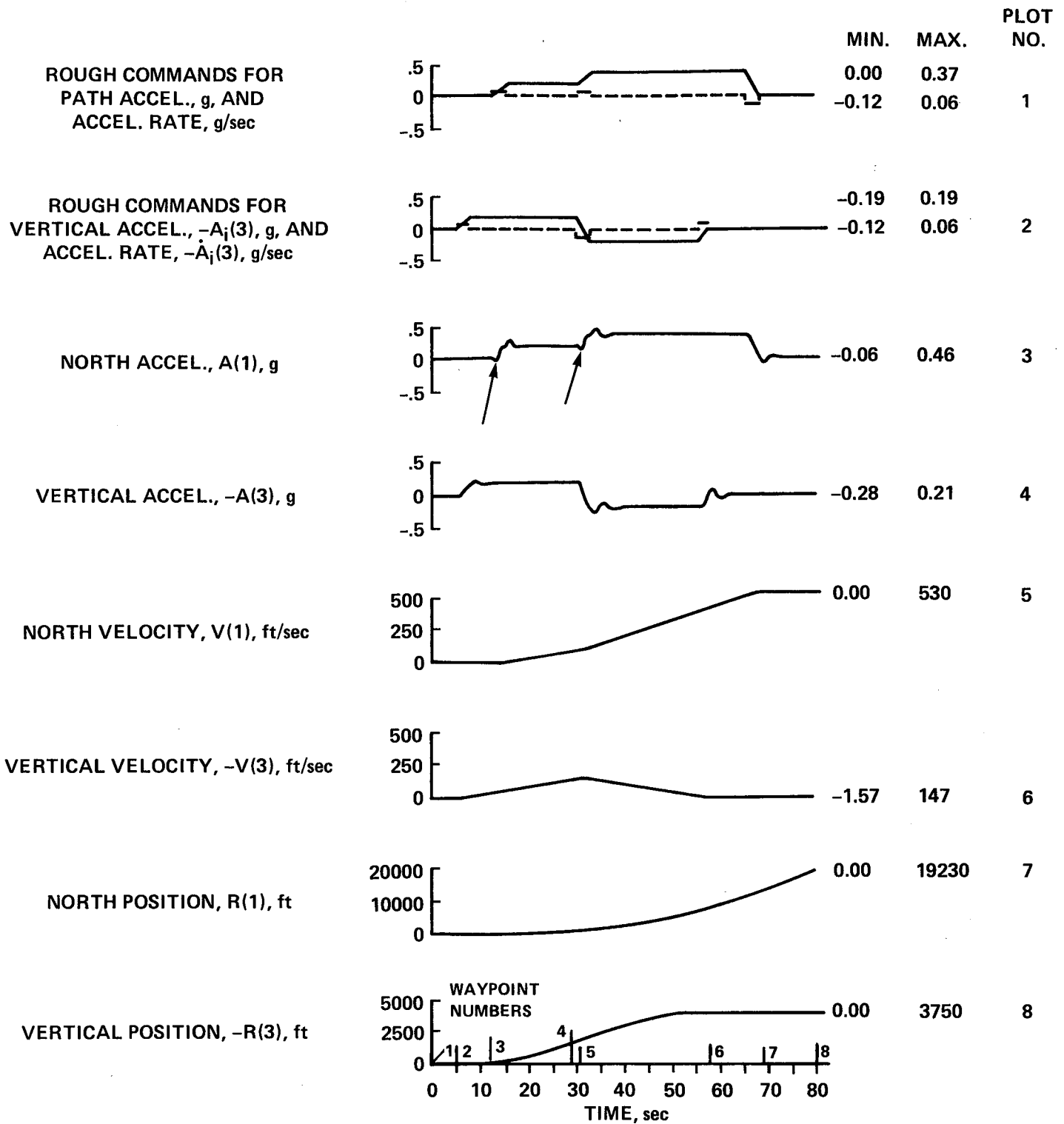


Figure 10(b).- Run 5. Continued.

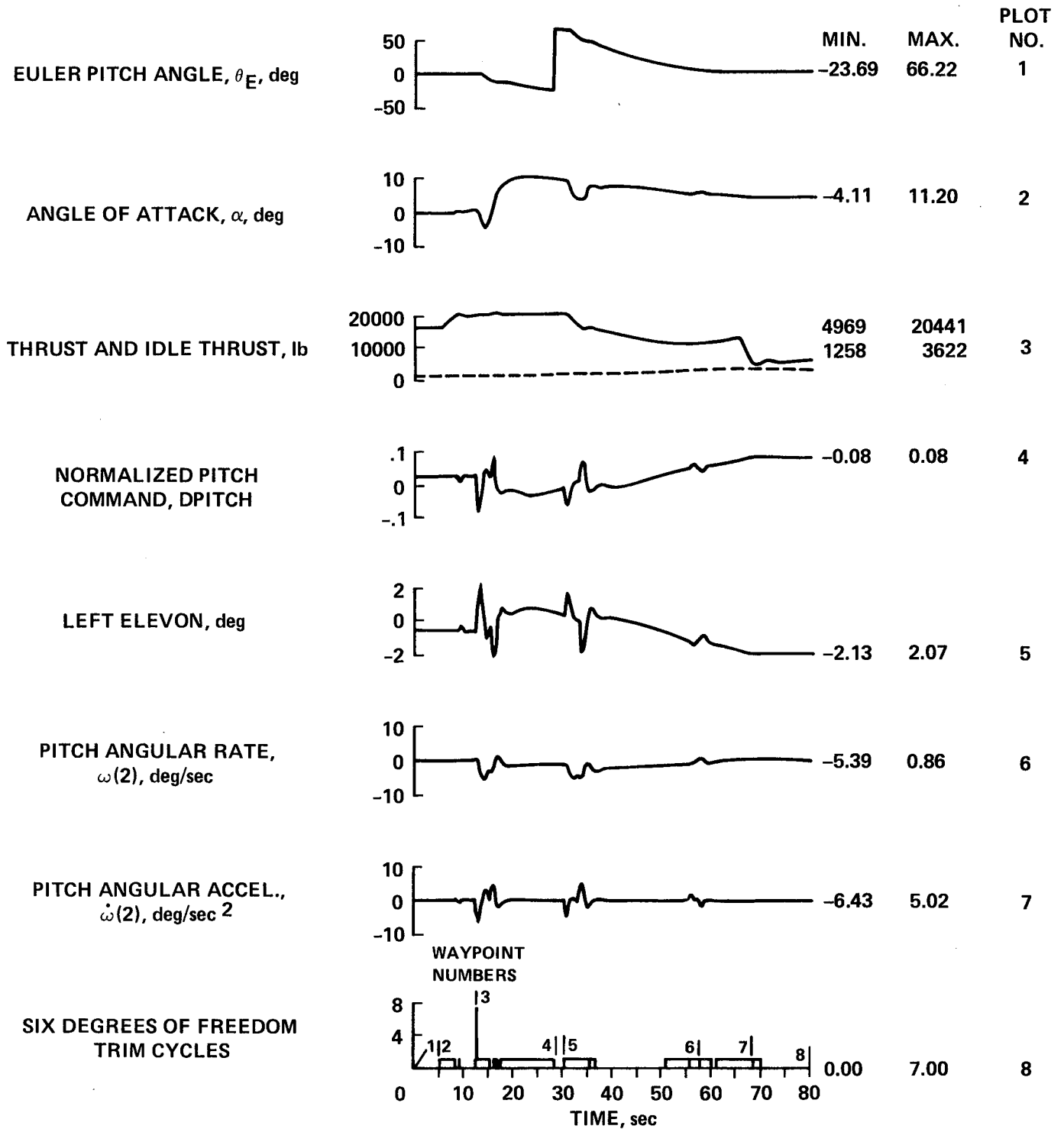


Figure 10(c).- Run 5. Concluded.

vertical deceleration command of 0.2 g was applied until the vertical velocity command became zero at 57 sec (WP6). The north acceleration command was reduced to zero at 68 sec (WP7) and straight, level, constant-velocity flight was commanded until the run terminated at 80 sec (WP8).

The aircraft north and vertical accelerations are shown in the third and fourth plots, velocities are shown in the fifth and sixth plots and displacements are shown in the seventh and eighth plots of figure 10(b). The north acceleration shows nonminimum phase effects at the small arrows but no such effect is seen in the vertical channel because its acceleration results from thrust and not from a nozzle deflection. The horizontal velocity builds up smoothly to 530 ft/sec while the vertical velocity reaches a maximum of approximately 150 ft/sec. The aircraft achieved a range of approximately 20,000 ft in 80 sec with an altitude gain of 3700 ft.

The pitch angle in the first plot of figure 10(c) shows that the switch from the perpendicular axis system to Earth-reference axes occurred at 28 sec. After a negative transient caused by the initial reversed (nonminimum phase) horizontal acceleration, the angle of attack remained less than  $12^\circ$  so no lift-curve slope reversal was involved. The thrust in the third plot required afterburner during the vertical acceleration but it was reduced to approximately 6000 lb for level constant-velocity flight. The only significant control command was in the pitch channel as shown in the fourth plot. Its reversed and direct images are seen in the elevon deflection of the fifth plot and in the pitch-angular acceleration of the seventh plot. The count for the four-degree-of-freedom trim never exceeded one, but the final plot shows that the six-degree-of-freedom trim required seven trim cycles when the horizontal acceleration was applied at 12 sec although it did not exceed one count otherwise.

DATA FOR RUN 6

TABLE 6.- WAY POINT TABLE FOR RUN 6

Way point, WP	Time	Velocity		Heading	Trajectory situation
		North	Vertical		
1	0	0	0	0	Hover
2	5	0	0	0	Accelerate north
3	26	42	0	0	Accelerate up
4	45	42	32	0	Heading rate
5	65	42	36	90	End of run 6

Run 6. Simple Maneuvers in Hovering Flight

The situation in hovering flight is somewhat different from what has been discussed so far. The first three runs were entirely conventional flight, and the fourth and fifth runs spent only brief periods during the terminal portion of the runs in the vertical attitude. For this run the aircraft is in a vertical attitude throughout the maneuver so that the attitude reference is always measured with respect to the perpendicular reference system. Furthermore, although the aircraft acceleration is still the essential input, the actual primary inputs are steps of acceleration rather than of acceleration rate. This process was more convenient for these tests, it might correspond to inputs from a pilot, and it demonstrated the flexibility of the system. However, these steps were sent through a low-pass filter before going to the command generator. The velocities are relatively low so aerodynamic forces are of secondary importance. Angle of attack and sideslip show unusual variations as the aircraft moves in both directions along all axes. The primary control forces and torques arise from the engine thrust and nozzle deflections as the aircraft operates in the tail-sitting mode. The maneuvers for this run are confined to the vertical plane which is defined by the north and vertical axes.

The vertical flight profile is shown with way point numbers in figure 11(a). The plots of figure 11(b) show the acceleration commands and the aircraft accelerations along the north and vertical axes and the heading rate and angle commands about the vertical axis. The run starts in hover (WP1) in a vertical attitude with the landing gear pointing north at zero elevation. For this mode, heading is defined as the angle between north and the horizontal projection of the aircraft landing gear. At 5 sec (WP2) a step command of approximately 0.1 g north is given as is shown by the dashed line in the first plot. This step command is passed through a first-order filter with a time constant of 1 sec as shown by the solid-

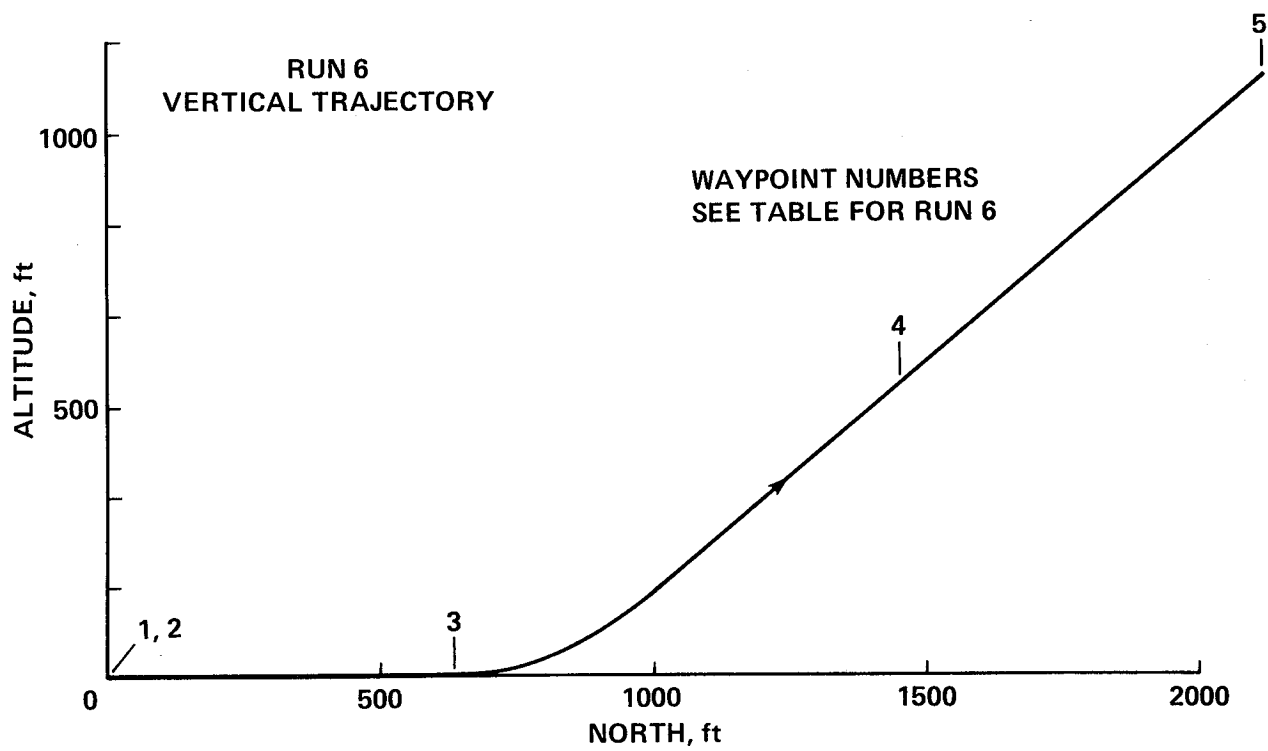


Figure 11(a).- Run 6. Simple maneuvers in hovering flight.

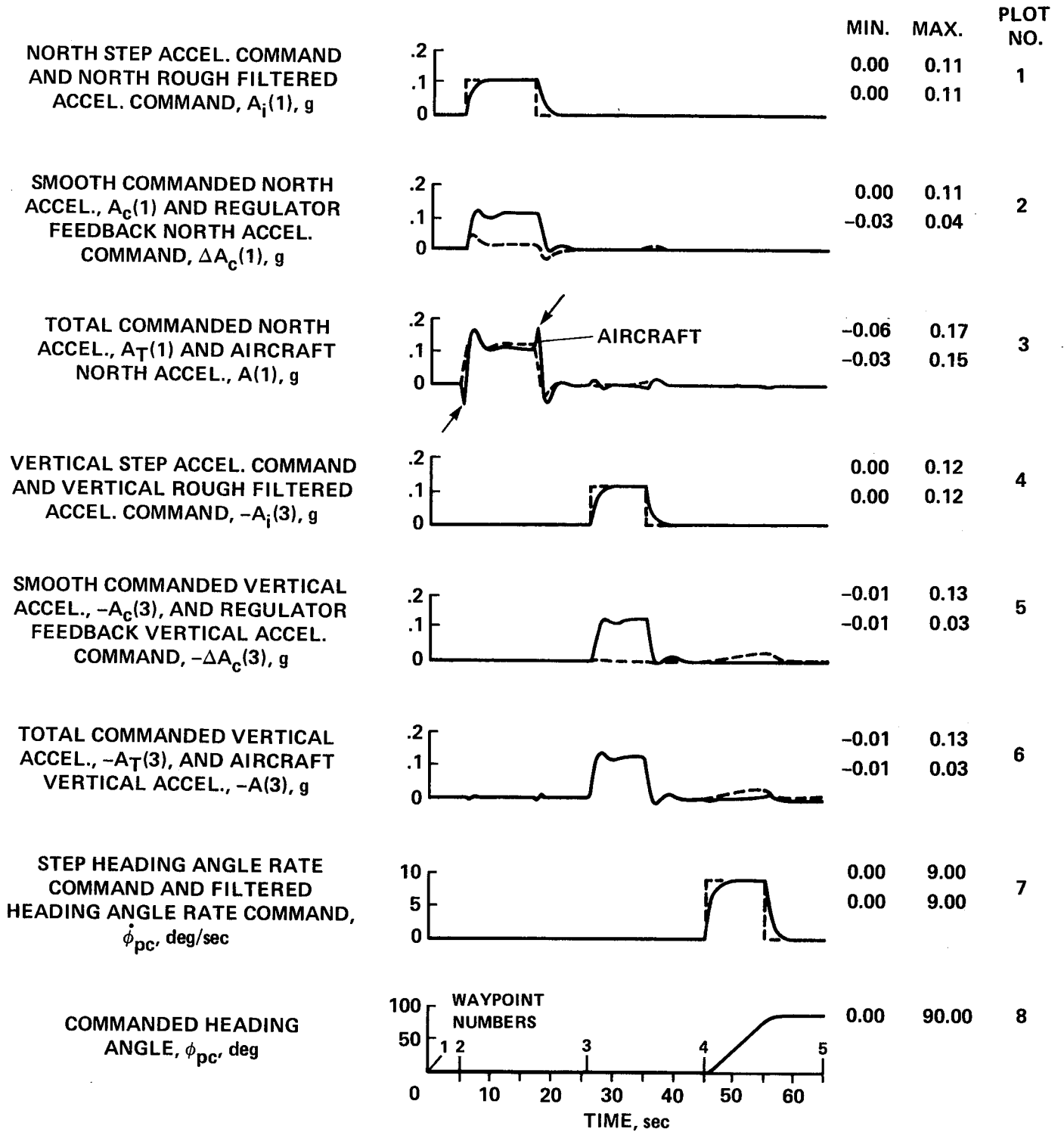


Figure 11(b).- Run 6. Continued.

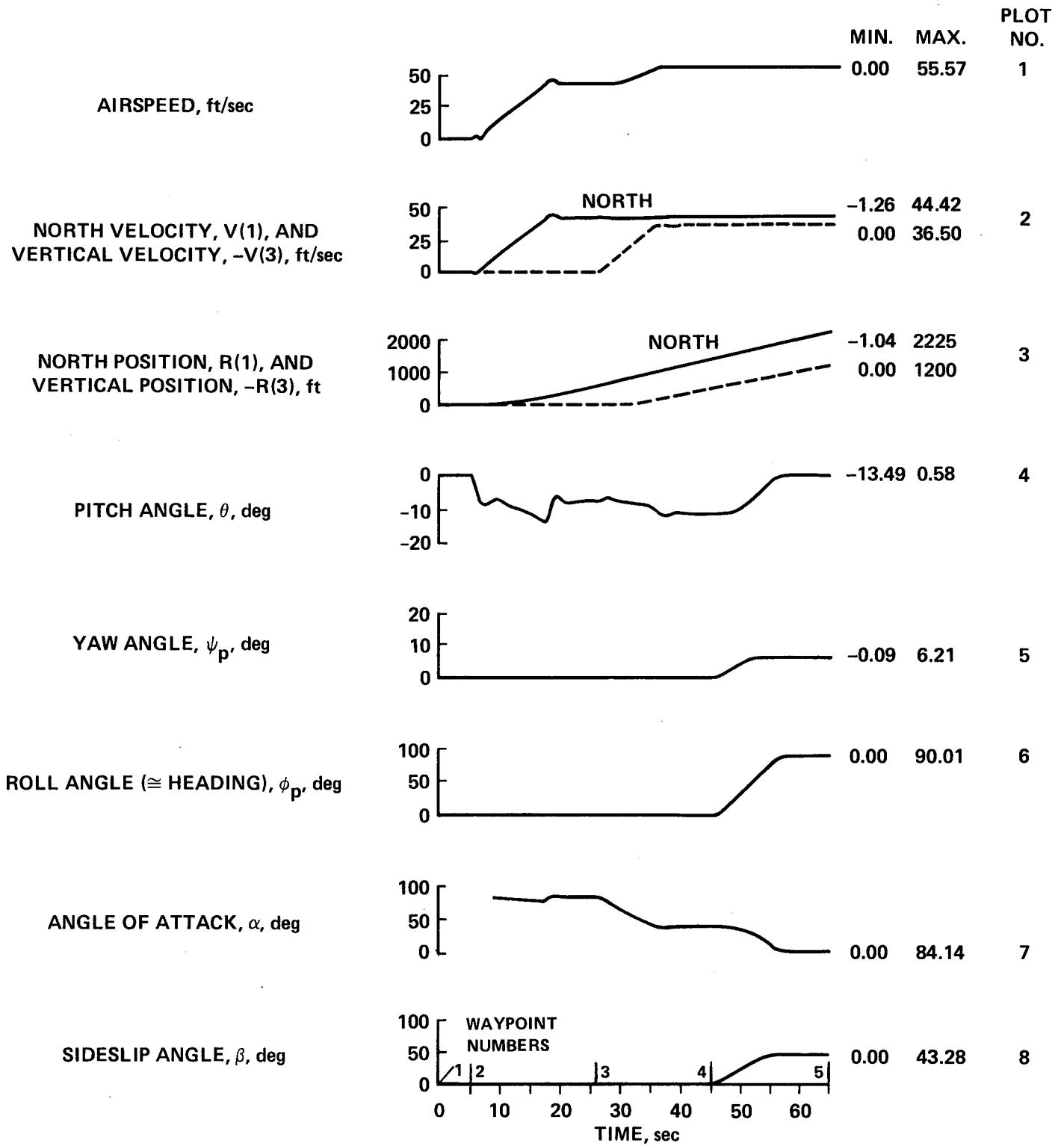


Figure 11(c).- Run 6. Continued.

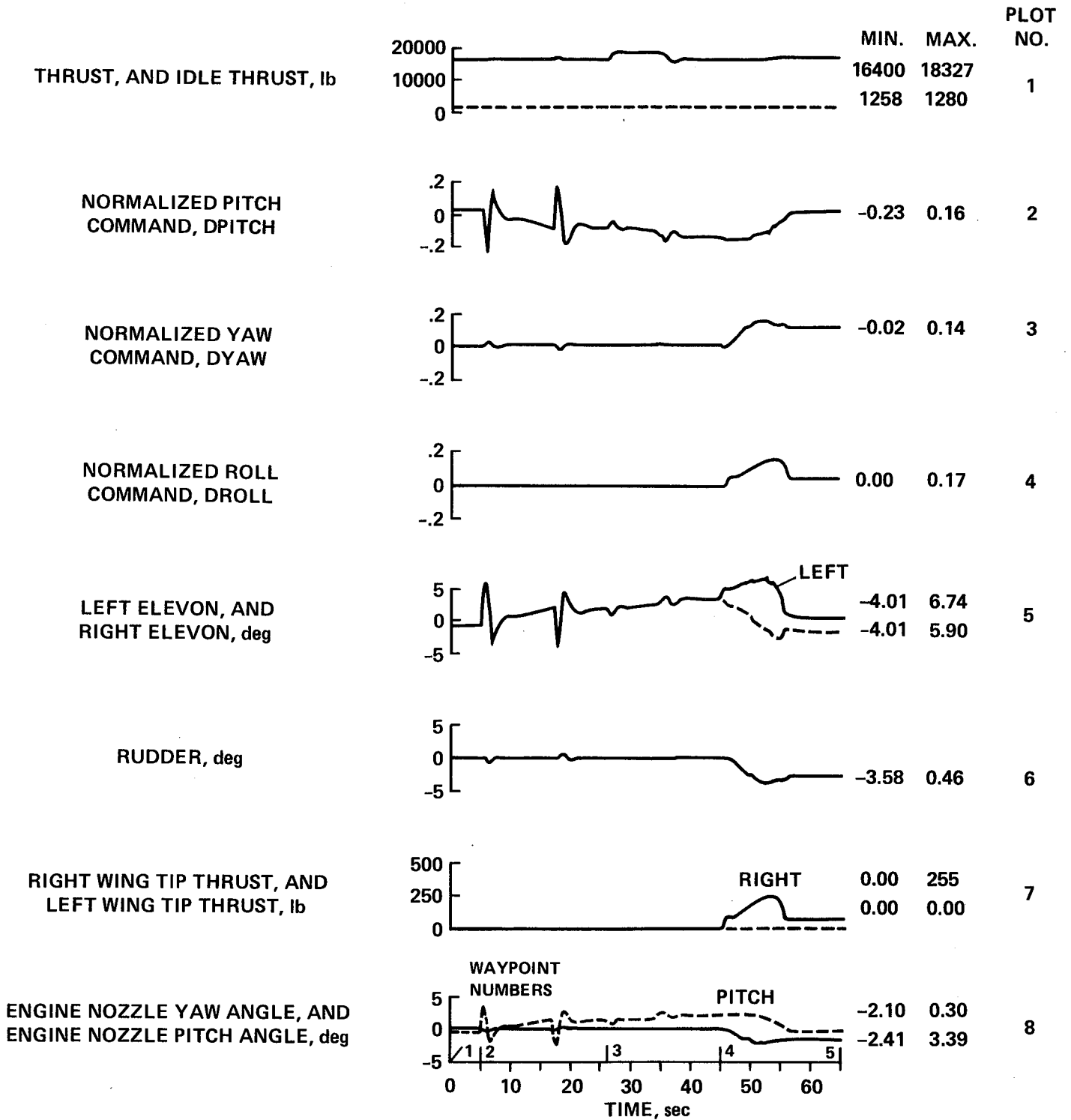


Figure 11(d).- Run 6. Continued.

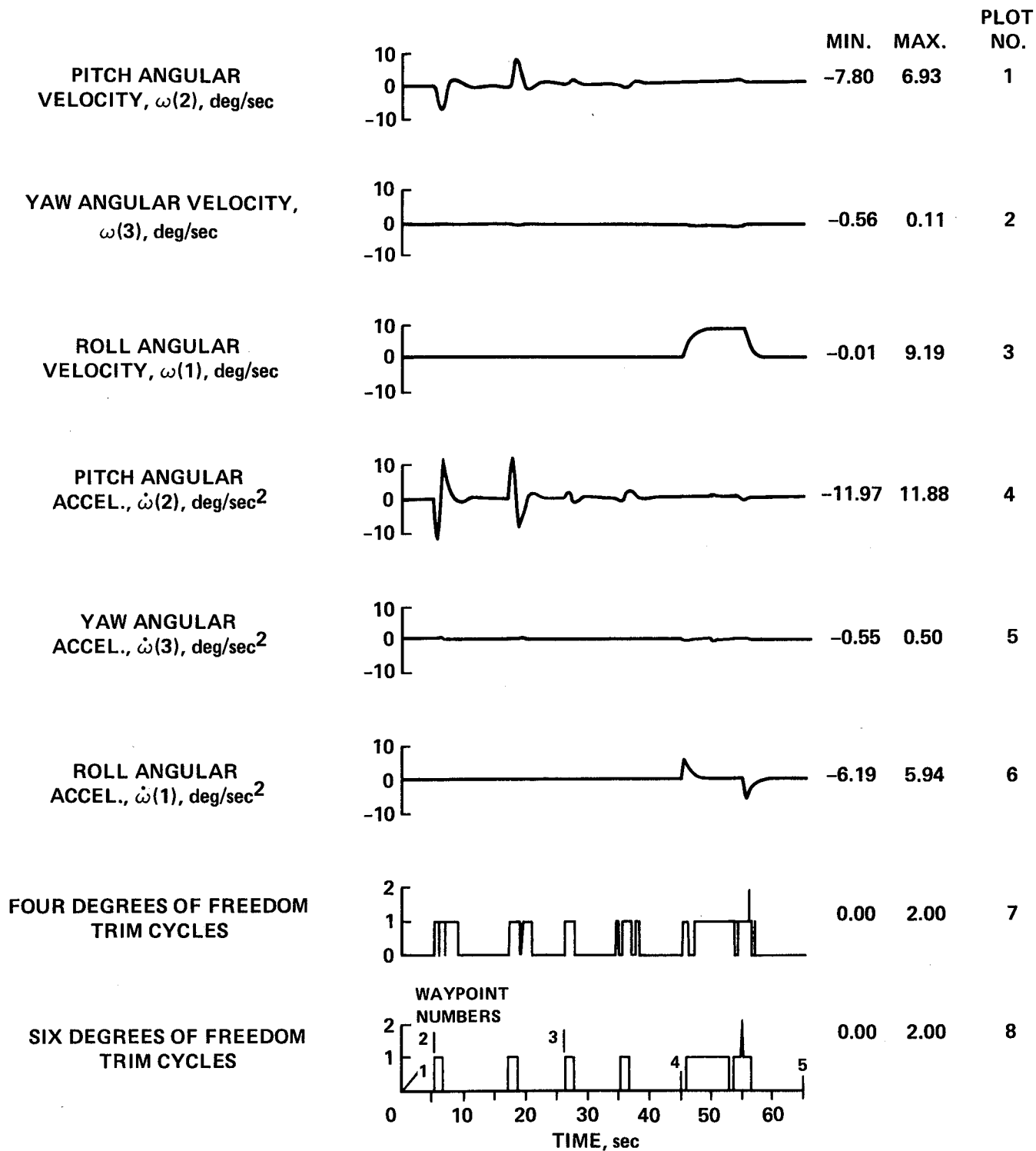


Figure 11(e).- Run 6. Concluded.

line curve to produce the rough acceleration command ( $A_i$ , in fig. 5). This input is maintained until 17 sec, then the resulting north-velocity command of 42 ft/sec is held for the duration of the run. The smooth acceleration command,  $A_c$ , and the closed-loop acceleration correction command,  $\Delta A_c$ , are shown in the second plot. Note that the feedback signal is small when compared to the feed-forward signal. The total north-acceleration command,  $A_T$  is shown in the dashed curve of the third plot and the actual north aircraft acceleration is shown by the solid curve. Note that the nonminimum phase effects are indicated by the small arrows. At 26 sec (WP3) a step-vertical acceleration command shown by the fourth plot results in a vertical velocity command of 36 ft/sec for the last half of the run. The vertical acceleration command signals in the fifth plot show even less  $\Delta A_c$  feedback signal than they do for the horizontal axis. This result is explained by the sixth plot, which shows no nonminimum phase effects in the vertical channel so that the aircraft follows the total command signal closely.

At 45 sec (WP4) when the aircraft is moving north at 42 ft/sec and up at 36 ft/sec, a step command of  $9^\circ/\text{sec}$  heading-angle rate (roll about the aircraft's longitudinal axis) was given as shown by the dashed curve in the seventh plot. This command is filtered as shown by the solid curve and is integrated as shown by the commanded angle in the last plot. It will be recalled that in the vertical attitude, the aircraft-direction cosine matrix with respect to the perpendicular reference system is TBP which is constructed from the three Euler angles. The first Euler angle is the landing-gear roll angle about the vertical axis which is essentially heading in the hover mode. This is the commanded heading angle as shown in the final plot. The other two Euler angles are the fifth and sixth trim variables in the six-degree-of-freedom trim. The heading command reaches  $90^\circ$  at 55 sec so that the aircraft is moving sidewise and up for the final 10 sec of this trajectory with the landing gear point west.

The velocity, position, and angular responses of the aircraft are shown in figure 11(c). The airspeed in the first plot reaches 55 ft/sec. The north and vertical velocities are shown in the second plot, and the respective positions are shown in the third plot. The pitch angle about the aircraft's lateral axis is shown in the fourth plot. Note that it is higher during acceleration. Roughly 0.1 radian of tilt is needed to give the 0.1-g acceleration initially. This tilt builds up more to overcome aerodynamic forces as speed is increased and it then drops back to a value sufficient to overcome the aerodynamic drag forces during the constant velocity trajectory. The tilt shifts from pitch to yaw as the aircraft rolls about the vertical axis but the aircraft continues to move in the north direction. As the roll angle increases in the sixth plot, the aircraft's attitude changes from pitch to yaw as shown in the fourth and fifth plots. The resulting behavior of angle of attack and sideslip is shown in the last two plots where the erratic initial behavior of angle of attack has been suppressed.

The control commands and responses are shown in figure 11(d). The first plot shows that thrust remains essentially equal to the aircraft weight of 16,400 lb but increases somewhat for the vertical-acceleration portion of the trajectory. The pitch command in the second plot produces the aircraft tilt that is necessary for

horizontal translation. Pitch trades off with yaw command as the roll angle goes to  $90^\circ$  in response to the roll command shown in the fourth plot. The elevon commands in the fifth plot follow the pitch command with reversed sign initially, but response to the mixture of pitch and yaw commands gives different deflections for the left and right elevons as shown after 45 sec. The rudder deflection in the sixth plot follows the yaw command with a reversal of sign. The roll command in the fourth plot increases initially and then drops when  $90^\circ$  of roll is attained but remains positive to balance aerodynamic and propulsion forces. The right wing-tip bleed air jet in the seventh plot follows the roll command but the left jet never comes on as shown by the dashed line. The pitch and yaw engine nozzle angles in the last plot follow the pitch and yaw commands with reversed signs but remain well below their mechanical limits of  $\pm 15^\circ$ .

The aircraft angular velocities are shown in the first three plots of figure 11(e). The pitch angular velocity in the first plot shows a response when the vehicle tilts to establish the initial acceleration at 5 sec and again when the acceleration is terminated at 17 sec. The roll angular velocity in the third plot occurs between 45 and 55 sec as the aircraft rolls  $90^\circ$  about the vertical axis. The angular accelerations in the next three plots are seen to be the derivatives of the angular velocities. The trim counts in the last two plots exceed one only when the roll is terminated at 55 sec. The trim cycle numbers in the last two plots show long periods when no perturbation cycle was required and only one instance of two trim cycles, which occurred when roll rate was terminated at 55 sec.

DATA FOR RUN 7

TABLE 7.- WAY POINT TABLE FOR RUN 7

Way point, WP	Time	Velocity			Heading	Trajectory situation
		North	East	Up		
1	0	0	0	0	0	Vertical attitude hover
2	5	0	0	0	0	East acceleration
3	15	0	24	0	0	North acceleration
4	25	18	24	0	0	Vertical acceleration
5	35	18	24	30	0	Heading rate
6	50	18	24	30	120	Reverse commands
7	72	0	0	0	0	End of run 7

Run 7. Complex Maneuvers in Hovering Flight

Figure 12 presents the results of a 72-sec vertical attitude run during which individual maneuvers were made in each channel and then simultaneous maneuvers were made in all channels. The ground track with way point numbers is shown in figure 12(a) along with a plot of altitude against time.

For the vertical attitude maneuvers, the primary commands are accelerations along the three axes of the perpendicular reference system and angular rates about the vertical. The run started in the vertical attitude with zero altitude and zero heading angle (the landing gear pointing north (WP1)). The second plot in figure 12(b) shows (dotted curve) that a step acceleration command of 0.2 g was applied in the east direction at 5 sec (WP2). The dashed curve shows the resulting smooth command,  $A_c$ , and the solid curve is the actual aircraft acceleration response in the sideways direction which exhibits a nonminimum phase effect. Curves of other internal commanded acceleration components in the side direction were recorded but are not shown as they were generally similar to those shown previously.

The first plot of figure 12(b) shows that at 15 sec (WP3) when the aircraft is moving sideways at 24 ft/sec a step acceleration command of 0.2 g north is given for 3 sec. The other usual acceleration curves are also given for the north axis in the first plot. The third plot shows that at 25 sec (WP4) a step vertical acceleration command of 0.2 g is given for 5 sec. At 25 sec the vehicle is moving 18 ft/sec north and 24 ft/sec east. At 35 sec (WP5) the aircraft is moving east at 24 ft/sec, north at 18 ft/sec, and up at 30 ft/sec. Note that there is no nonminimum phase effect in the vertical channel so the aircraft acceleration follows the smooth

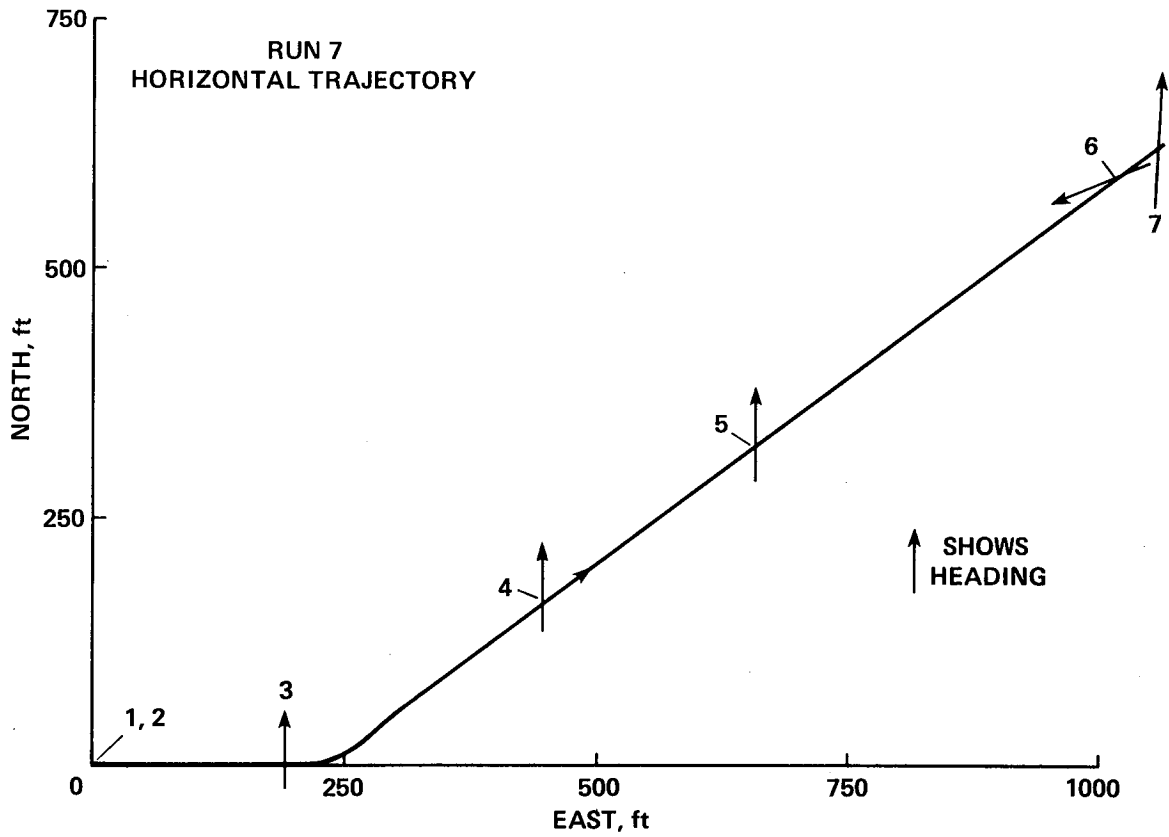
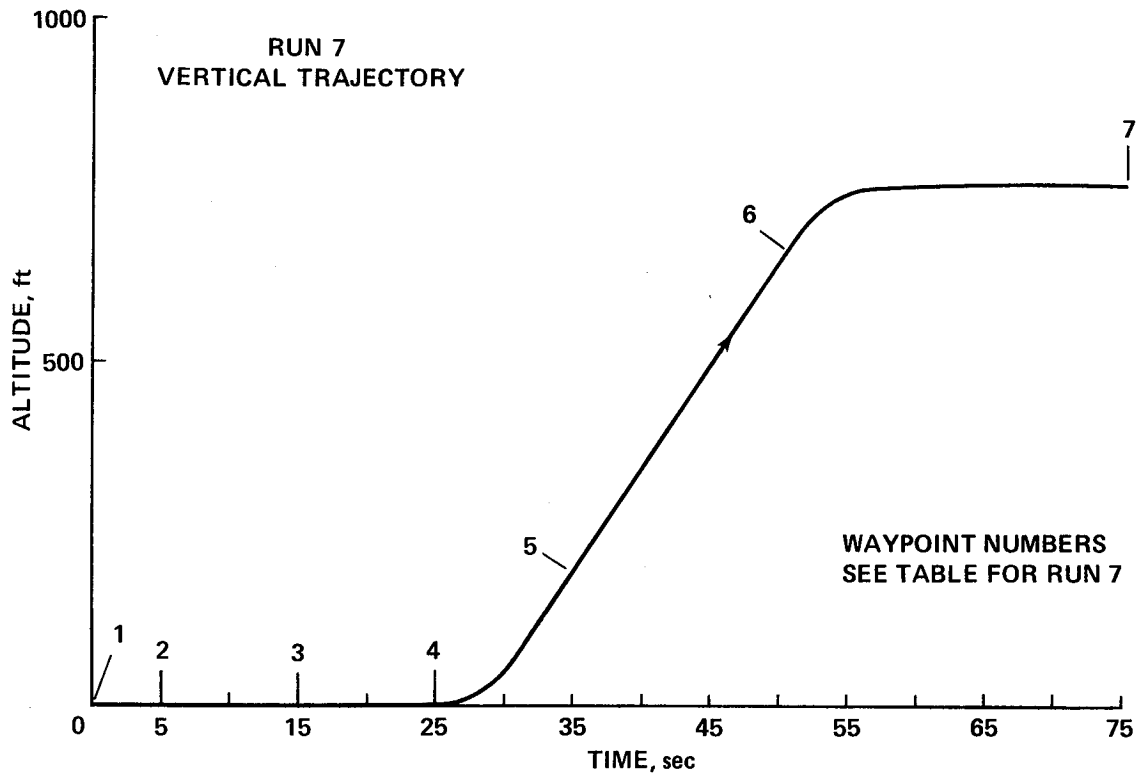


Figure 12(a).- Run 7. Complex maneuvers in hovering flight.

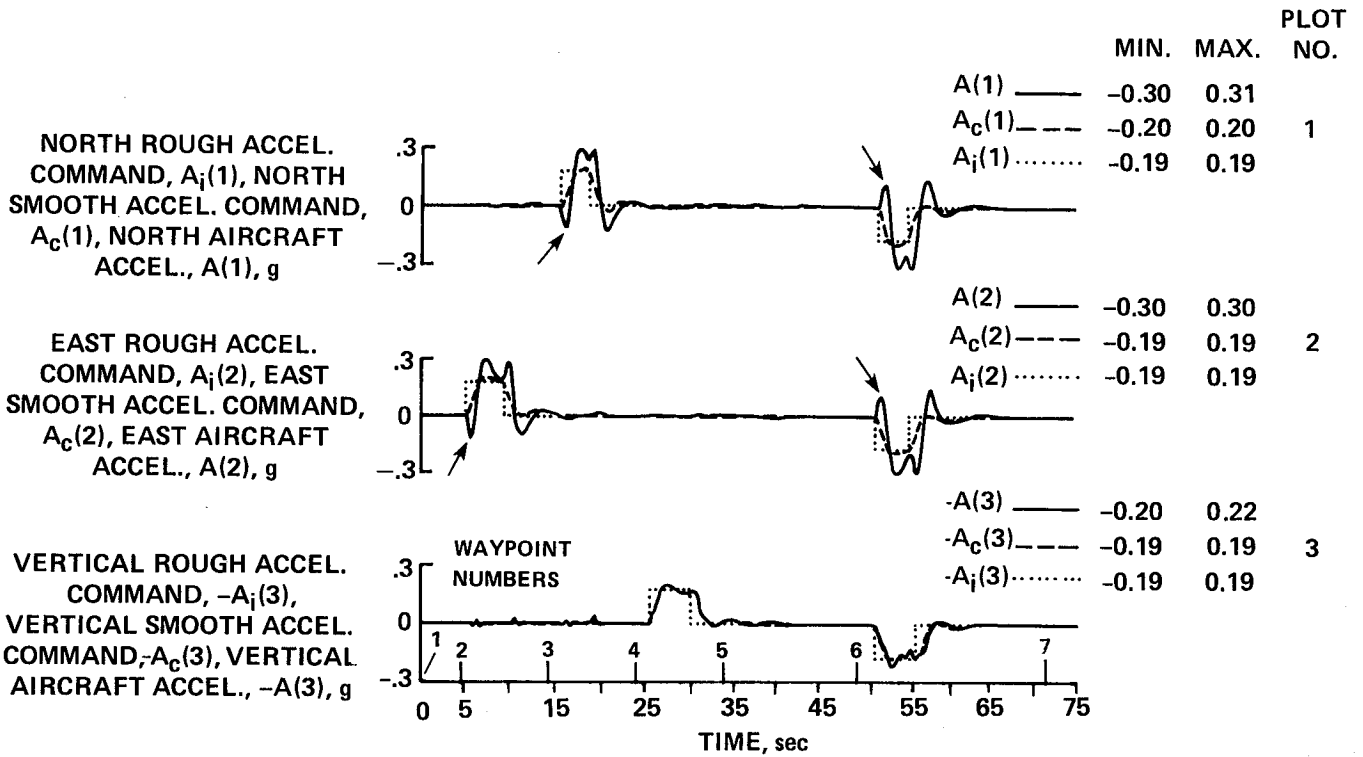


Figure 12(b).- Run 7. Continued.

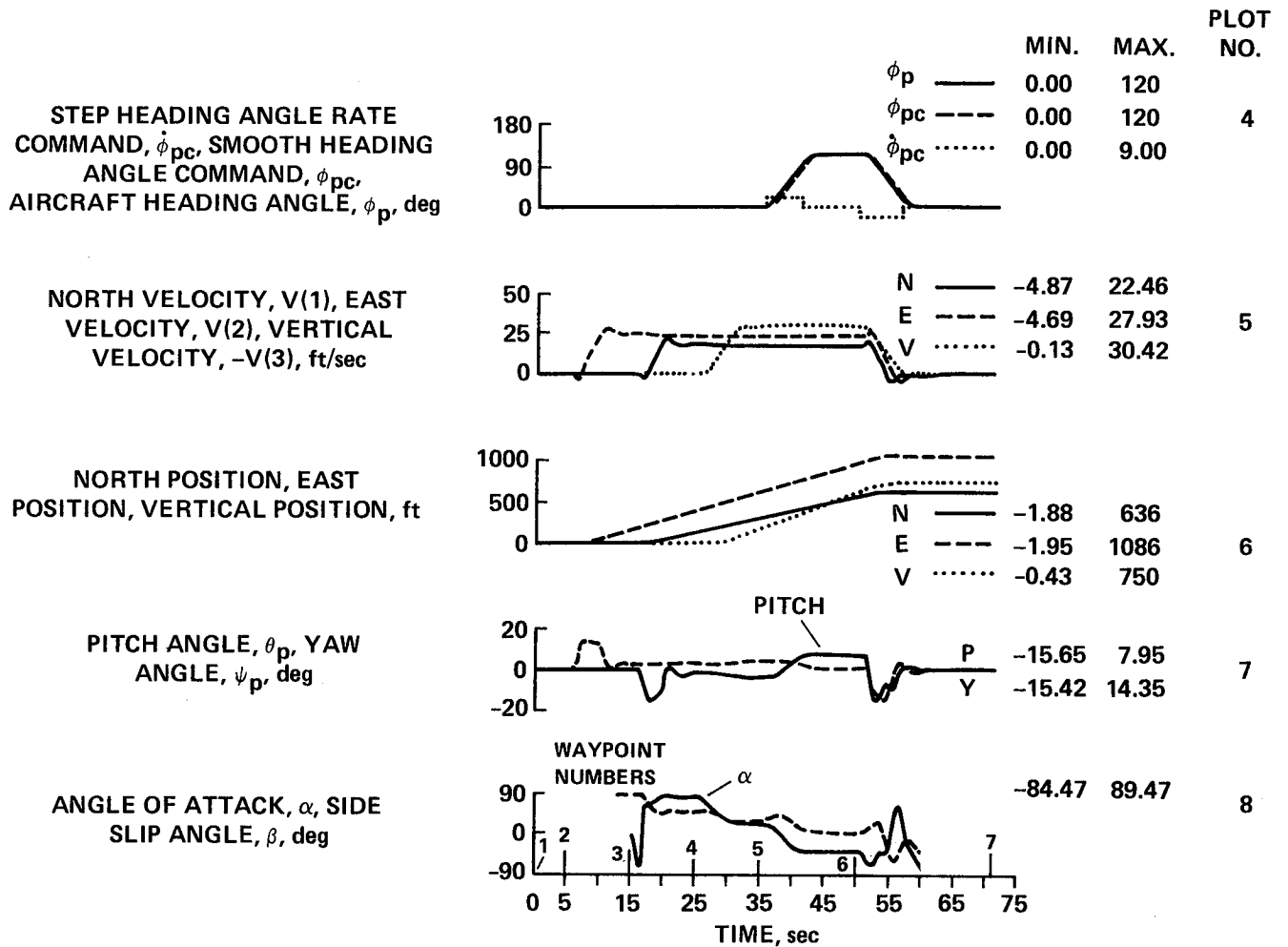


Figure 12(c).- Run 7. Continued.

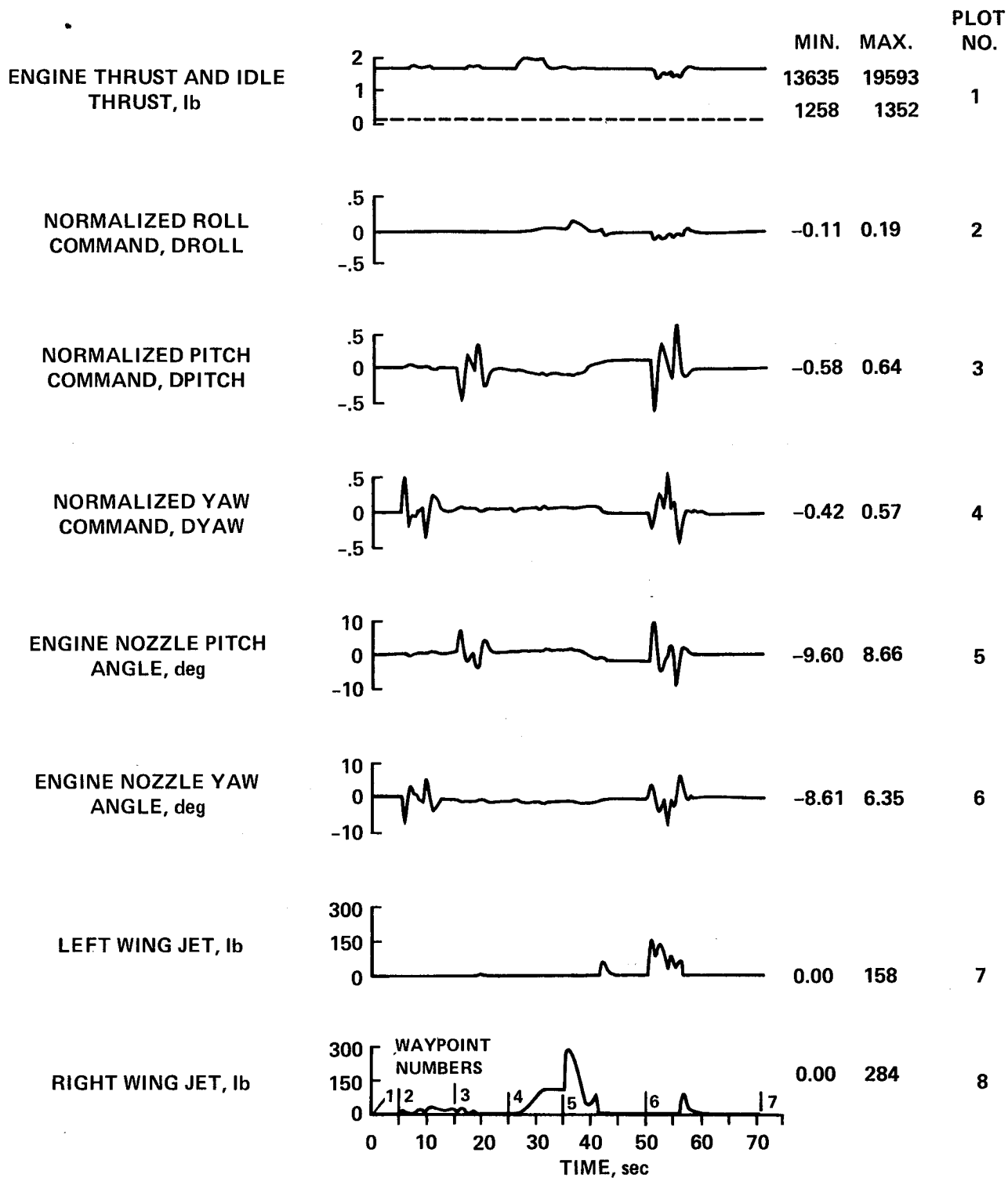


Figure 12(d).- Run 7. Continued.

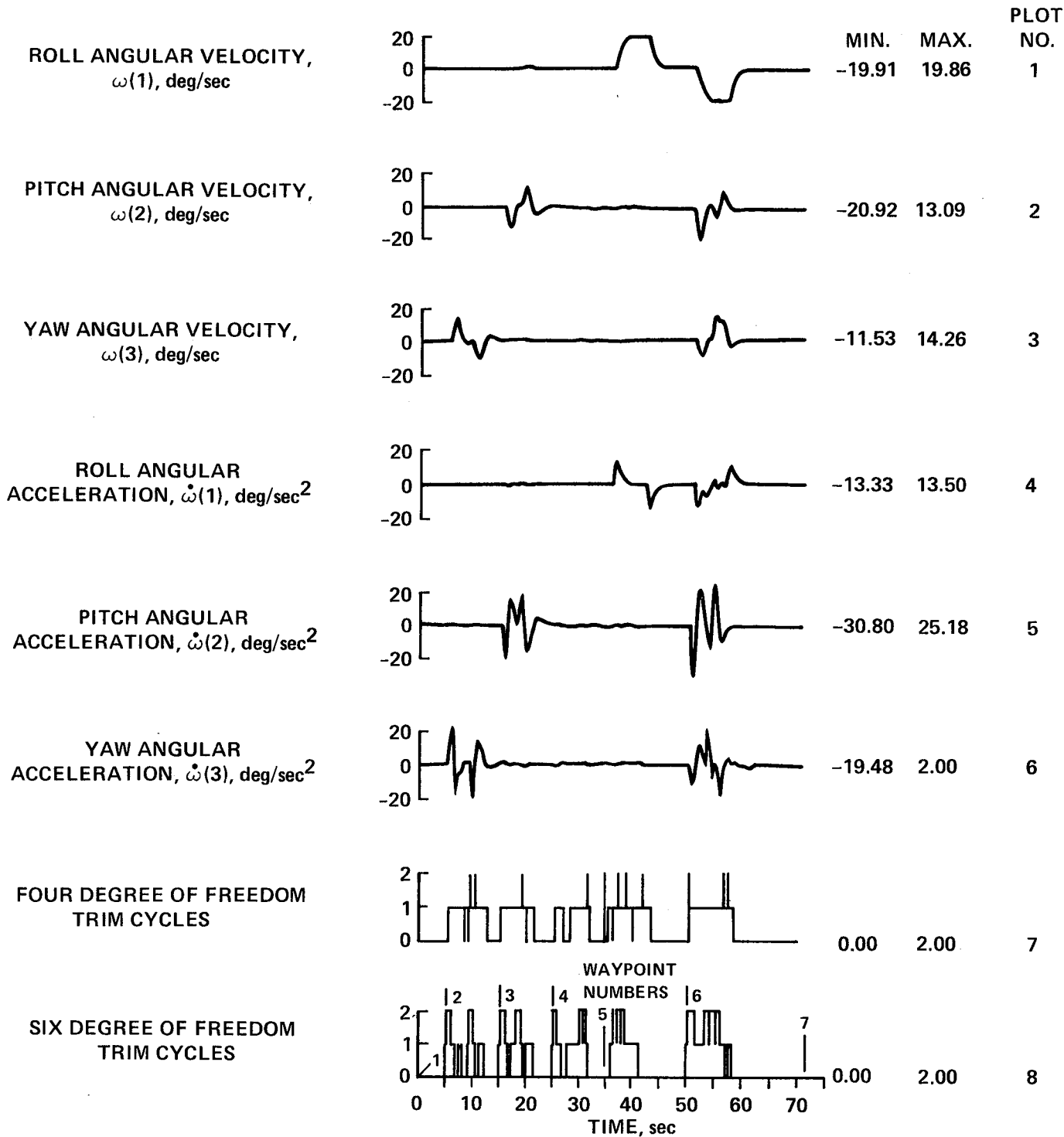


Figure 12(e).- Run 7. Concluded.

vertical command quite closely. The first plot of figure 12(c) shows that at 35 sec a step heading-angular-velocity command of  $20^\circ/\text{sec}$  about the vertical axis is applied for 6 sec until the aircraft is moving with the same velocities with respect to the ground, but with the landing gear facing southwest. At 50 sec (WP6) all the prior step commands are reversed simultaneously and the aircraft comes to rest hovering in the original attitude but displaced 635 ft north, 1085 ft west, and 750 ft above the original position at 72 sec (WP7) as shown by the curves of the third plot. The corresponding velocities are shown in the second plot. The yaw and pitch Euler angles are shown in the fourth plot. The roll angle is shown in the first plot. Angle of attack and sideslip are shown in the last plot; they are somewhat erratic at very low speeds when the aircraft may be moving in a transient manner in both directions along all axes and so are suppressed.

Figure 12(d) shows the control commands and the actual control displacements for this maneuver. The first plot shows that the thrust remains essentially equal to the aircraft weight with an increase during vertical acceleration. The roll, pitch, and yaw commands in the next three plots are three of the trim variables from the four-degree-of-freedom trim. Significant pitch and yaw excursions occur only when the attitude is changing to produce horizontal accelerations with the vehicle in the vertical attitude. The pitch and yaw nozzle-angle deflections in the fifth and sixth plots are, as usual, scaled negative versions of the roll and yaw commands. The left and right wing-tip bleed-air jet thrusts in the last two plots follow the roll command.

The roll, pitch, and yaw angular acceleration responses in the fourth, fifth, and sixth plots of figure 12(e) follow the roll, pitch, and yaw commands of the second, third, and fourth plots of figure 12(d) closely. It will be noted that the simultaneous angular velocity responses at 50 sec in the first three plots of figure 12(e) are very nearly the inverses of the individual responses earlier in the run. Only rather minor cross coupling effects are observable as this fairly violent maneuver is executed. The trim cycle counts in the last two plots never exceed two but several more double trim cycles are required for the six-degree-of-freedom trim.

DATA FOR RUN 8

TABLE 8.- WAY POINT TABLE FOR RUN 8

Way point, WP	Time	Position			Trajectory situation
		North	East	Up	
1	0	0	0	1000	Vertical attitude hover
2	5	-20	-20	980	Trajectory offsets
3	25	0	0	1000	Wind gusts
4	35	14	11	1000	Recovery
5	70	22	12	1000	End of run

Run 8. Initial Displacements and Steady Winds in Vertical Attitude Hover

The run started in vertical attitude hover at an altitude of 1000 ft. At 5 sec the aircraft was displaced by 20 ft in each axis and allowed to recover to the initial commanded position. At 25 sec a steady wind of 10 ft/sec was applied to each axis. The ground track and the trajectory profile in the north-up (vertical) plane are shown in figure 13(a).

The solid curve in the first plot in figure 13(b) is the step gust which was the same for each channel. The dotted curve is the wind estimate as computed by the air data sensor on the aircraft, assumed to have a 25 sec time-constant. The three final plots in figure 13(b) show the constant commanded position in the dotted curves and the aircraft position response in the solid curves. All three positions have returned to their commanded values by 25 sec. The vertical response, controlled by thrust magnitude, is considerably faster than are the horizontal responses that require the aircraft to tip and which show a nonminimum phase characteristic.

The velocity and acceleration response in each axis is shown in figure 13(c). The nonminimum phase effect in the horizontal channels is evident. No integral error signals were included in this design, so the steady wind causes a constant displacement although the velocity and acceleration return to zero. The vertical wind effect is extremely small. The aircraft angular change in the first two plots of figure 13(d) is less than 2° in response to the gusts. The nozzle pitch and yaw angles in the fourth and fifth plots have, as usual, the same shape as do the Dpitch and Dyaw commands and as the pitch and yaw angular accelerations which are omitted. The aircraft attitude and control responses in the figure indicate very tight, stable performance, and they suggest that operation in the vertical-attitude

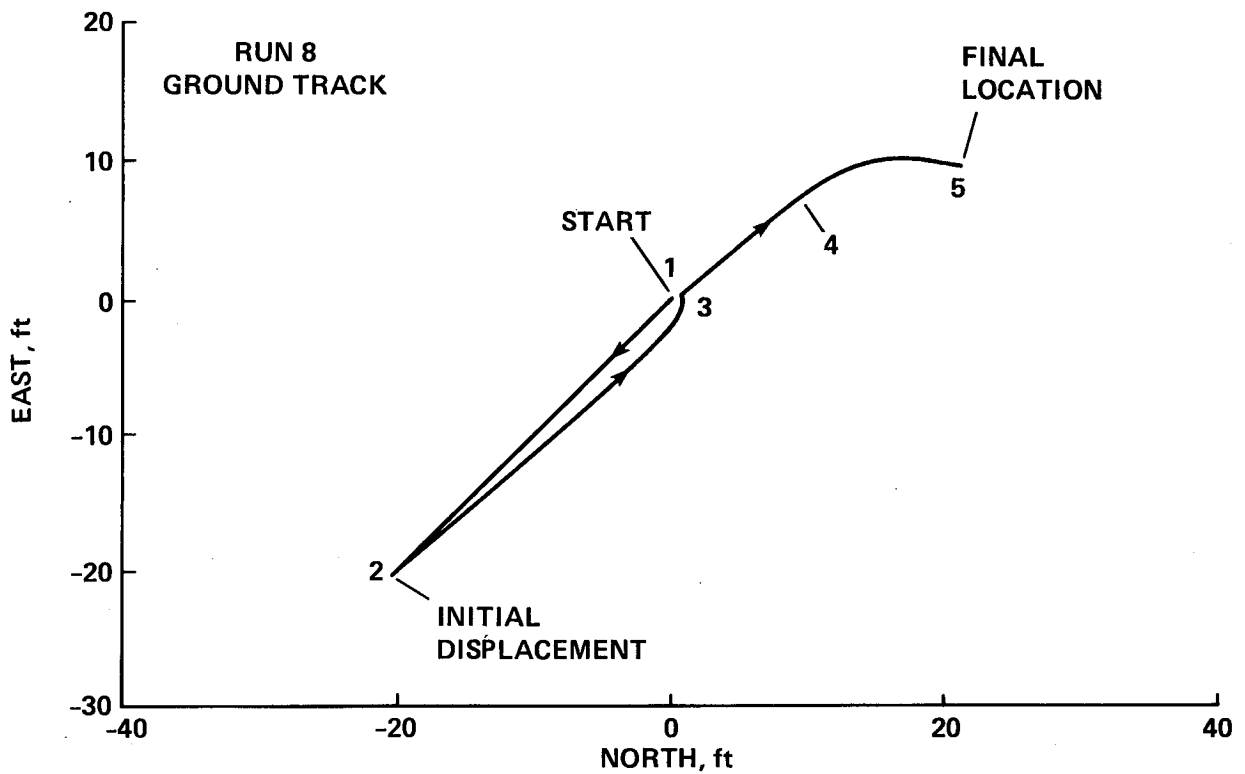
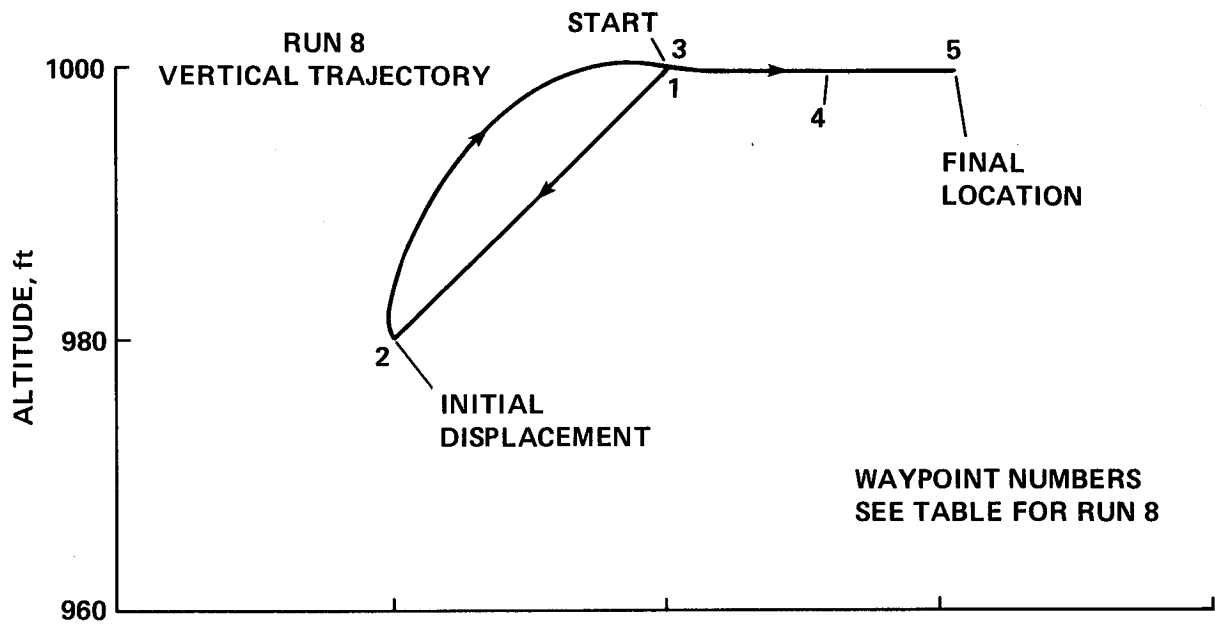


Figure 13(a).- Run 8. Disturbances in hovering flight.

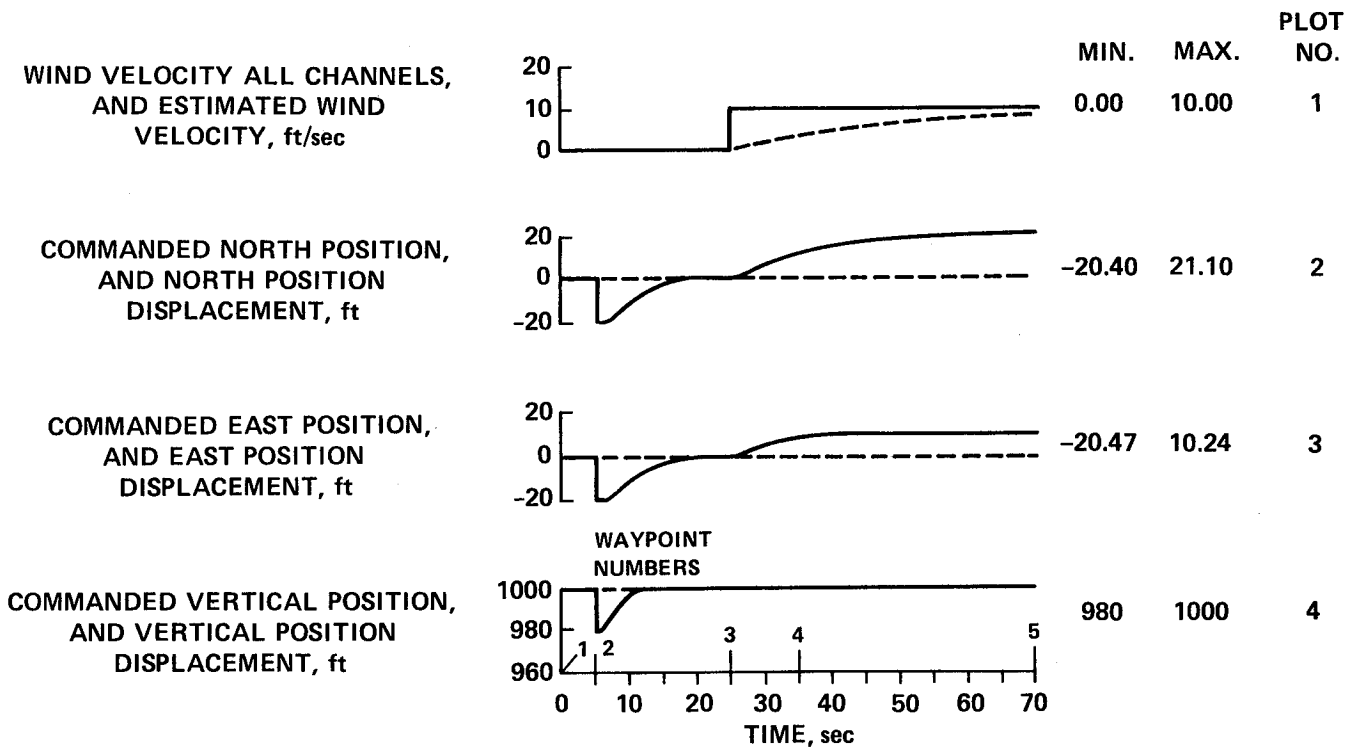


Figure 13(b).- Run 8. Continued.

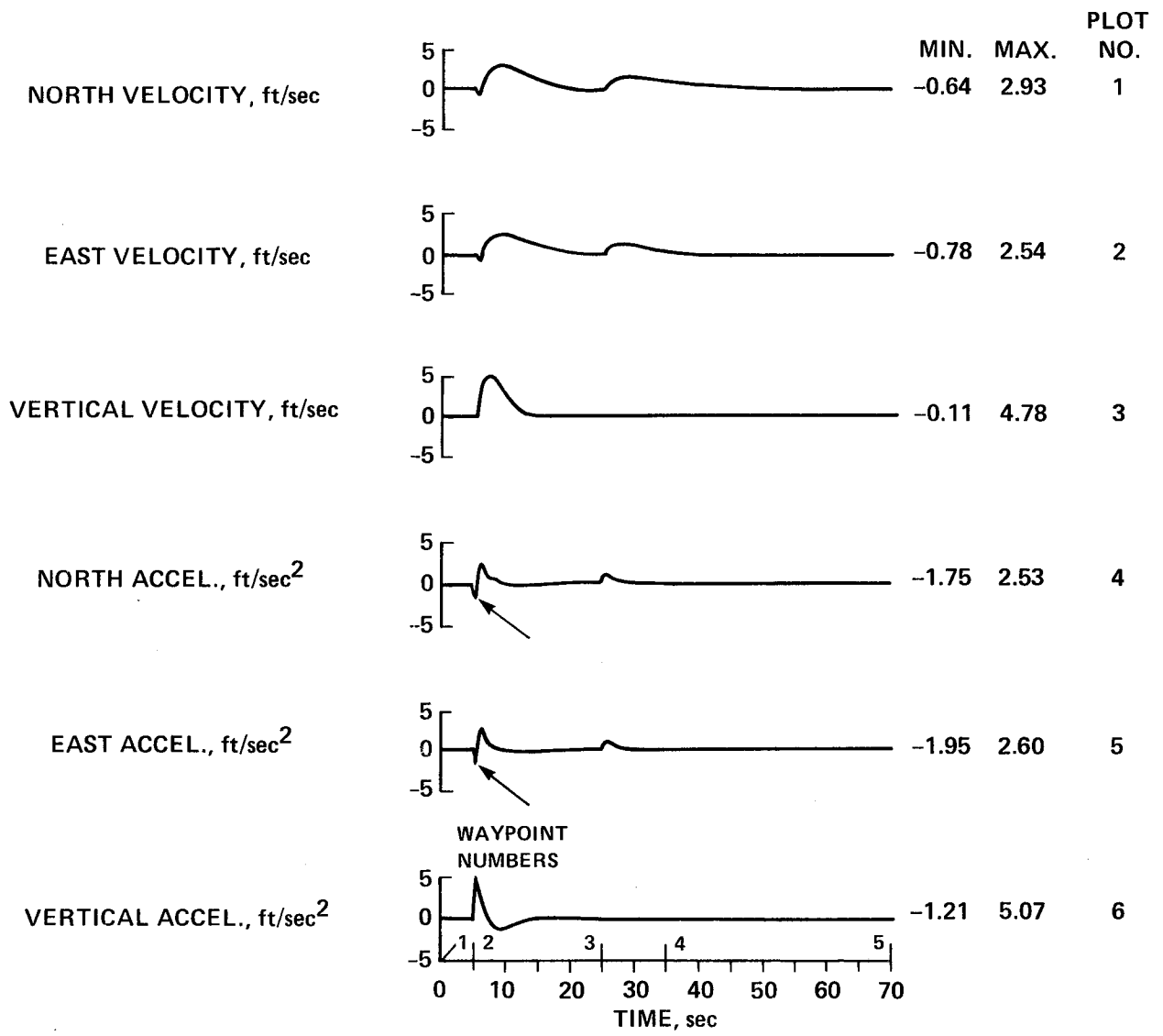


Figure 13(c).- Run 8. Continued.

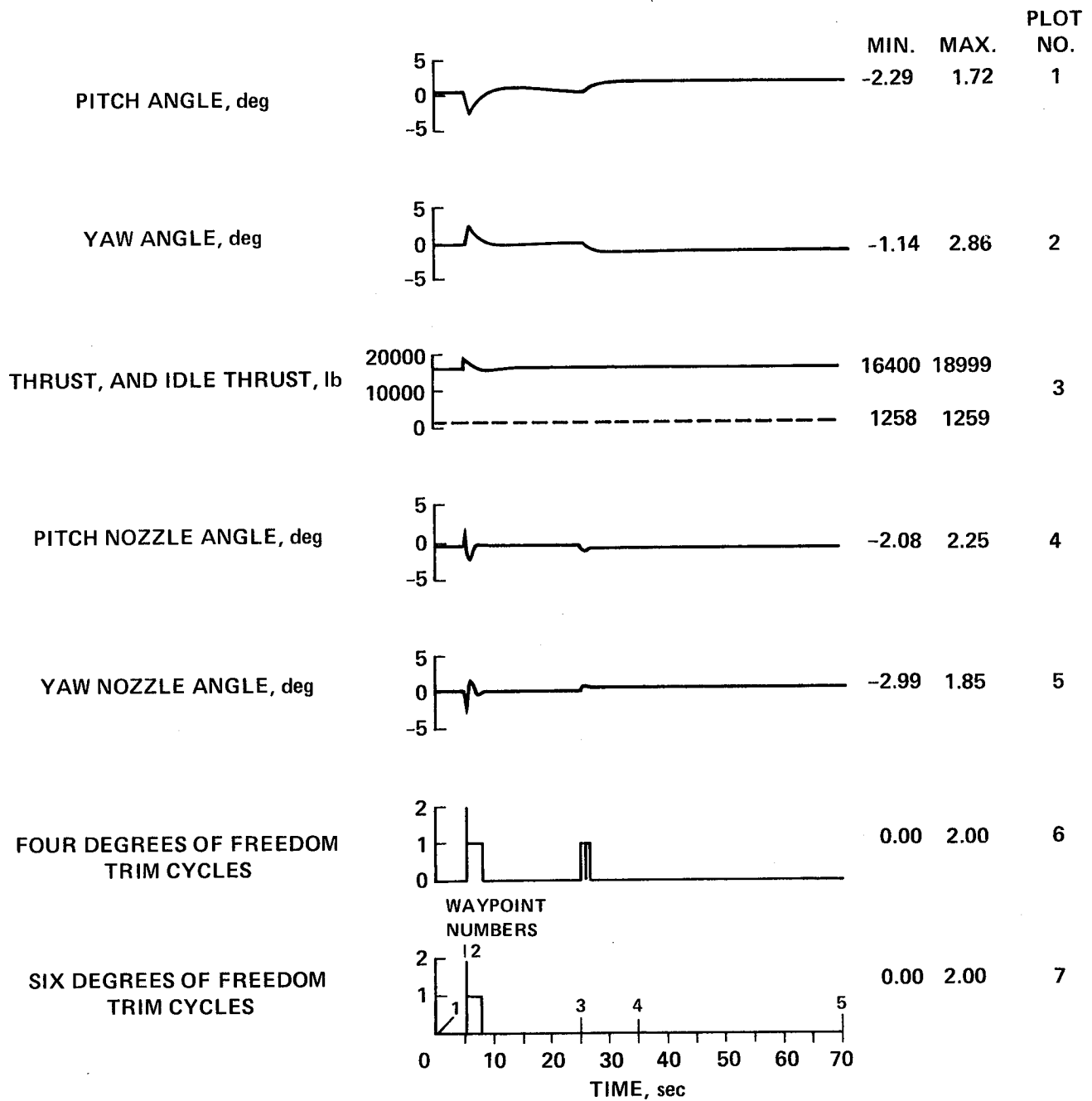


Figure 13(d).- Run 8. Concluded.

hover mode can be simple, straightforward, and precise. The final two plots in figure 13(d) record the number of trim cycles required, and they show that the variation of aircraft characteristics in the region is so slight that the same Jacobian matrix can be used for almost the entire flight. It will be recalled that if no trim cycle is required, the previous Jacobian matrix is used with the present errors to provide a control correction for even these small errors.

#### CONCLUDING REMARKS

The simulation data which has been presented and discussed, and experience with previous simulations and flight tests form the basis for the following comments.

1. Aircraft controlled by this system concept have shown smooth and acceptable transient responses to a wide variety of trajectory commands. They have followed trajectories involving accelerating, decelerating, turning, and climbing with high accuracy. Lags in executing extreme maneuvers cause some buildup of errors in the translational regulator but they are quickly eliminated in steady flight.

2. The use of limiters in the command generators and regulators allows the aircraft to make a smooth acceptable response to nonexecutable commands. A satisfactory recovery with reasonable control deflections and aircraft attitudes is made from very large trajectory offsets. Although offsets of only 100 ft were shown in the data, essentially similar results were found for much larger initial trajectory errors.

3. Complex trajectory commands are effectively decoupled and sent only to the appropriate axis. This decoupling is facilitated by the fact that aerodynamics and propulsion are completely integrated. Only the total acceleration command is sent to the inversion process which selects the required mixture of force generators to achieve the command.

4. This procedure essentially splits the design problem into two separate parts. The first part, not emphasized in this report, is to design a command section that will create suitable executable trajectory acceleration commands in response to a variety of inputs. The second part, the focus of this report, is to design a control section that will force the aircraft to follow the acceleration commands. How well this objective is achieved may be observed by comparing the total commanded acceleration with the actual aircraft acceleration.

5. It is believed that future airborne digital computers will have enough speed and capacity to easily carry out the extensive calculations required for this control system approach. The majority of computation time is required to calculate the inverse aircraft model accelerations in response to control inputs. The six repetitions of the model calculations required for the six-degree-of-freedom trim all start from the same conditions except for one input perturbation; therefore, they could all be calculated simultaneously by using a parallel computation. The

same is true for the four-degree-of-freedom trim, hence a parallel computation could save time by a factor of almost ten.

6. The six-degree-of-freedom trim in figure 5 is done with zero commanded angular acceleration and angular velocity so that it gives a commanded aircraft attitude consistent with a steady state linear acceleration command. The four-degree-of-freedom trim, most easily visualized in the hover mode, has a commanded angular acceleration input and thus gives the control deflections needed to produce it. A forward (positive north) linear acceleration requires a forward tip of the aircraft. In the vertical attitude this is a negative pitch angle about the aircraft's horizontal axis. The negative angular acceleration to produce this angle requires the nozzle at the rear of the aircraft to point forward so its reaction force is in a rearward or negative direction. This initial linear acceleration in the wrong direction is a nonminimum phase effect.

7. The nonminimum phase effect which occurs in the actual aircraft does not show up in the trim for reasons that may not be immediately apparent. It is not seen in the six-degree-of-freedom trim because the trim equations assume zero angular acceleration. The four-degree-of-freedom trim uses the three moment equations and only the force equation along the first or longitudinal aircraft axis. The generation of an angular acceleration about the aircraft's second or third axis requires a nozzle deflection that produces a force along the aircraft's third or second axis, respectively, and none along the longitudinal axis so it has no effect on the longitudinal force trim equation. In other words, a portion of the aircraft's rotational dynamics is not modeled. This deficiency in dynamic modeling places an extra burden on the regulators and causes the aircraft linear acceleration response to have a significant transient overshoot in the horizontal axis (most easily seen in the vertical attitude mode) compared to the total linear acceleration command.

## APPENDIX

### COMMAND GENERATORS AND REGULATORS

Symbols (Some Specialized for Appendix)

- $A_c$  smooth commanded acceleration vector
- $A_i$  rough commanded acceleration vector
- DT integration time-step = 0.05 sec
- F system matrix,  $12 \times 12$
- G gain matrix,  $3 \times 3$
- G1 translational command generator, position-error gain vector
- G2 translational command generator, velocity-error gain vector
- G3 translational command generator, series-gain vector
- G4 translational command generator, acceleration-rate gain vector
- G5 translational regulator, position-error gain vector
- G6 translational regulator, velocity-error gain vector
- G7 rotational command generator, attitude-error gain vector
- G8 rotational command generator, angular-velocity error-gain vector
- G9 rotational regulator, attitude-error gain vector
- G10 rotational regulator, angular-velocity error-gain vector
- I identity matrix,  $3 \times 3$
- $I_{12}$  identity matrix,  $12 \times 12$
- Q(T) vector function of matrix T, where
- $$Q(T) = \frac{1}{2} \begin{vmatrix} T_{23} - T_{32} \\ T_{31} - T_{13} \\ T_{12} - T_{21} \end{vmatrix}$$
- R aircraft position vector

$R_c$  smooth-commanded position vector  
 $R_i$  rough-commanded position vector  
 $R(1)$  first component of  $R$ , etc.  
 $s$  Laplace variable  
 $S(\omega)$  matrix function of vector  $\omega$ , where
 
$$S(\omega) = \begin{vmatrix} 0 & \omega(3) & -\omega(2) \\ -\omega(3) & 0 & \omega(1) \\ \omega(2) & -\omega(1) & 0 \end{vmatrix}$$
  
 $T$  general orthogonal matrix,  $3 \times 3$   
 $T_{11}$  first element of  $T$  matrix, etc.  
 $TBR$  aircraft attitude matrix  
 $TBR_c$  rough-commanded attitude matrix  
 $TBR_{sc}$  smooth-commanded attitude matrix  
 $V$  aircraft velocity vector  
 $V_c$  smooth-commanded velocity vector  
 $V_i$  rough-commanded velocity vector  
 $z$  computer cycle, time-delay operator  
 $\alpha_c$  commanded angle of attack  
 $\beta_c$  commanded sideslip angle  
 $\phi_c$  commanded roll angle  
 $\psi_c$  commanded heading angle  
 $\Gamma_c$  commanded flightpath angle  
 $\epsilon_0$  command generator, total-error vector  
 $\epsilon_1$  command generator, position-error vector  
 $\epsilon_2$  command generator, velocity-error vector

$\epsilon_3$	command generator, acceleration-rate error vector
$\omega$	general angular velocity vector
$\omega(1)$	first element of $\omega$ vector, etc.
$\omega_i$	rough-commanded, angular-velocity vector
$\omega_c$	smooth-commanded, angular-velocity vector
$\omega_F$	translational command generator, natural frequency, force factor
$\omega_T$	translational command generator, natural frequency, trajectory factor
$\omega_n$	rotational command generator, natural frequency
$\omega_s$	rotational regulator, natural frequency
$\delta_F$	translational command generator, damping ratio, force factor
$\delta_T$	translational command generator, damping ratio, trajectory factor
$\delta_n$	rotational command generator, damping ratio
$\delta_s$	rotational regulator, damping ratio
$\Delta A_c$	acceleration correction vector
$\Delta T$	angular error matrix
$\Delta \dot{\omega}_c$	angular acceleration, correction vector

#### TRANSLATIONAL COMMAND GENERATOR

The function of the translational command generator in figure 5 is to

- (1) accept the rough input, trajectory command vectors of position  $R_i$ , velocity  $V_i$ , and acceleration  $A_i$ , which may not be executable by the aircraft because of missing vector components, excessive rates of change or discontinuities; and
- (2) provide smooth, executable, consistent trajectory command vectors  $R_c$ ,  $V_c$ , and  $A_c$ . The command generator achieves these objectives by taking the form of a canonical model of the aircraft with a dynamic response which is the desired dynamic response of the aircraft.

The canonical model represents the aircraft as three strings of four integrators each, with each string corresponding to one of the Earth reference axes (north, east, and down). Figure A1 shows a single string representing the first channel

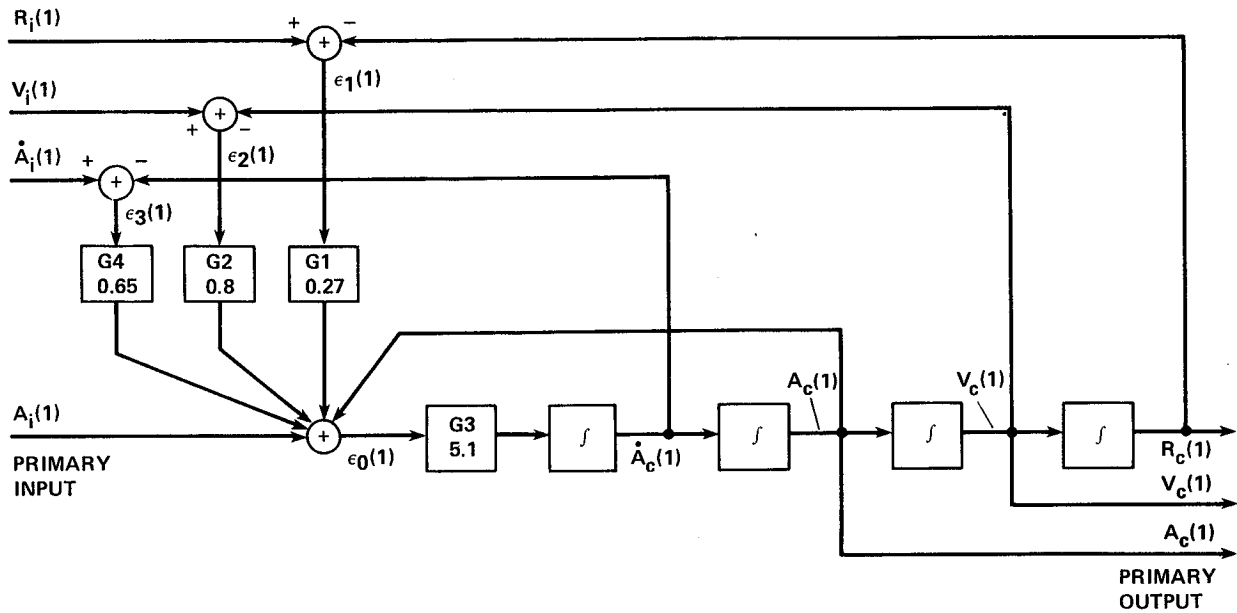


Figure A1.- Translational command generator canonical model, single channel.

with the integrator outputs as position, velocity, acceleration, and acceleration rate. The input of primary interest for this discussion is the rough acceleration command  $A_i(1)$ , and the corresponding output is the smooth acceleration command  $A_c(1)$ . Feedback loops within the command generator are formed with error signals between corresponding input and output quantities. The transient response of this system depends on the feedback gains which can be selected by various pole placement methods.

For steady state and slowly varying inputs, the feedback loops will tend to maintain low values of the primary error signal  $\epsilon_0(1)$  and of the secondary error signals between input and output quantities  $\epsilon_1(1)$ ,  $\epsilon_2(1)$ , and  $\epsilon_3(1)$  whenever possible; but if an input is missing or is inconsistent, the other errors will adjust to keep the primary error low at the expense of standoff errors between the other variables. In any event, the output quantities  $R_c(1)$ ,  $V_c(1)$ , and  $A_c(1)$  will be a smooth consistent set of position velocity and acceleration since they are the outputs of consecutive integrators. A further discussion of the canonical model from a theoretical standpoint can be found in reference 2.

The actual command generator used for this simulation was designed as shown in figure A2, which is the complete three-dimensional flow diagram with vector quantities and three channel integrators. A number of amplitude and rate limiters are included as well as a differencing circuit to calculate the derivative of input acceleration. The limiters are adjusted to limit the output commands to suitable levels as discussed more fully in reference 1. The following discussion of the gain selection process will neglect the limits and consider the frequency response of the acceleration input.

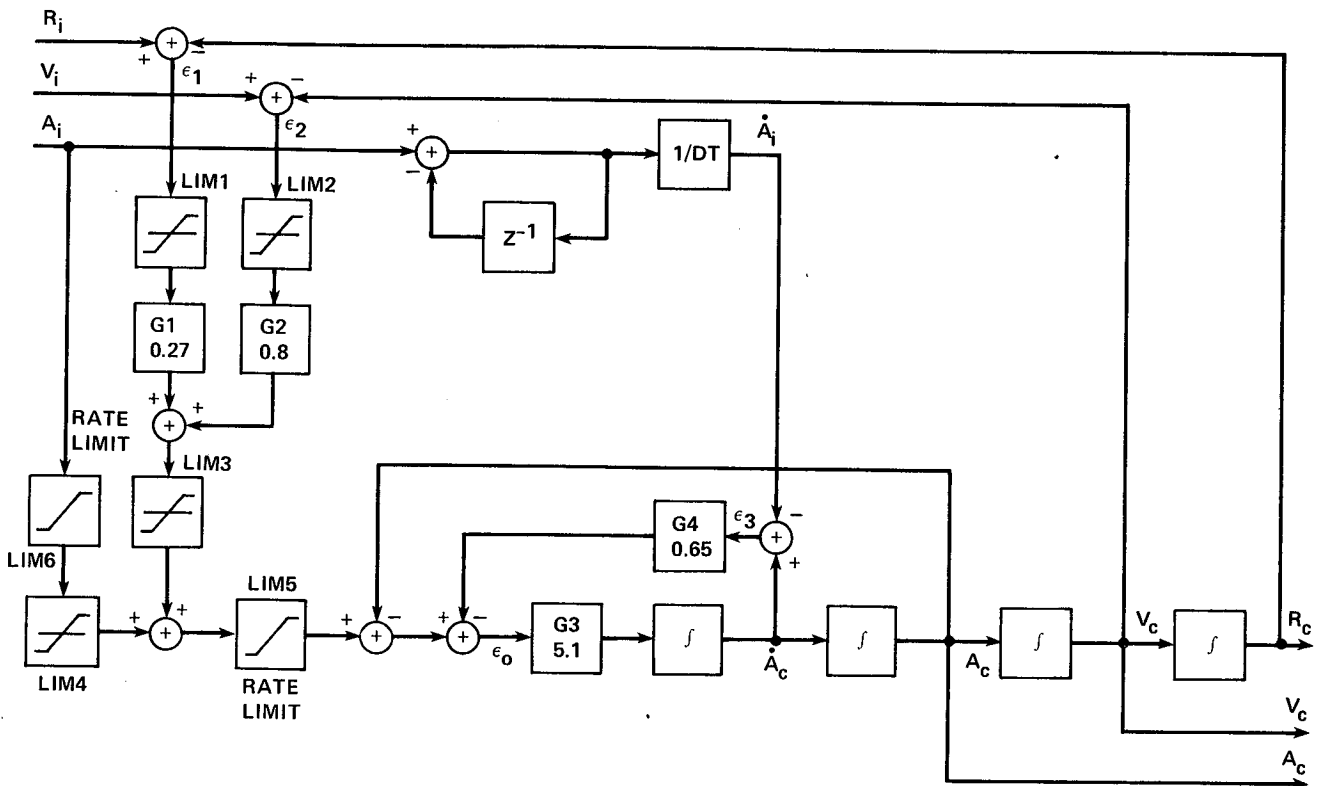


Figure A2.- Translational command generator, complete configuration.

The perturbation model of the command generator for a linear frequency analysis is shown in figure A3 where only the acceleration input has a nonzero value. This is a three-dimensional model with vector quantities. The input  $A_i$  is the trajectory acceleration command which does not include the effect of gravity so the output of the second integrator, which is smoothed acceleration, is a specific force in a gravity-free environment. The structure is that of a three-channel servomechanism. The state space has dimension 12 and is defined by the outputs of the integrators. The position and velocity are defined by the last two three-channel integrators. The remaining 6 dimensions are used to model the force generation process which is represented as a simple force generation servo.

The commands to the outer loops are zero for the frequency response analysis, but in actual operation will force the command generator output to asymptotically follow the rough trajectory input.

The gains in figure A3 could be selected by several different methods. For this investigation, where the main emphasis was on demonstrating the operation of the Newton-Raphson inversion process, a simple approach to gain selection was employed. More sophisticated optimization methods could certainly be used to advantage and would be useful for a serious design effort. In fact, a major focus in applying the inverse model control scheme to future aircraft will be in the area of

FOR TRANSFER FUNCTION ANALYSIS

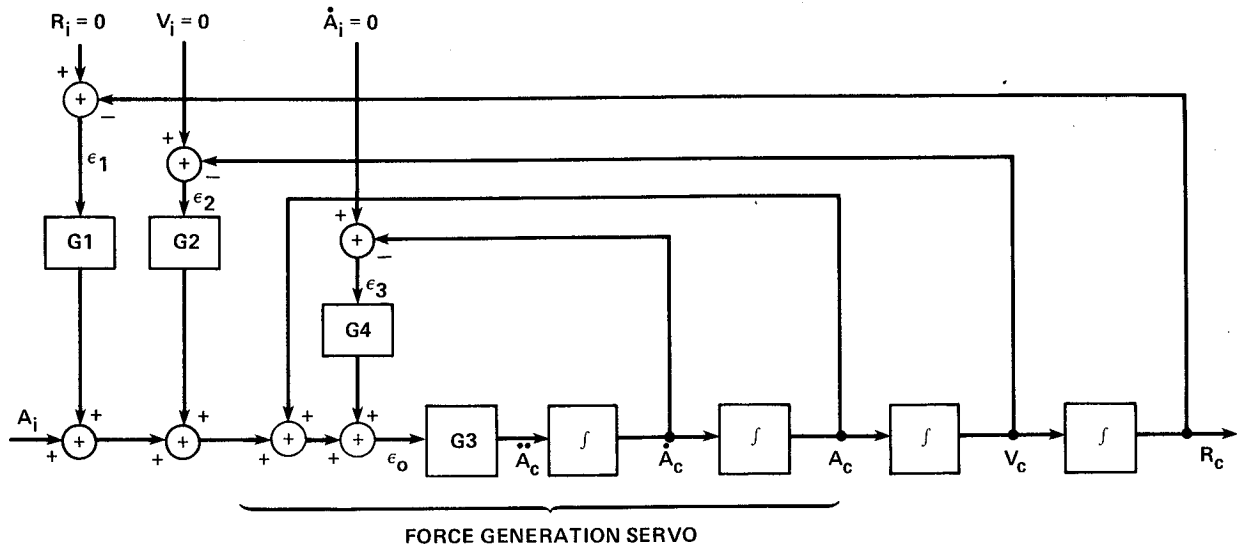


Figure A3.- Translational command generator, perturbation model.

command generator design once it has been demonstrated that the technique can force the aircraft to follow, quite closely, the output of the command generator.

The following paragraphs explain how the gains of figure A3 were chosen using linear control theory. The variables are three component vectors (with the command subscripts dropped) such as

$$R = \begin{vmatrix} R(1) \\ R(2) \\ R(3) \end{vmatrix}$$

and the gains are three-by-three diagonal matrices such as

$$G_1 = \begin{vmatrix} G_{11} & 0 & 0 \\ 0 & G_{12} & 0 \\ 0 & 0 & G_{13} \end{vmatrix}$$

The integrator outputs were chosen as the state variables. The unforced state equations--in vector matrix form--are

$$\begin{vmatrix} \dot{R} \\ \dot{V} \\ \dot{A} \\ \ddot{A} \end{vmatrix} = \begin{vmatrix} 0 & I & 0 & 0 \\ 0 & 0 & I & 0 \\ 0 & 0 & 0 & I \\ -G_1 G_3 & -G_2 G_3 & -G_3 & -G_4 G_3 \end{vmatrix} \begin{vmatrix} R \\ V \\ A \\ \dot{A} \end{vmatrix}$$

A1

where  $I$  is the three-by-three identity matrix and  $0$  is a three-by-three matrix of zeros. The characteristic equation of the system is  $\det(sI_{12} - F) = 0$ , where  $F$  is the system matrix and  $I$  is the twelve-by-twelve identity. This leads to the determinant equation

$$\begin{vmatrix} Is & -I & 0 & 0 \\ 0 & Is & -I & 0 \\ 0 & 0 & Is & -I \\ G_1G_3 & G_2G_3 & G_3 & (Is + G_4G_3) \end{vmatrix} = 0 \quad A2$$

which yields

$$Is^4 + G_4G_3s^3 + G_3s^2 + G_2G_3s + G_1G_3 = 0$$

This vector equation represents a three-axis decoupled system because the gain matrices are diagonal. Thus each of the corresponding scalar equations represents a single channel.

The roots of a scalar characteristic equation are the poles of the transfer function of the corresponding channel. The gains can be determined by any of the conventional pole placement techniques. For this study they were determined as follows. The force generation servo that was essentially represented by the first two integrators was specified to have a second-order response, natural frequency of  $\omega_F = 1.2$  rad/sec and a damping ratio  $\delta_F = 0.6$ . The translational response associated with the last two integrators was specified to have a second-order response with natural frequency  $\omega_T = 0.98$  rad/sec and a damping ratio  $\delta_T = 0.96$ . This leads to a desired transfer function that is a cascade of two second-order systems. The denominator of this transfer function then determines the characteristic equation:

$$(s^2 + 2\delta_F\omega_Fs + \omega_F^2)(s^2 + 2\delta_T\omega_Ts + \omega_T^2) = 0 \quad A3$$

When this desired characteristic equation is set equal to the first channel of the characteristic equation of figure A3 we have

$$\begin{aligned} s^4 + s^3(2\delta_F\omega_F + 2\delta_T\omega_T) + s^2(4\delta_F\delta_T\omega_F\omega_T + \omega_F^2 + \omega_T^2) + s(2\delta_F\omega_F\omega_T^2 + 2\delta_T\omega_T\omega_F^2) + \omega_F^2\omega_T^2 \\ = s^4 + s^3G_{31}G_{41} + s^2G_{31} + sG_{31}G_{21} + G_{31}G_{11} \end{aligned} \quad A4$$

A direct matching of the coefficients gives the gains,  $G_{11} = 0.27$ ,  $G_{21} = 0.8$ ,  $G_{31} = 5.1$ , and  $G_{41} = 0.65$ .

One interesting feature of figure A3 is the inclusion of the gain  $G_{31}$  in the direct path. This prevents the representation from being exactly in controller canonical form, but permits unity feedback to close the force generation servo loop. This also gives a direct physical representation for convenient numerical

checking during system tests and observation of limiting behavior. For these tests the same gains were chosen for all three channels but a more realistic design would give different dynamic response characteristics for each channel which is easily accomplished as the channels are decoupled.

The translational regulator was designed on similar principals. As shown in figure 5 it generates an acceleration correction signal,  $\Delta A_c$ , which is a sum of weighted errors between smooth-commanded and actual position and velocity vectors as shown in figure A4. The position and velocity error gains were initially selected to be the same as the position and velocity error gains in the command generator. This is a reasonable approach to close the outer loops around the aircraft with the same gains that were used to close the loops around the canonical model. This gave generally satisfactory response. However, some improvement in the first two channels was seen when the gains in the first two channels were reduced to the values shown on figure A4.

$$G5 = \begin{bmatrix} 0.07 \\ 0.07 \\ 0.27 \end{bmatrix} \quad G6 = \begin{bmatrix} 0.4 \\ 0.4 \\ 0.8 \end{bmatrix}$$

A5

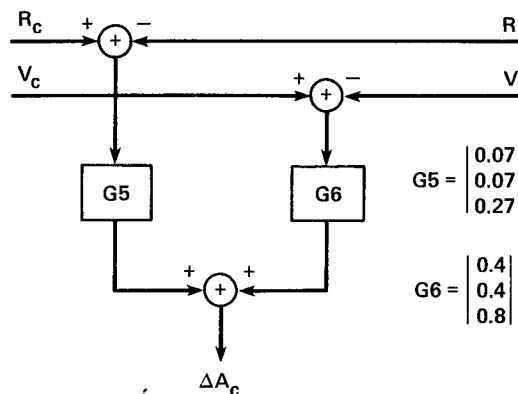


Figure A4.- Translational regulator.

## ROTATIONAL COMMAND GENERATOR

The function of the rotational command generator in figure 5 is to accept the rough-commanded attitude matrix  $TBR_c$  from the six-degree-of-freedom trim and the rough-commanded trajectory angular velocity, vector  $\omega_i$ , from the translational command generator, and to provide a smooth, executable, consistent commanded-angular acceleration vector,  $\dot{\omega}_c$ , to the four-degree of freedom trim, and to provide a commanded angular velocity vector,  $\omega_c$ , and attitude matrix,  $TBR_{sc}$ , to the rotational regulator. This arrangement differs somewhat from the translational command generator. There is no rough angular acceleration input, and the input angular-velocity command,  $\omega_i$ , is only a part of the total commanded aircraft angular velocity. It will be recalled that the commanded aircraft attitude,  $TBR_c$ , is the product of five angular rotations. Two of these rotations  $\psi_c$  and  $\Gamma_c$  represent the commanded velocity vector, and their rates of change can be calculated from the commanded trajectory accelerations to yield  $\omega_i$ . This process, however, gives only part of the total aircraft angular velocity as the rates of change of angle of attack, angle of sideslip, and roll angle are neglected. Nevertheless, this provides useful partial information and essentially complete information in steady turns where  $\alpha_c$ ,  $\beta_c$ , and  $\phi_c$  remain constant.

Figure A5 is a signal flow diagram of the rotational command generator. The rotational command generator is a canonical model of the desired aircraft angular response and consists of three strings of two integrators each. The first integration is a straightforward calculation of  $\omega$  from its derivative  $\dot{\omega}$ . The second

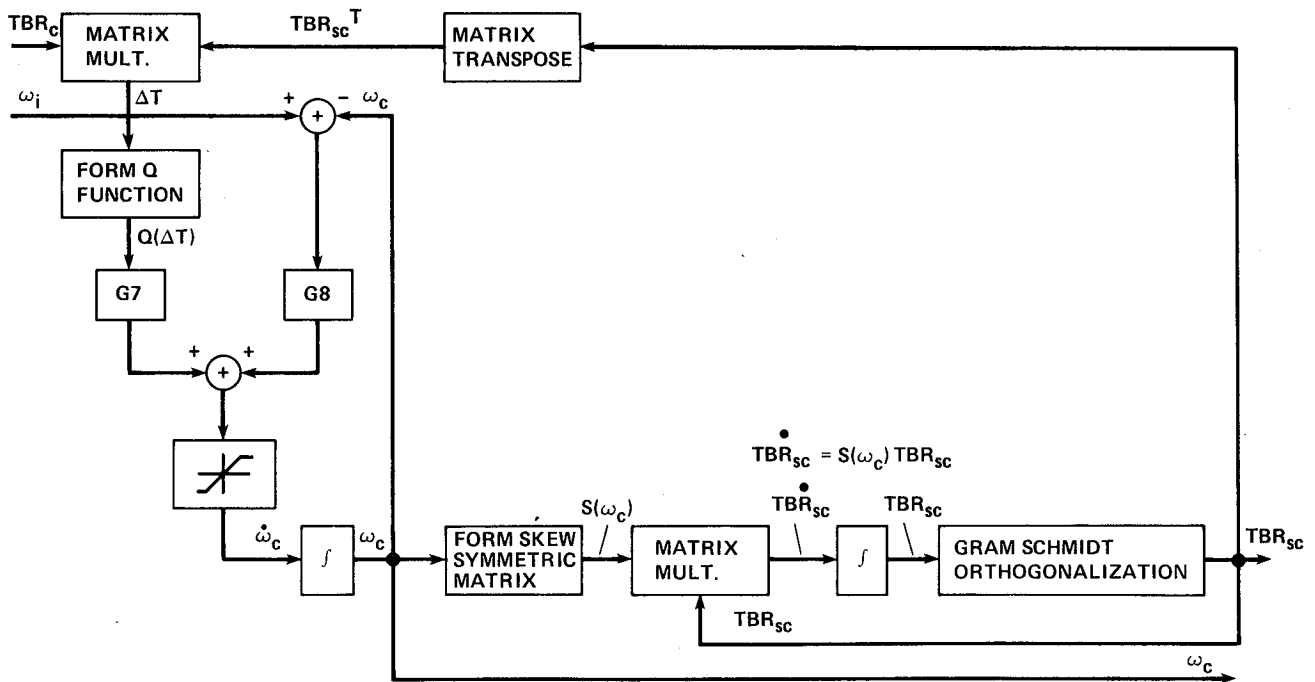


Figure A5.- Rotational command generator, complete configuration.

integration has the attitude matrix TBRsc as output. The derivative of an orthogonal-direction cosine matrix T is the matrix product  $\dot{T} = S(\omega)T$  where  $S(\omega)$  is the skew symmetric matrix function of the angular velocity.

The calculations are shown symbolically in figure A5 which also indicates how the input and output attitude matrices are multiplied (after transposition of the output matrix) to give an error matrix,  $\Delta T$ , which is then expressed as an error vector by the function  $Q(\Delta T)$  so that it can be combined with the angular-velocity error vector to form the input to the first integrator. The attitude matrix performs a positive rotation and its inverse (transpose) performs a negative rotation so the product represents the error between input and output. For a small rotation, the elementary direction-cosine-matrix sine terms equal the rotation angles; and since infinitesimal Euler angles can be treated as a vector, they can be represented by the Q vector function.

One limiter is shown in figure A5 and additional limiters and rate limiters have been successfully employed in other applications. The outer loop is closed through an attitude comparison so the outputs and inputs of the integrators will form a consistent set of angular orientation, angular velocity, and angular acceleration. The circuit is essentially a complementary filter that provides angular acceleration and angular velocity vectors primarily from an attitude input. It was necessary to employ a Gram Schmidt orthogonalization at each integration cycle to maintain an orthogonal output matrix.

The perturbation model for a linear frequency analysis is shown in figure A6. For a frequency response analysis an input acceleration command can be assumed with zero values for the other inputs. For this simple, two-integrator case, the natural frequency is  $\omega_n = \sqrt{G7}$  and the damping ratio is  $\delta_n = G8/(2\sqrt{G7})$ . A natural frequency of 3.5 rad/sec and a damping ratio of 0.75 were used for these tests to give values of  $G7 = 12.25$  and  $G8 = 5.25$ .

The rotational regulator in figure 5 generates an angular acceleration correction signal  $\Delta\dot{\omega}_c$  which is a sum of weighted errors between smooth-commanded and actual attitude and angular velocity as shown in figure A7. The same scheme for

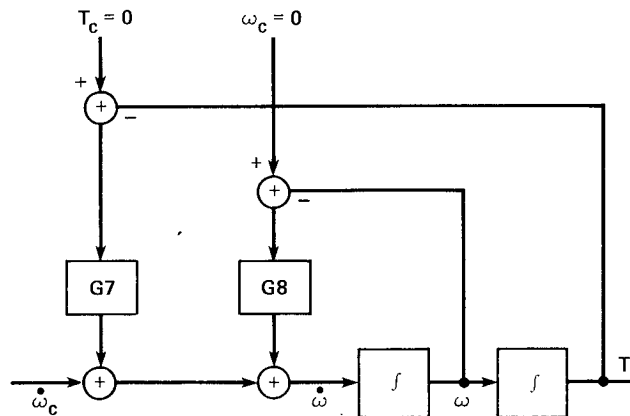


Figure A6.- Rotational command generator, perturbation model.



## REFERENCES

1. Smith, G. Allan; and Meyer, George: Application of the Concept of Dynamic Trim Control to Automatic Landing of Carrier Aircraft. NASA TP-1512, 1980.
2. Meyer, George: The Design of Exact Nonlinear Model Followers. Proceedings of the Joint Automatic Control Conference, University of Virginia, Charlottesville, Va., June 1981.
3. Meyer, George: Nonlinear Systems Approach to Control System Design. First Annual Aircraft Controls Workshop, NASA Langley Research Center, Hampton, Va. NASA CP-2296, 1983.
4. Meyer, George; and Cicolani, Luigi: Application of Nonlinear System Inverses to Automatic Flight Control Design--System Concepts and Flight Evaluations. AGARDograph No. 251, Theory and Applications of Optimal Control in Aerospace Systems, July 1981.
5. Meyer, George; and Wehrend, William: DHC-6 Flight Tests of the Total Automatic Flight Control System (TAF COS) Concept on a DHC-6 Twin Otter Aircraft. NASA TP-1513, 1980.
6. Meyer, George; Hunt, Robert L.; and Su, Renjeng: Design of a Helicopter Autopilot by Means of Linearizing Transformations. Guidance and Control Panel 35th Symposium, Lisbon, Portugal. AGARD Conference Proceedings No. 321, 1983.
7. Smith, G. Allan; and Meyer, George: Total Aircraft Flight Control System--Balanced Open and Closed Loop Control with Dynamic Trim Maps. IEEE Cat. No. 79CH1518-0, Proceedings of 3rd Digital Avionics Systems Conference, Fort Worth, Tex., Nov. 1979.
8. Smith, G. Allan; and Meyer, George: Application of the Concept of Dynamic Trim Control and Nonlinear System Inverses to Automatic Control of a Vertical Attitude Takeoff and Landing Aircraft. Proceedings of the 4th Digital Avionics Systems Conference, St. Louis, Mo., Nov. 1981.
9. Smith, G. Allan; and Meyer, George: Aircraft Automatic Digital Flight Control System with Inversion of the Model in the Feed-Forward Path. Proceedings of the 6th Digital Avionics Systems Conference, Baltimore, Md., Dec. 1984.
10. Driggers, H. R.: Study of Aerodynamic Technology for VSTOL Fighter/Attack Aircraft. NASA CR-152132, 1978.

11. Fortenbaugh, Robert L.: A Mathematical Model for Vertical Attitude Takeoff and Landing (VATOL) Aircraft Simulation. Prepared under contract NAS2-10249 by Vought Corporation, Dallas, Tex., for NASA Ames Research Center, Dec. 1980.
12. USAF Stability and Control, DATCOM. Air Force Flight Dynamics Laboratory, Wright-Patterson AFB, Ohio, Oct. 1960 (Apr. 1978 revision).

~~END~~

~~DATE~~

~~JAN. 27, 1987~~

1. Report No. NASA TM 88209		2. Government Accession No.		3. Recipient's Catalog No.	
4. Title and Subtitle AIRCRAFT AUTOMATIC-FLIGHT-CONTROL SYSTEM WITH INVERSION OF THE MODEL IN THE FEED-FORWARD PATH USING A NEWTON-RAPHSON TECHNIQUE FOR THE INVERSION				5. Report Date July 1986	
				6. Performing Organization Code	
7. Author(s) G. Allan Smith, George Meyer, and Maurice Nordstrom* (*Work done while employed by Informatics General Corporation, now Sterling Software, Palo Alto, California)				8. Performing Organization Report No. A-86092	
				10. Work Unit No.	
9. Performing Organization Name and Address Ames Research Center Moffett Field, CA 94035				11. Contract or Grant No.	
				13. Type of Report and Period Covered Technical Memorandum	
12. Sponsoring Agency Name and Address National Aeronautics and Space Administration Washington, DC 20546				14. Sponsoring Agency Code 505-34-01	
				13. Type of Report and Period Covered Technical Memorandum	
15. Supplementary Notes Point of Contact: G. Allan Smith, Ames Research Center, MS 210-3, Moffett Field, CA 94035 (415)694-5444 or FTS 464-5444					
16. Abstract <p>A new automatic flight-control system concept suitable for aircraft with highly nonlinear aerodynamic and propulsion characteristics and which must operate over a wide flight envelope has been investigated at NASA Ames Research Center. This exact model follower inverts a complete nonlinear model of the aircraft as part of the feed-forward path. The inversion is accomplished by a Newton-Raphson trim of the model at each digital computer cycle time of 0.05 seconds.</p> <p>The combination of the inverse model and the actual aircraft in the feed-forward path allows the translational and rotational regulators in the feedback path to be easily designed by linear methods. An explanation of the model inversion procedure is presented. An extensive set of simulation data for essentially the full-flight envelope for a vertical attitude takeoff and landing aircraft (VATOL) is presented. These data demonstrate the successful, smooth, and precise control that can be achieved with this concept. The trajectory includes conventional flight from 200 to 900 ft/sec with path accelerations and decelerations, altitude changes of over 6000 ft and 2g and 3g turns. Vertical attitude maneuvering as a tail sitter along all axes is demonstrated. A transition trajectory from 200 ft/sec in conventional flight to stationary hover in the vertical attitude includes satisfactory operation through lift-curve slope reversal as attitude goes from horizontal to vertical at constant altitude. A vertical attitude takeoff from stationary hover to conventional flight is also demonstrated.</p>					
17. Key Words (Suggested by Author(s)) Automated flight control system Inversion of model Inverse model control system Newton-Raphson Inversion of aircraft model				18. Distribution Statement Unlimited  Subject category - 08	
19. Security Classif. (of this report) Unclassified		20. Security Classif. (of this page) Unclassified		21. No. of Pages 96	22. Price*